DEPLOYMENT DYNAMICS OF INFLATABLE WINGS

By

Weng Kheong Loh (BEN)

Bachelor of Science in Mechanical and Aerospace
Engineering
Oklahoma State University
Stillwater, OK, USA
2006

Submitted to the Faculty of the
Graduate College of
Oklahoma State University
in partial fulfillment of
the requirements for
the Degree of
MASTER OF SCIENCE
December, 2008

DEPLOYMENT DYNAMICS OF INFLATABLE WINGS

Thesis Approved:

Dr. Jamey Jacob

Thesis Advisor

Dr. Andy Arena

Dr. Ronald Delahoussaye

Dr. A. Gordon Emslie

Dean of the Graduate College

ACKNOWLEDGMENTS

I would like to express my sincere appreciation to my advisor, Prof. Jamey Jacob, for his intelligent supervision, constructive guidance, patience, financial support, inspiration, motivation and friendship. I am proud of working with him for the past two and a half years in a one-of-a-kind inflatable wing project. I would like to thank Prof. Andy Arena for being the motivator for me to continue my persuasion in M.S. after being through the sweet success in the Design/Build/Fly competition in 2006. I would like to thank Prof. Ronald Delahoussaye for serving on my committee. I would also like to thank Johnny Chandler and Eric Johnson for their help and useful suggestions. I wish to extend my appreciate to Prof. Suzanne Smith and Dr. Andrew Simpson from the University of Kentucky on BIG BLUE and inflatable wing research. Without their references, i would not have the in-depth understanding of the inflatable wing technology. I wish to extend my gratitude to all members who has contributed to the MARS and BIG BLUE project for their passion, team spirit and unforgettable friendship. Without them, i personally could not envision the potential of inflatable wing technology. I'd also like to thank ILC Dover, particularly Dave Cadogan, Steve Scarborough and Dan Gleeson for providing us with the wings and many helpful discussions.

Most importantly, I wish to express my sincere thanks to my parents and sibling for their confidence in me in OSU for the past 7 years. I would like to thank them for their encouragement at times of difficulty, and understanding to shape who I am today. I also want to thank my distant girlfriend, Inhu Ko, who is currently staying in South Korea. Thanks for her patience, love and companionship through the window

messenger for the past few months as I slowly worked on my thesis until completion.

Finally, i would like to thank the OSU School of Mechanical and Aerospace Engineering for providing me with the opportunity to pursue a M.S. and the financial support of Oklahoma NASA EPSCoR, the Oklahoma Space Grant Consortium, and NextGen Aeronautics.

TABLE OF CONTENTS

LIST OF FIGURES

Figure Page

CHAPTER 1

Introduction

1.1 Scope

Inflatable structures have been used in both the civilian and military sectors for decades. The complexity of these structures range from life rafts and shock absorbers to solar arrays and solar sails. These structures are commonly designed to take up the least amount of space thereby maximizing overall storage capacity, which also optimizes transportation. This thesis will describe an approach that combines this technology and aircraft wing design.

Since 1930, inflatable concepts has been proposed and integrated into the aviation development. Various patents using inflatable structure were filed on some of the early concepts, which include an inflatable spar vehicle proposed by McDaniel, shown in fig.1.1, an inflatable reentry vehicle by Aerospace Corporation as shown in fig.1.2 and several variation of inflatable spar wing design shown in fig.1.3. All previously described patents are inflatable spar orientated designs and can be manufactured easily; however, their concept was poorly designed to resist bending loads. All prototypes were apparently not developed beyond their patent stage.

ILC Dover is one of the leading manufacturer of soft good products and space suits. Since 1970, ILC Dover has employed the inflatable wing technology and developed Lighter than Air (LTA) Structure like the Aerostat. Currently, University of Kentucky (UK), Oklahoma State University (OSU) and ILC's Dover is working closely to expand the potentials and productivities of inflatable wing technology. Inflatable wing technology is relatively new as compared to conventional wing design, therefore,

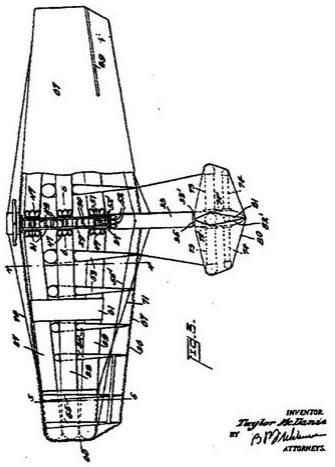

Figure 1.1: Inflatable spar vehicle [1]

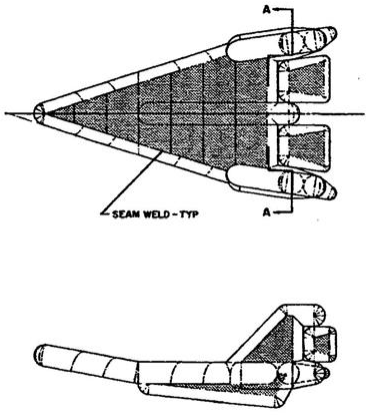

Figure 1.2: Reentry vehicle designed by Aerospace Corporation

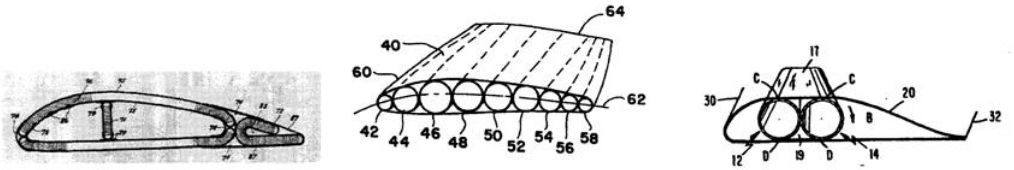

(a) Bain, 1963 (b) Sebrell, 1976 (c) Priddy 1988

Figure 1.3: Earlier circular inflatable wing concepts [2, 3, 4]

different aspects of inflatable wings have to be evaluated before this technology can be fully utilized in the aircraft designs. Till today, inflatable wings technology has

been tested on UAVs and spacecraft design for planetary exploration [11, 8]. The Inflatable winged aircraft not only reduce the storage capacity prior to its flight, but it might also allow a single aircraft to perform multiple tasks by changing it wing shape during flight.

Here are some of the outlined benefits and drawsback associated with inflatable wing technology as stated by Cadogan *et al.* [12]

Benefits

1. High packing efficiency (low packed volume)
2. High G deployable
3. Robust/simple/reliable (no moving parts)
4. Low Cost
5. Long Storage Life
6. Recoverable/Durable/Reusable
7. Can be morphed or shape modified for control
8. Can recover shape if buckling occurs during flight (gust load)
9. Inflatable structures dampen vibrations well

Drawbacks

1. Potential for leakage/ballistic penetration
2. Thicker airfoil required for high stiffness, thus, less efficient aerodynamically
3. Aspect ratio limited for high wing loading
4. Inflation system mass burden

5. Need for make-up gas (thermal/altitude excursions)

Many of the drawbacks can be addressed by applying a material technology known as rigidization. Rigidization is the action by which a flexible inflatable structure is converted into a rigid composite structure. Cadogan *et.al* [12] and Simpson *et.al* [8] has discussed the methodology of rigidization.

1.2 Motivation and Objectives

Most of the inflatable wing research conducted in wind tunnel and flight tests mainly focused on pre-inflated wing configuration. In contrast, NASA I2000 has conducted mid-air deployment at rapid deployment rate. The designed inflation system was successfully tested and able to inflate the wings in less than a fraction of a second until the internal pressure reaches 300 psi. I2000 was lifted to mid-air using an aircraft carrier before transition from wingless to winged aircraft. No significant flight instability was observed and the unpowered flight was safely returned to the ground. However, the following questions were raised :

- What would happen if the inflation rate was slower than expected due to mechanical failure or leakage in the system?
- If a lower pressure wing was used, would it be able to completely deploy under dynamic pressure without significantly disrupting the flight stability?
- What kind of behavior would the inflatable wings exhibit during slow inflation in flight?
- How can we control the wing deployment with slower flow rate?

The motivation of this research is to develop an recoverable in-flight aspect ratio morphing UAV using a low pressure inflatable wing designed by ILC Dover. An powered inflatable winged aircraft was proposed to conduct takeoff, deploy, cruise and

land independently in contrast with NASA I2000. Fig 1.4 depicts the aspect ratio morphing wing concept using inflatable wings. However, to answer those questions regarding the stability of in-flight deployment, the deployment behavior has to be investigated before integrated onto an UAV design.

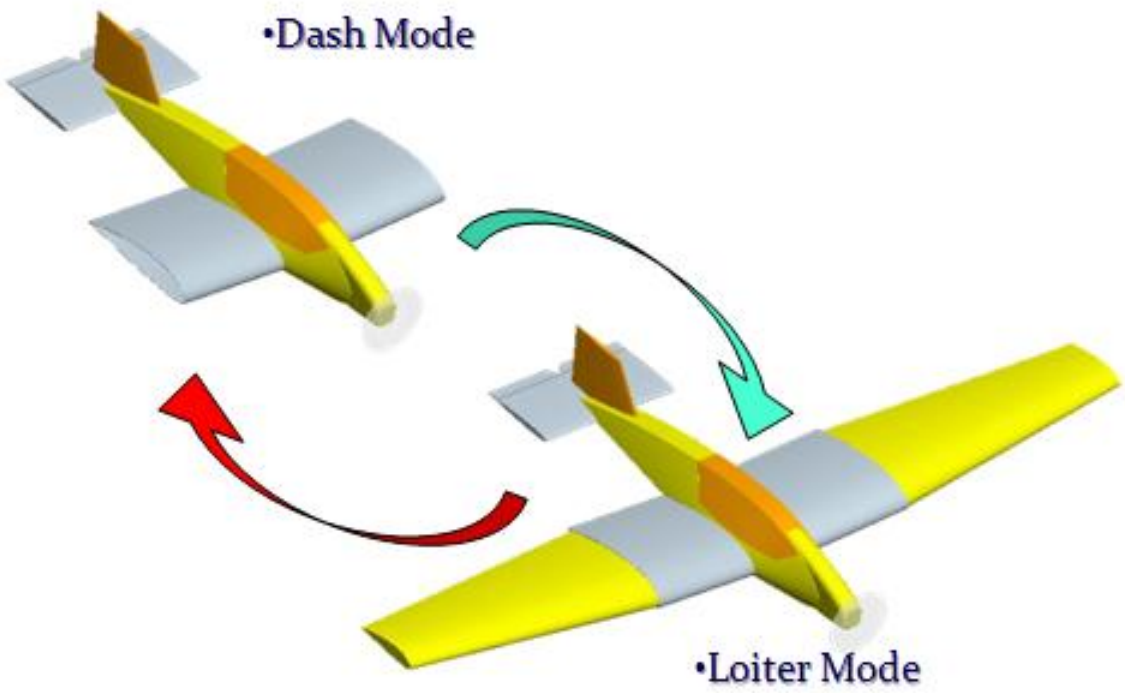

Figure 1.4: Wing morphing using inflatable wing

Therefore, wind tunnel deployment test is needed to verify the impact of dynamic pressure on the inflatable wing at slow deployment rate. This helps simulate in-flight deployment to prove the morphing capability using inflatable wing. Here are the objectives outline in this research.

- Investigate the dynamic response of inflatable wing upon deployment
- Investigate the impact of dynamic pressure on the wing pressure
- Investigate the deployment behavior at varying AOA various angle of attack,

even though straight flight was expected prior to deployment sequence.

- Explore potential methods/techniques to improve the deployment sequence and maintain stability during in- flight

1.3 Thesis Outline

Chapter 2 presents the previous works of various morphing wing aircraft that categoried into three sections: Morphing wing, Rigid Folding Wing, and Inflatable Wing. This chapter also explains the motivation and the goal of this research. Chapter 3 present the experimental set up used to investigate the dynamic deployment of inflatable wing. Chapter 4 deals with the inflatable wing characteristics and construction methods. Five preliminary morphing concepts using inflatable wings were also discussed. Chapter 5 presents the results and discussions of both the wind tunnel experiments and full scale test . Chapter 6 describes the research aircrafts used for this research. Finally, chapter 7 presents the summary of the work contained herein as well as possibilities of future work.

CHAPTER 2

Background

2.1 Previous Work on Wing Morphing

Most modern Unmanned Aerial Vehicles (UAVs) are designed for a single mission such as attack or reconnaissance. The design characteristics of an aircraft are dictated by the vehicle's primary mission and is not optimized for other mission segments or roles. This results in reduced range, loiter times, and the inability to operate from some airfields. The capability to change the wing profile or geometry would allow a single vehicle to conduct multiple missions that are beyond its designed capabilities. The capability is termed wing morphing which is the ability of the wing structure to automatically reconfigure its shape or surface textures to adapt to changes in flight conditions.

Research on wing morphing has increased in recent years to improve aircraft performance, expand its flight envelope, replace conventional control surfaces and reduce drag [13, 14, 15]. UAVs are ideal platforms to test this new technology, as pilot safety is not a concern. Some morphing wing work has been inspired by the study of birds or insects, and can also be dated back to Wright Brothers flight in 1903. Wing twist was used on the Wright Brothers Flyer for roll control, a method inspired by the Wrights' observations of the way turkey vultures soared over the Miami River near their Ohio home [16]. The purpose of aircraft morphing is the ability to perform drastically different mission roles during a single flight. There are several government agencies, universities and companies in the United States spending an increasing amount of resources on morphing technology in the next sections.

2.1.1 Rigid Morphing Wing

A. F/A 18 and Morphing Wing Research Aircraft

(a) F/A 18 using Active Aeroelastic Wing

(b) NASAs latest morphing aircraft concept

Figure 2.1: NASA's morphing wing research aircrafts.

NASA was one of the earlier developers that joined with US Air Force to conduct research on morphing wing technology with Advanced Fighter Technology Intergration (AFTI) program began [13]. To improve the maneuverability of future high-performance military aircraft, programs such as the Mission Adaptive Wing (MAV) and Active Aeroelastic Wing Program (AAW) made use of lighter-weight flexible wings.

The MAV wing was built by Boeing Aircraft and integrated with a NASA F-111As wing. MAV wings had an internal mechanism controlled operated by an onboard digital flight control system to modify the camber section to change the wing is skin. This aircraft was testing in-flight at subsonic, transonic, and supersonic speeds. A total of 59 flights were conducted over 3 years beginning in 1985. The test data showed a drag reduction of around 7 percent at the wing design cruise point to over 20 percent at an off-design condition[13].

In 1996, AAW was developed and validated by NASA, the US Air Force and Boeing is Phantom Works to demonstrate roll control improvement through aerodynamically induced wing twist on the F/A 18 as shown in fig. 2.1 (a). The research was

made possible by using modern composites and actuators. The F-18s leading edge flap was divided into inboard and outboard segments. Each segments was operated separately using actuators to demonstrate wing twist. The aerodynamic force on the twisted wing provide the roll forces desired [17].

Currently, NASA researchers are working on an advance-morphing-aircraft concept that could become reality by 2030. This aircraft has the ability to respond to constantly varying conditions using sensors to monitor pressure variations over the entire surface of the wing. This concept design is shown in fig. 2.1 (b). The feedback response to these measurements will direct an internal motion-generating actuator to alter the wing shape to an optimal configuration. The wing will sweep depending on the flight mission/conditions. In addition, the engine inlet and nozzles are designed to morph as well. A tail could be deployed to provide additional control [16].

B. Morphing Tomahawk

Raytheon Missile Systems received a $4.1 million contract from the Defense Advanced Research Projects Agency (DARPA) for its work on the Morphing Aircraft Structures program [15]. Raytheon is proposing new airframe elements for cruise missiles, which will be able to change in flight, adapting to the mission requirements, and other changes in the combat zone. Missile like the one shown in fig. 2.2, can be enhanced to travel to the target area at high speed, loiter and then move to another target area, at speed from 0.3 Mach and 3.0 Mach.

Figure 2.2: Modified Tomahawk.

C. Sliding Wing

NextGen Aeronautics is currently designing a hunter-killer UAV using a sliding skin concept as shown in fig. 2.3. NextGens morphing wing has flexible, stretchable skin panels attached to an articulated lattice structure with actuators in the joints. Successful flight test show that this UAV is capable of independently varying wing area and sweep. This wing demonstrates a wing area change of 145%, aspect ratio changes of 440% and thickness/chord changes of 280%.

Figure 2.3: NextGen Aeronautics shape-changing UAV.

D. Pneumatic Morphing Aspect Ratio Rigid Wing

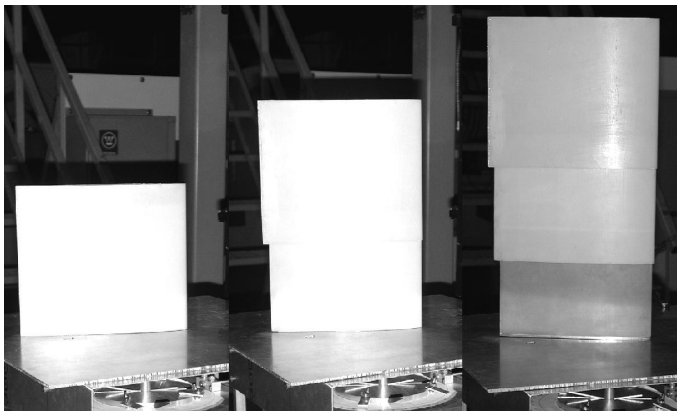

Figure 2.4: Morphing wing using Inflatable telescopic spar.

The University of Maryland is currently developing a small scale morphing aspect ratio wing as shown in fig. 2.4, using an inflatable telescopic spar that may be possible to develop a UAV with variable aspect ratio wings. Hollow fiberglass shells are used

to preserve the span-wise airfoil geometry and ensure compact storage and deployment of the telescopic wing. The telescopic wing consists of three concentric circular aluminum tubes of decreasing diameter and increasing length that deploy under pressurized air to produce various wingspan configurations. This wing could extend or retract its span from 7 inches to 15 inches, about 114% increase. The telescopic wing was tested in four different configurations and experimental results were compared to finite wing theory results. The preliminary aerodynamic results are promising for the variable aspect ratio telescopic wing. It was expected that the telescopic wing at maximum deployment should incur a slightly larger drag penalty and a reduced lift to drag ratio [18].

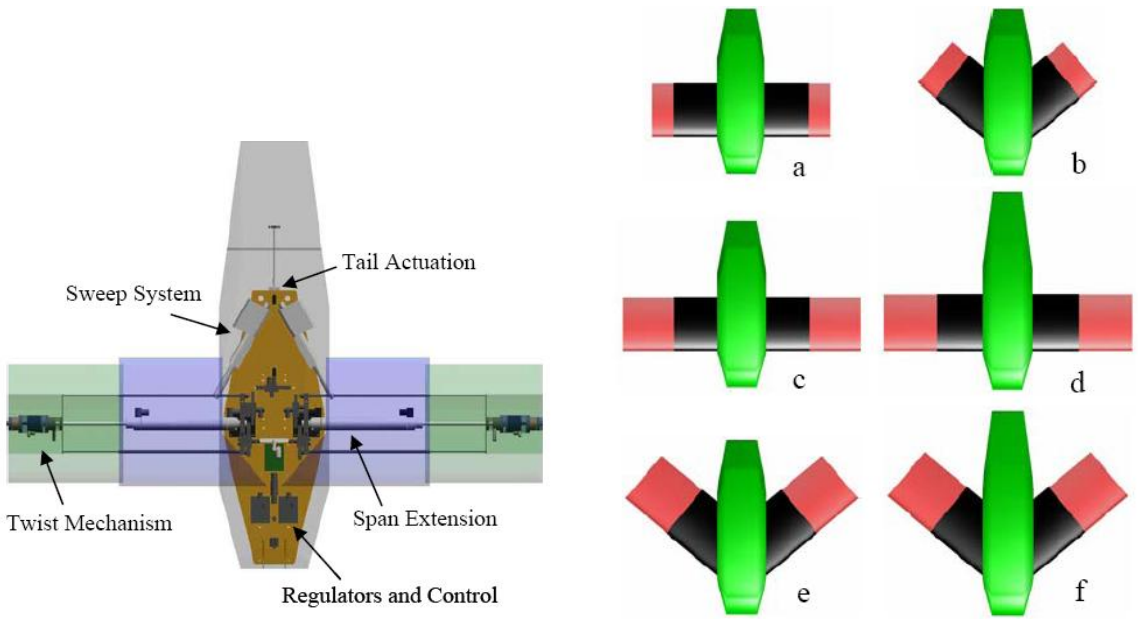

(a) Internal structure (b) various configuration

Figure 2.5: Fully adaptive aircraft model.

Virginia Tech conducted similar approach. A fully adaptive aircraft configuration as shown in fig. 2.5 was used as an experimental test bed for aerodynamic modeling and flight control. The adaptive model is designed to achieve large-scale shape changes in order to investigate morphing for multi-mission UAVs. There are five independent planform changes along with independent twist control on each wing. Wind tunnel

testing was conducted to analyze the aerodynamic characteristic and evaluate the usefulness of having a UAV with multiple configuration capability. Wind tunnel tests of various planform configurations indicate that different configurations yields minimum drag over a range of flight conditions [7].

However, both pneumatic wings have only been tested in wind tunnels at a range of Reynolds numbers and not yet fully designed for actual flight testing due to the complexity and bulkiness of the telescoping mechanism.

2.1.2 Rigid Folding Wing

A. FLYRT

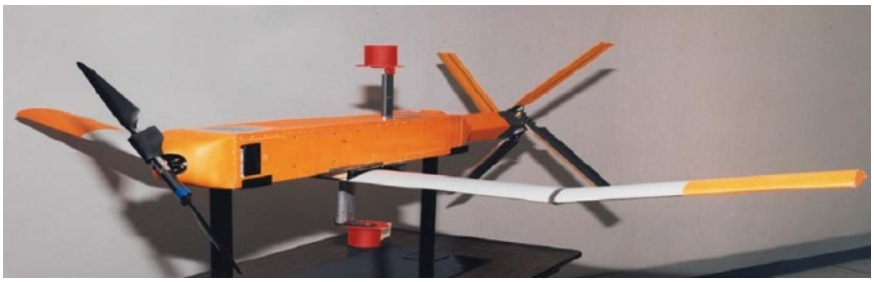

Figure 2.6: Flying radar target UAV.

In 1990, the Naval Research Laboratory (NRL) built and tested an experimental non-recoverable ship-launched expendable radar decoy, FLYRT (Flying Radar Target) as shown in Fig. 2.6. The first test flight occurred in September 1993. FLYRT was launched with rigid folded wings and tail surfaces from a MK 36 launcher by using a solid-propellant rocket motor, which burned for about 1.6 seconds. The fully expanded rigid wing has a span of 2.4 meters and weight of 60kg. Immediately after launch, the tail fins were unfolded mechanically to control the vehicle during ascent. After the booster had been jettisoned, the UAV coasted to the apogee of the launch trajectory, where the rigid wings were unfolded and the electric motor started. A total of 13 drones were built before the program ended, and the decoy successfully

demonstrated the defense of a variety of ships against simulated radar threats.

B. Bat Wing and Z-wing

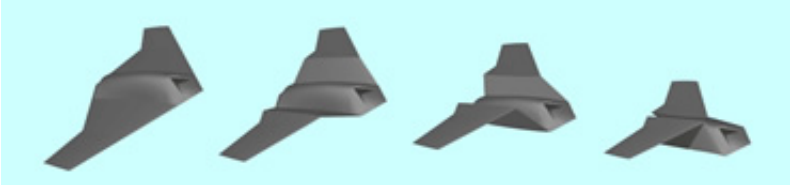

Figure 2.7: AFRL Z-wing concept.

Lockheed-Martin Skunk Works and AFRL are developing an aircraft that has the ability to significantly alter its rigid wing shape to modify the flight performance characteristics to accommodate a variety of missions including combat and reconnaissance. Two very different morphing wing concepts are currently under development that could perform a 150% change in surface area through the morphing process the bat wing and the Z-wing. The bat wing will extend and retract in a planar motion and the Z-wing will transition from full extension to a position resembling that of a bird's folded wing. Fig. 2.7 is showing the z-wing concept aircraft [15, 19]

C. MPUAV Concept

Figure 2.8: The Cormorant.

A Multi-Purpose Unmanned Aerial Vehicle (MPUAV) briefly considered by Lockheed Martin called the Cormorant, is shown in fig. 2.8. The idea is that the drone could handle all-weather reconnaissance, battle damage assessment, or specialized mission support for the submarine. This UAV could be launched from a submarine, then perform wing shaping for a different mission and return to the ship [15].

C. ALICE

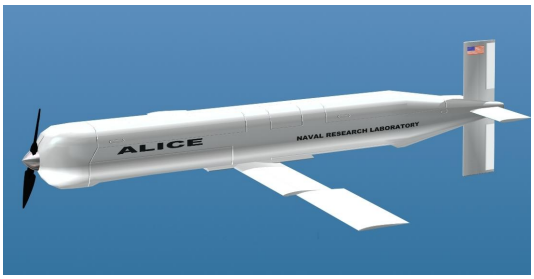

Figure 2.9: ALICE.

ALICE is an unmanned platform that can be air launched from a tactical aircraft at speeds of up to 0.8 Mach and altitudes of up to 45,000 ft. The design is shown in fig. 2.9. After launched from the tactical aircraft, ALICE glides using tail control surfaces until it reaches a speed of approximately 250 knots. The rigid wing and propeller then deploy and the fuel engine starts. ALICE will cruise to approximately 200 nautical miles per one hour before the outer rigid wing panels deploy for loiter. In the loiter mode, it will operate at 65 knots with a two hour endurance and carry a 25 lb payload. Research efforts included development of the polymorphic wing, a JP-8 fueled rotary engine, a high efficiency starter/generator, a folding variable pitch propeller, and an advanced EW payload [20].

Figure 2.10: ARES [5].

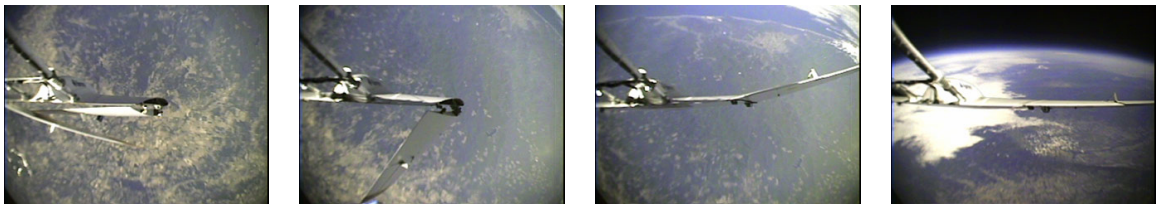

(a) Stowed (b) Unfolding (c) Fully Deployed (d) Gliding

Figure 2.11: Deployment test [5].

D. Mars Prototype - ARES

Aerial Regional-scale Environmental Survey of Mars (ARES) is shown in fig. 2.10 (a), was proposed by Langley Research Center and was selected as the NASAs next Mars Scout Mission. ARES is an autonomous powered aircraft with a folding wing blended body design. It has a 6.1 m (22ft) span wing with 4.9 m (16ft) long body, which is similar in size as the Cessna. In order to pack this high aspect ratio wing spacecraft into the volume limited space capsule, the tail is folded above the body and the wings are folded beneath the body. A successful flight test was conducted on September 19, 2002 using a half scale model as shown in fig. 2.11 [5].

2.1.3 Inflatable Wing

Inflatable wing was developed and integrated in aircraft design decades ago, including the development of lighter-than-air (LTA) vehicles, manned inflatable heavier-than-

air vehicles and UAVs. While LTA vehicles also include inflatable structures, our main focus herein is on the inflatable wing used solely for lift generation. Inflatable wings are a promising method for aircraft design that required the wing to be stowed when not in use. Inflatable wings are conceptually possible for any wing span and have been developed with a wing span as small as 15 cm (6in) for missile fins and as large as 9.14m (30ft) or more for LTA vehicles. The ability of the inflatable wing to be stowed has many incentives. Inflatable wing structures have the benefit of an extremely low packing volume without affecting it structural integrity. The packing volume can be more than ten times smaller than their deployed volume. Inflatable wing can be folded and stowed inside the fuselage and inflated to its designated pressure when needed. Conversely, one major concern to the inflatable wing design is the lack of roll control actuator compared with conventional rigid wing design that has flap and ailerons. This problem can be tackled in several ways. One option is a servo actuation technique used to deform the wing shape to provide roll control, since inflatable wings are deformable by nature. This method is discussed in a later section.

A. Goodyear Inflatoplane

The Inflatoplane was an experimental aircraft made by the Goodyear Aircraft Company as shown in fig. 2.12. The Inflatoplane was successfully developed and demonstrated as an inflatable manned aircraft in February 1956. The Inflatoplane had a wing span of 8.53 m (28ft) and was designed as a military rescue aircraft. The Inflatoplane was a single-seated aircraft and a two seated version was introduce later. This concept was developed as a rescue tool to be packed inside a small lightweight package and parachuted to a downed airman behind enemy lines for self-rescue. Only 12 Goodyear Inflatoplanes were constructed, but development was continued until the project was cancelled in 1973 when it could not find a valid military use for an

aircraft that could be brought down by a well-aimed bow and arrow. Based on the wind tunnel test conducted on Inflatoplane at NASA Langley, this airplane was longitudinally stable, and had adequate roll and pitch control. However, aeroelasticity effects were a concern. The aircraft performance was acceptable at low speed and with low load factor between 1 and 1.5. However, as the speed increased, wing twisting was observed and an increased in the lift-curve slope that causes a loss of stability. Column-type buckling of the wing was occurred at load factor just over 2 and caused the inboard wing section to fold up and invariably contact the engine above the wing. The wing structure buckled at a speed of 71 mph and at an angle of attack 5 degrees, and at a load factor of slightly in excess of 2. The buckling occurred suddenly after about 30 seconds at this loading condition [8, 21].

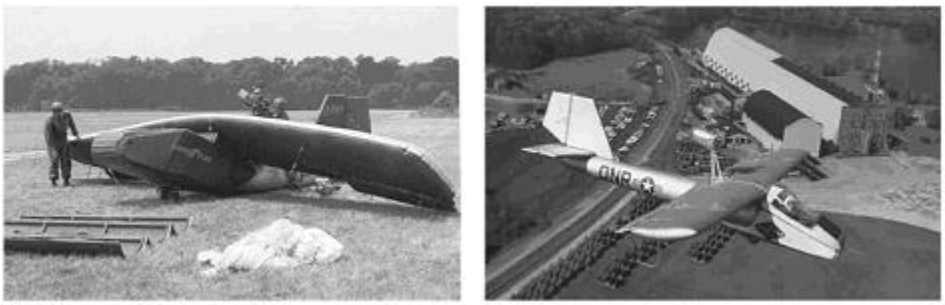

Figure 2.12: Goodyear's Inflatoplane.

B. ILC Dovers Apteron

ILC Dover was one of the earliest aerospace companies in the 1970s to develop inflatable winged UAVs [8, 12]. The Apteron UAV as shown in fig 2.13 had 1.55m (5.1ft) wing span. It had a tractor configuration using a 373W (0.5 hp) engine, with a gross weight of 3.18 kg (7lb) and was remotely-controlled via elevons mounted on the trailing edge. The Apteron was proven in flight but was never put into production by ILC Dover. Since then, three types of inflatable wings have been designed and manufactured by ILC Dover: the Inflatable-rigidizable wing, Vectran wing and

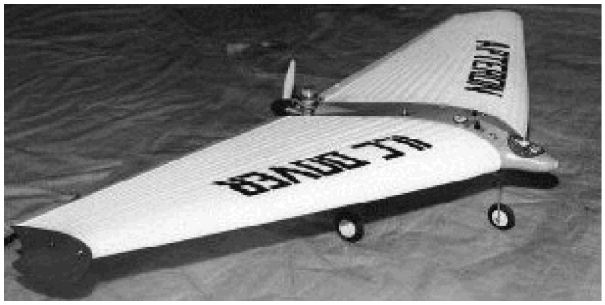

Figure 2.13: Apteron.

polyurethane coated nylon wing. These designs are discussed in later sections.

C. NASA Dryden I2000

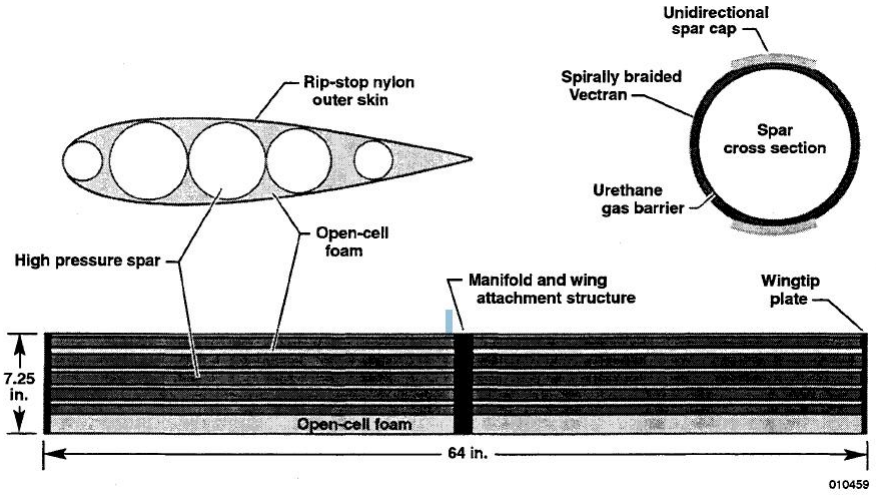

Figure 2.14: Vertigo wing layout [6].

In 2002, a small-scale unpowered inflatable wing aircraft was tested and evaluated at the NASA Dryden Flight Research Center. The inflatable wing used in this program was designed and fabricated by Vertigo, Inc (Lake Elsinore, California) for the U.S. Navy Gun Launched Missile program. It was a design integrated into missile systems for in-flight high speed deployment. This 6.4 m (64 in) span inflatable wing contains five high pressure inflatable cylindrical spars than run span-wise from tip to tip with a chord is 0.18m (7.25 in). Between the spars and the trailing edge of the

Figure 2.15: NASA Dryden I2000 in-flight deployment sequence [6].

wing was open-cell foam bonded to the spars and to a rip-stop nylon outer skin. Additionally, a rib at each tip rigidly connected all the spars to establish wing torsional stiffness. Thermally activated adhesives are used to bond the spars, foam, and the nylon skin into a contiguous wing structure. The airfoil profile is a NACA0021 and does not contain any control surfaces; therefore, full three axis control was affected only by the tail control surface. This inflatable wing consisted of a manifold at the center of the wing to hold the wing spars in position. Fig. 2.14 shows the wing layout of the I2000 inflatable wing. A small COTS with a volume of approximately 35 cubic inches was selected for the high pressure tank. Nitrogen gas was selected as the pressurizing gas. At 1800 psig was reduced to a wing pressure between 150 psig to 300 psig using an adjustable pressure regulator. By using this high pressure inflation system, the inflatable wing could be rapidly inflated during flight within one-third of a second. Fig. 2.15 shows the partially deployed inflatable wing after launched from an aircraft carrier. The wing immediately deployed upon released from the aircraft carrier. No indications of instability or divergence was evident as it transitioned from wingless to winged flight. The unpowered I2000 glided down to a smooth landing under complete control [6].

D. Pneuwing

Pneuwing is a foldaway wing designed by Prospective Concepts, a Swiss company. The inflatable wing is filled to 9.7 bar, about one third of the typical tire pressure. Pneuwing is a two-seater airplane and powered by a Rotary Wankel 814 engine. It has a wingspan of 8.2 meter and wing area of 16.5 m^2. The maximum allowable g-load was recorded at 6 g with speed range from min 50 km/h to max 150 km/h. While the ailerons are operated in the conventional way by means of wires, the landing flaps change their curvature by varying the internal air pressure, which is a plus for the aerodynamics. The first flight test was conducted in 1998 in St. Stephen and over 150 additional flights followed. However, mass production was not possible due to lack of interest from prospective investors [9, 22].

(a) Deflated planform (b) Pneuwing during approach landing

Figure 2.16: Pneuwing.

E. AIRCAT

The University of Kentucky (UK) has been working with ILC Dover, manufacturers of space suits and inflatable space structures to develop Epplerinflatable wings that can be used on future space exploration aircraft [23]. Extensive experimentation has been done at UK regarding the aerodynamic performance of the inflatable wings made by ILC Dover. ILC Dover has provided NACA 4318 based tapered wings that include a two piece construction. The interior is a polyurethane bladder while the exterior is composed of excess Vectran from the construction of the crash bags used on the Mars Rover. The polyurethane/Vectran composition of the wings make them relatively heavy for their size and also requires an operating inflation pressure of 15 - 18 psi. High pressure inflation makes these wings extremely rigid but also making deformation and warping difficult. Each pair of the Vectran wings, also known as FASM wings, are handmade making mass production difficult. Each pair of the FASM wings also has a unique bolt pattern at the root chord requiring experimentalists to fabricate unique test fixtures for each set of wings. The FASM wings were used in BIG BLUE IV where they flew a lifting body test bed at 39 lbs with a 4.5hp 50cc engine. A picture of the AIRCAT testbed flying with the inflatable wings is seen in fig. 2.18

The most recent wings that ILC Dover have provided to the UK for analysis are made of rip-stop nylon and possess the capability of being mass produced. These wings also use the NACA 4318 profile. The UK has also created a unique inflatable wing design that possesses the ability to become rigid when exposed to UV rays. These wings are packaged with a light-curing resin that hardens upon exposure to UV rays in the upper atmosphere. The success of the BIG BLUE (Baseline Inflatablewing Glider, Balloon-Launched Unmanned Experiment) Project in May of 2004 demonstrated these capabilities.

F. BIG BLUE V

(a) Low altitude test

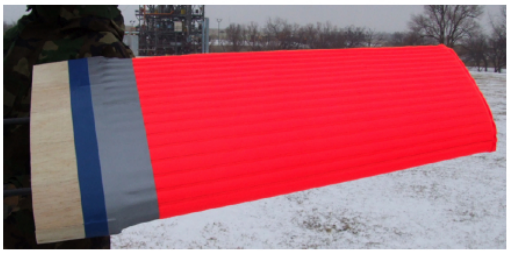

(b) Inflatable taper wing

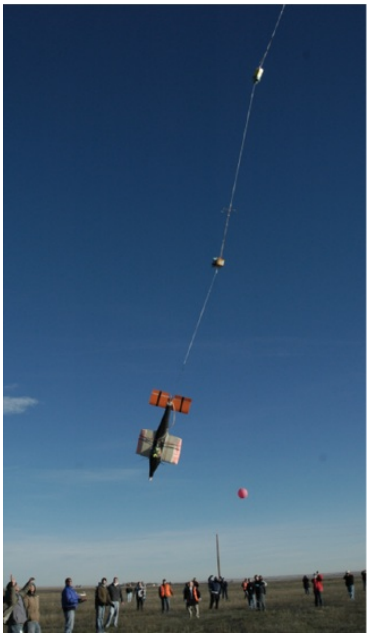

(c) High altitude launch at Colorado

Figure 2.17: BIG BLUE V.

MARS, the Mars Aircraft Realization System, is the part of the program at Oklahoma State University (OSU) to develop, construct and test airplane designs for flight on Mars [11]. It is a component of BIG BLUE V. BIG BLUE is a high-altitude experiment developed, designed, built, conducted and evaluated primarily by undergraduate students in the College of Engineering at the University of Kentucky. The

goal of BIG BLUE is to demonstrate the feasibility of inflatable wings for flight in the low-density atmosphere of planet Mars. While most designs use folding wings like the ARES [5], MARS uses inflatable wings to overcome the packing problem in the spacecraft carrier. In the high altitude flight test discussed herein, the completed and semi-autonomous aircraft ascends via weather balloon to a targeted altitude of 100,000 feet in order to simulate the density present in the Martian atmosphere. The inflatable wings are inflated to a 5 - 8 psi and a release mechanism is triggered that allows the aircraft to parachute to an altitude of 5,000 feet above ground level, where it is flown under autonomous guidance, and then lands under human control. The inflatable wings were manufactured by ILC Dover, Inc. out of polyurethane coated rip-stop nylon. The airfoil profile is NACA 4318. Each wing semi-span has a root chord of 19.5 inches and a tip chord of 13.5 inches with a semi-span of 36 inches. The wings were constructed in two semi-spans such that they could be mounted externally to a fuselage, but they did not include mounting attachments. The wings were attached to a balsa sandwich wing mount using a light weight low temperature fiberglass tape with a silicon based adhesive. The wing mounts were in turn connected to one another using two carbon fiber rods. Full three axis control was affected only by the tail control surface. A small scuba air tank was selected as the pressure tank source. The fuselage was initially constructed out of a composite using a balsa sandwich as shown in Fig. 2.17 (a). While this design was used for low altitude flight testing, later designs used a composite with a card stock sandwich to reduce weight. This design was used for the high altitude mission as shown in Fig. 2.17 (c).

2.2 Wing Planform Effects

Since our proposed research aircraft wing will expand in the span-wise direction, the wing morphing will affect the drag and lift characteristic. This section here will briefly discuss about the effect of variable planform on drag at low speed flight. The

Figure 2.18: UK's Aircat.

analysis presented here will follow Inman *el.at*'s [7] discussion of variable span effects for low speed flight. Consider the un-swept planform geometry shown in fig. 2.19. The planform area can be written as

$$S = S_1 + 2\Delta bc \tag{2.1}$$

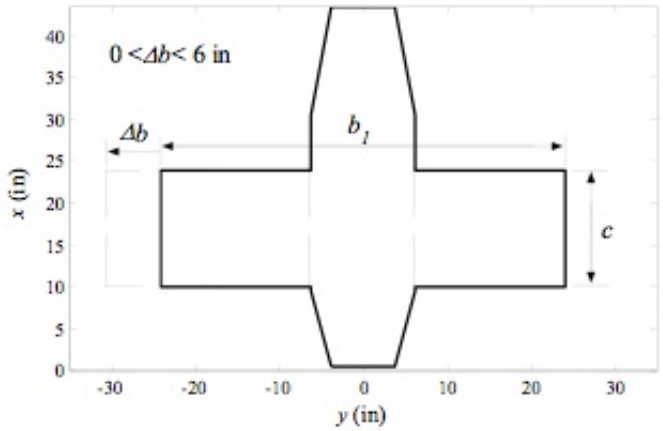

Figure 2.19: Illustrated planform parameter for an unswept configuration [7].

The wing planform is a low aspect ratio when the inflatable is stowed, thus as-

suming the rigid wing planform only. This simplification makes $\Delta b = 0$ and c is the chord length of the outer wing section. The reference area S_{ref} will be defined as S_1. For the rigid wing planform shown in fig. 2.19, the profile drag can be written as

$$D_p = qS_{ref}C_{dp} + 2\Delta bc(1 + \frac{2\Delta bc}{S_{ref}}) \tag{2.2}$$

where q is the dynamic pressure and C_{dp} may be considered a 2D profile drag coefficient (which is a function of the Reynold number).The induced drag for an elliptic load distribution can be written as

$$D_i = \frac{L^2}{\pi q b^2} \tag{2.3}$$

where L is the lift force and b is the total wing span. A span efficiency factor as a function of Δb could be added to Eq. 2.3 to account for the effect of non-elliptic load distribution. This is not included here because the dominant effect of span is captured in the b^2 term in the dominator of Eq. 2.3.The total wing span for the unswept configuration can be written as

$$b = b_1 + 2\Delta b \tag{2.4}$$

where b_1 is the total span of the unextended-span, un-swept configuration. The total drag can be written by combining Eq. A.1 to Eq. 2.4 as

$$D = qS_{ref}C_{dp} + 2\Delta bc(1 + \frac{2\Delta bc}{S_{ref}}) + \frac{L^2}{\pi q b^2} \tag{2.5}$$

This equation may be used to determine the Δb that achieves a given L with minimum D. This is done by taking the derivative of Eq. 2.5 with respect to Δb and setting it equal to zero. the resulting equation for Δb is as follows

$$\Delta b = \frac{1}{2}\left[(\frac{2L^2}{\pi q^2 C_{dp} c})^{\frac{1}{3}} - b_1\right] \tag{2.6}$$

This equation shows that for minimum drag, Δb varies as $L^{\frac{2}{3}}$. Note that C_{dp} is in the denominator of Eq. 2.6. This indicated the expected result that as C_{dp} decreases, meaning the penalty for wetted area decreases, the Δb for minimum drag increases.

CHAPTER 3

Facilities and Diagnostics

Chapter 3 introduces the research equipment, experimental arrangements, and techniques used in this thesis. Primarily, most research was conducted in the wind tunnel at Oklahoma State University, Mechanical and Aerospace Engineering Department. Flight tests were performed by an expert-class ground based pilot using line of sight visual cues only at an RC field located in Guthrie, Oklahoma.

3.1 Wind Tunnel

3.1.1 Overview

The Oklahoma State University wind tunnel is an Eiffel type tunnel with a 1:16 contraction ratio. This open circuit wind tunnel is driven by a centrifugal motor with 125 hp located at the tunnel exit. The upstream of the wind tunnel has an inlet with a plastic honeycomb and high porosity screens to reduce the free stream turbulence. The wind tunnel has a 12′x 12′ inlet as shown in fig. 3.1. The test section consists of a 3′ x 3′ square transparent test section with a length of 6 ft ; with a pitot tube that could shift mechanically along the test section perpendicular to the air flow and connected to a manometer. Analog control was used to adjust the wind speed of the tunnel.

3.1.2 Imaging

Two Motion ProX3 as shown in fig. 3.2 (a) were used in the wind tunnel deployment tests. Each camera was set at pre-trigger mode to obtain pictures after the deployment

(a) 125Hp Wind Tunnel (b) 3' x 3' Transparent Test Section (c) 12' x12' Inlet

Figure 3.1: OSU Wind Tunnel.

began. Each Motion ProX3 was set to capture 30 frames per seconds to record the deployment sequence for Wing Alone (WA) deployment detailed in chapter 5. This model only capture images in black and white. The camera has 4GB internal memory image storage. All pictures can be transferred to the laptop by using a USB cable prior to the next experiment. As the research progress, Casio's Exilim camera as shown in fig. 3.2(b) was being used to replace the ProX3 due to it simplicity and faster processing time. The camera has 8GB memory card. This model provides 3 different video modes: high definition (HD), high speed (HS) and standard mode (STD). Only STD mode was being used and is sufficient for our research herein.

(a) Motion ProX3 (b) Casio's Exilim

Figure 3.2: Imaging equipments.

3.1.3 Aerodynamic Load Measurements

Aerodynamic loads were measured by using load cells connected to a strain gage conditioning amplifier. The amplifier has an adjustable gain ranging from 2 to 200 times. Maximum gain at 200 was used for our wind tunnel test to magnify the voltage signal obtained from the single point load cell. The load cell has a loading capacity of 1Kg (2.2 lb) and with a safe overload factor of 150%. The model is 2120B Strain Gage Conditioner and manufactured by Vishay Measurements Group. Each load cell was calibrated separately using lab-view prior to the wind tunnel test to find the relation of voltage in respect of load in pounds.

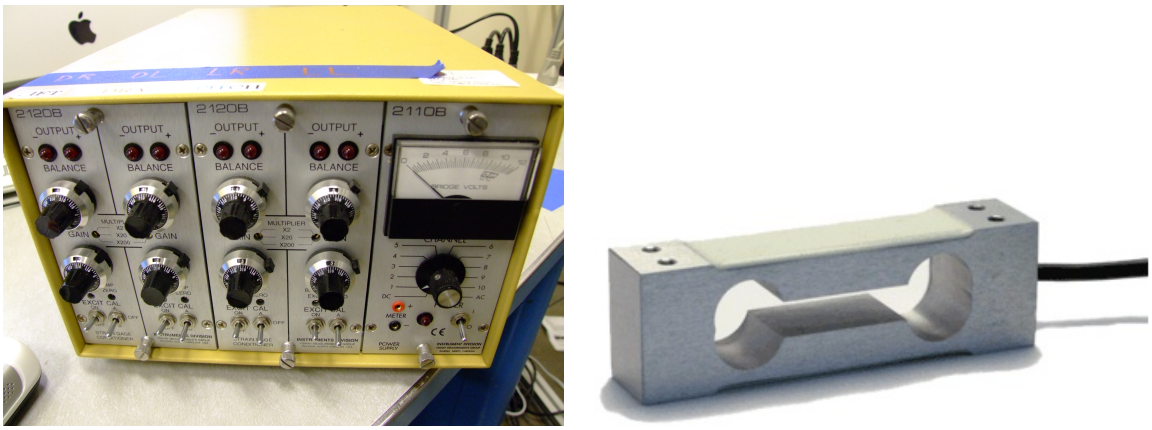

(a) Conditioning amplifier (b) Load cell

Figure 3.3: Load measurement system.

Labview was utilized as the data acquisition tool that interfaces with the conditioning amplifier and the low capacity single point load cell. Fig. 3.4 show the labview program used to measure the aerodynamic load for WSE and DCE deployment test. Pressure transducer as shown in fig. 3.9 (b) was later integrated into the lab-view to obtain pressure reading from DCE deployment test. The labview recorded the lift, drag, and pressure and stored as .lvm format. All data was later converted to Microsoft excel format for analysis.

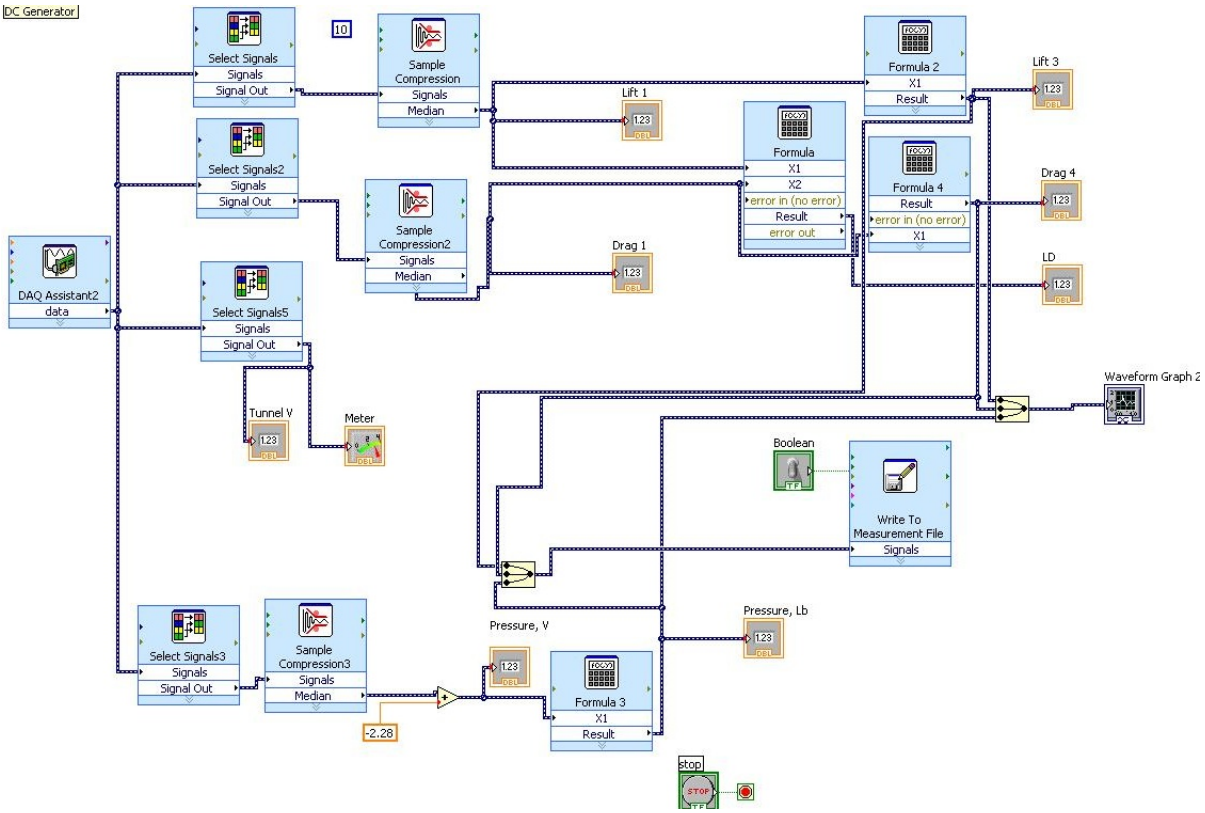

Figure 3.4: Labview schematic overview.

3.1.4 Test Section Arrangement

Wind tunnel deployment test was possible using a 17 inch span wing that has a 13.75 inch chord as shown in fig. 3.8 (a). This wing was constructed by ILC Dover in 2004 using the same material as the full scale wing. Different deployment tests were conducted throughout the research period. The wind tunnel set up schematic for each test are shown in fig. 3.5. Each wind tunnel set up was different based on three separate wing designs: Wing Alone (WA), Wing with Stiffener element (WSE) and wing with Deployment Control Element (DCE). Test results are shown in Chapter 5. A pitot tube attached to the top of the test section was connected to a manometer to measure the wind speed. The inflation system was directly connected to an adjustable pressure regulator (about 6 psi) to regulate down the compressed air hose available in the wind tunnel lab. For WA and WSE deployment test, a

cat-collar release mechanism was used to restrain the folded wing in the wind tunnel to simulate the stowed configuration. The collar will automatically release after the wing deployment begins. This restraint mechanism was used in BIG BLUE Project [11]. For DSE deployment test, Velcro was used as the wing constraint. For WA deployment test, a digital pressure transducer as shown in fig. 3.9 (b) was placed in the high speed camera's side of view to obtain the pressure reading. Later tests for WSE and DCE were interfaced with pressure transducer with max 5 psi input as shown in fig. 3.9 (a). The transducer was connected to Labview to obtain accurate change of pressure. Therefore, the inflation pressure for both tests was reducing to 5 psi. Single point load cell was available in this test to measure the lift and drag during the deployment.

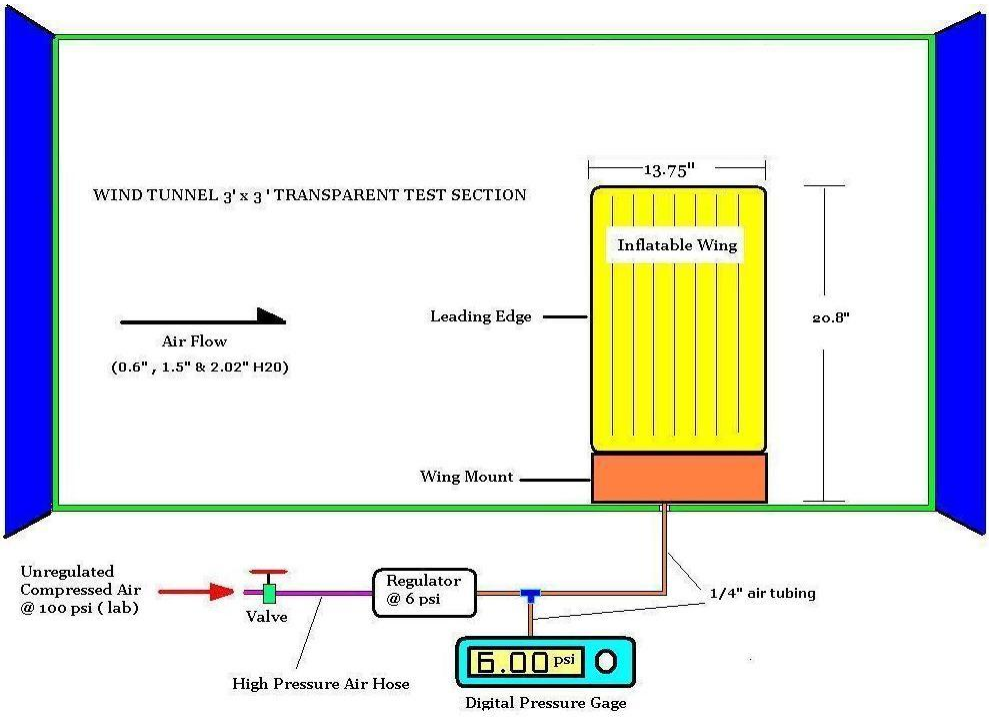

Figure 3.5: Wind tunnel set up schematic for Wing Alone (WA) deployment (not to scale).

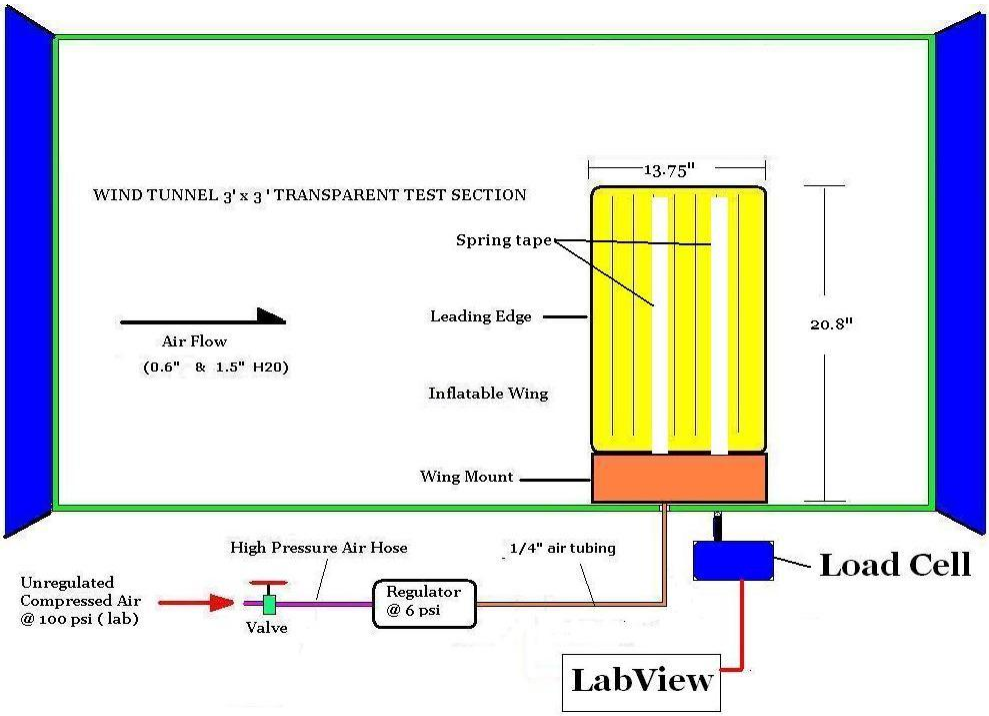

Figure 3.6: Wind tunnel set up schematic for Wing with Stiffener Element (WSE) deployment (not to scale).

3.2 Ground Tests

A wooden gimbal was constructed to mount the morphing wings on to determine the inertia effects during deployment. This was used in both static laboratory tests and dynamic ground tests. Dynamic tests were conducted by using a road vehicle to generate the in-flight aerodynamic loads.

3.2.1 Static Tests

Static laboratory tests was conducted using the gimbal as shown in fig. 3.10. The gimbal is designed to provide only roll and pitch motion with yaw motion restricted. The purpose of using this customized tool is to measure the dynamic motion of the deployment of the inflatable wings as it rotates freely on the dual axis. An adjustable 12 pound ballast was attached at the bottom of the frame for balance. The rigid wing

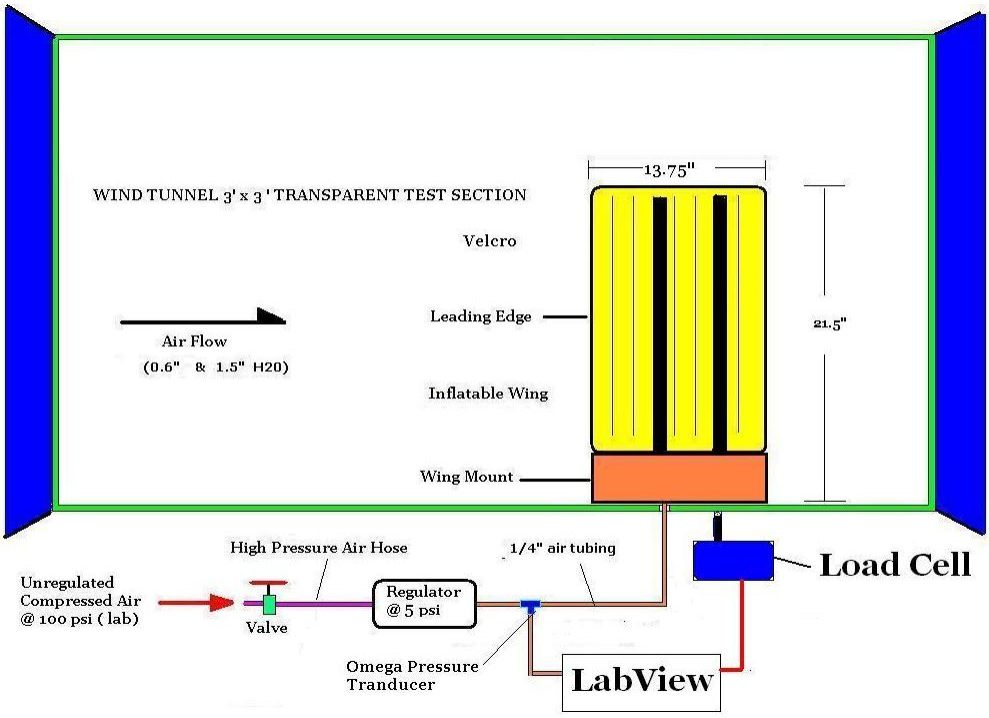

Figure 3.7: Wind tunnel set up schematic for Deployment Control Element (DCE) deployment (not to scale).

(a) Small scale inflatable wing

(b) Restraint mechanism

Figure 3.8: Inflatable wing.

section is attached to the gimbal by using stripes of Velcro. Static deployment test was conducted using a 3−axis accelerometer interfaced with Vernier ProLab as show in fig. 3.12 (a) and (b). The static test results are presented in Chapter 5.

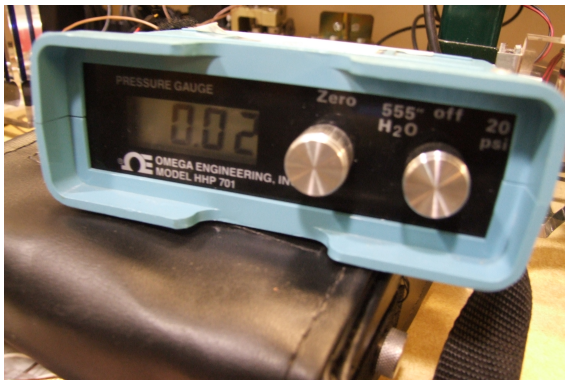

(a) Digital pressure gage

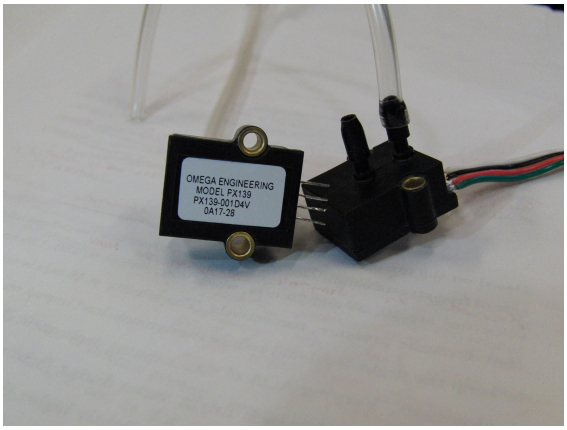

(b) Pressure transducer

Figure 3.9: Pressure measurement.

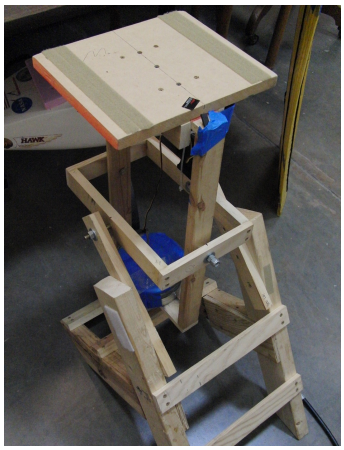

(a) Gimbal

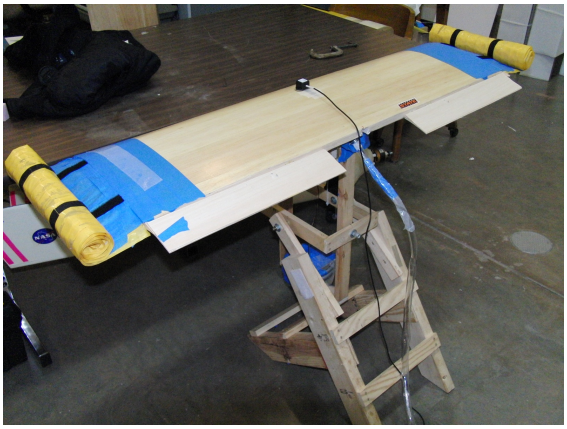

(b) Static deployment set up

Figure 3.10: Gimbal.

3.2.2 Road Vehicle Tests

The purpose of the road vehicle test is to provide a preliminary understanding of DCE method using one full span inflatable wing. The vehicle in motion relative to the wind speed helps simulate in-flight deployment. The rigid wing was mounted on the back of the truck as shown in fig. 3.11 with the inflatable wing section extended far away from the truck. A wind gage was also attached in front of the wing to measure the relative wind velocity. A CO2 canister was connected to a ball valve and manually controlled to inflate the wing as the vehicle is in motion.

Figure 3.11: Wing and a wind gage mounted behind a road vehicle.

3.2.3 Vernier LabPro

Vernier Lab Pro and 3− axis accelerometer were used on static deployment tests in the laboratory as discussed in the earlier section in Static Test. The direction of y-axis is the parallel in the span wise direction with positive direction pointing at the port wing. The x-axis is pointing at the front of the wing with z-axis pointing upward perpendicular to the wing surface. The accelerometer was placed at the quarter chord of the wing as shown in fig. 3.10 (b). The accelerometer will be showing an oscillating motion in respect of time as the gimbal rotates along its axis (pitch and roll).

3.3 X-foil

XFOIL is an interactive program for the design and analysis of subsonic isolated airfoils. Xfoil was used predict the aerodynamic parameters of the inflatable wing bumpy and smooth airfoil profile for calculation as shown in Appendix A. According to the Xfoil's website [24], X-foil consists of a collection of menu-driven routines which

(a) ProLab

(b) 3- axis accelerometer

Figure 3.12: Vernier data acquisition system.

perform various useful functions such as:

1. Viscous (or inviscid) analysis of an existing airfoil, allowing
   - forced or free transition
   - transitional separation bubbles
   - limited trailing edge separation
   - lift and drag predictions just beyond CLmax
   - Karman-Tsien compressibility correction
   - fixed or varying Reynolds and/or Mach numbers
2. Airfoil design and redesign by interactive modification of surface speed distributions, in two methods:
   - Full-Inverse method, based on a complex-mapping formulation
   - Mixed-Inverse method, an extension of XFOIL's basic panel method
3. Airfoil redesign by interactive modification of geometric parameters such as
   - max thickness and camber, highpoint position

- LE radius, TE thickness
- camber line via geometry specification
- camber line via loading change specification
- flap deflection
- explicit contour geometry (via screen cursor)

4. Blending of airfoils

5. Writing and reading of airfoil coordinates and polar save files

6. Plotting of geometry, pressure distributions, and multiple polars

CHAPTER 4

Wing Design

This chapter will discuss the unique characteristics demonstrated by an inflatable wing. Innovative approach and wing construction methods will be introduced and compared with its predecessor designs. Finally, five preliminary morphing wing concepts using inflatable wing will be discussed.

4.1 Inflatable Wing Design

Numerous advanced and commercial off-the-shelf material configurations have been investigated for inflatable wing construction by ILC Dover and University of Kentucky. These materials includes: vinyl, vectran, S/E Glass, 10mm polyurethane, and polyurethane coated nylon fabric. The list of major materials used in inflatable wing research are shown in fig. 4.1 (a) to (f).

According to Cadogan *et. al* [12], material selection for the inflatable wing is typically driven by the following:

1. Flex cracking and modulus at cold temperature
2. Manufacturing process
3. Resistance to gas permeation
4. Resistance to developing pinholes when folded or flexed

Furthermore, the materials used in the construction of the inflatable wings have low dielectric constant and therefore low observable from radar detection according to

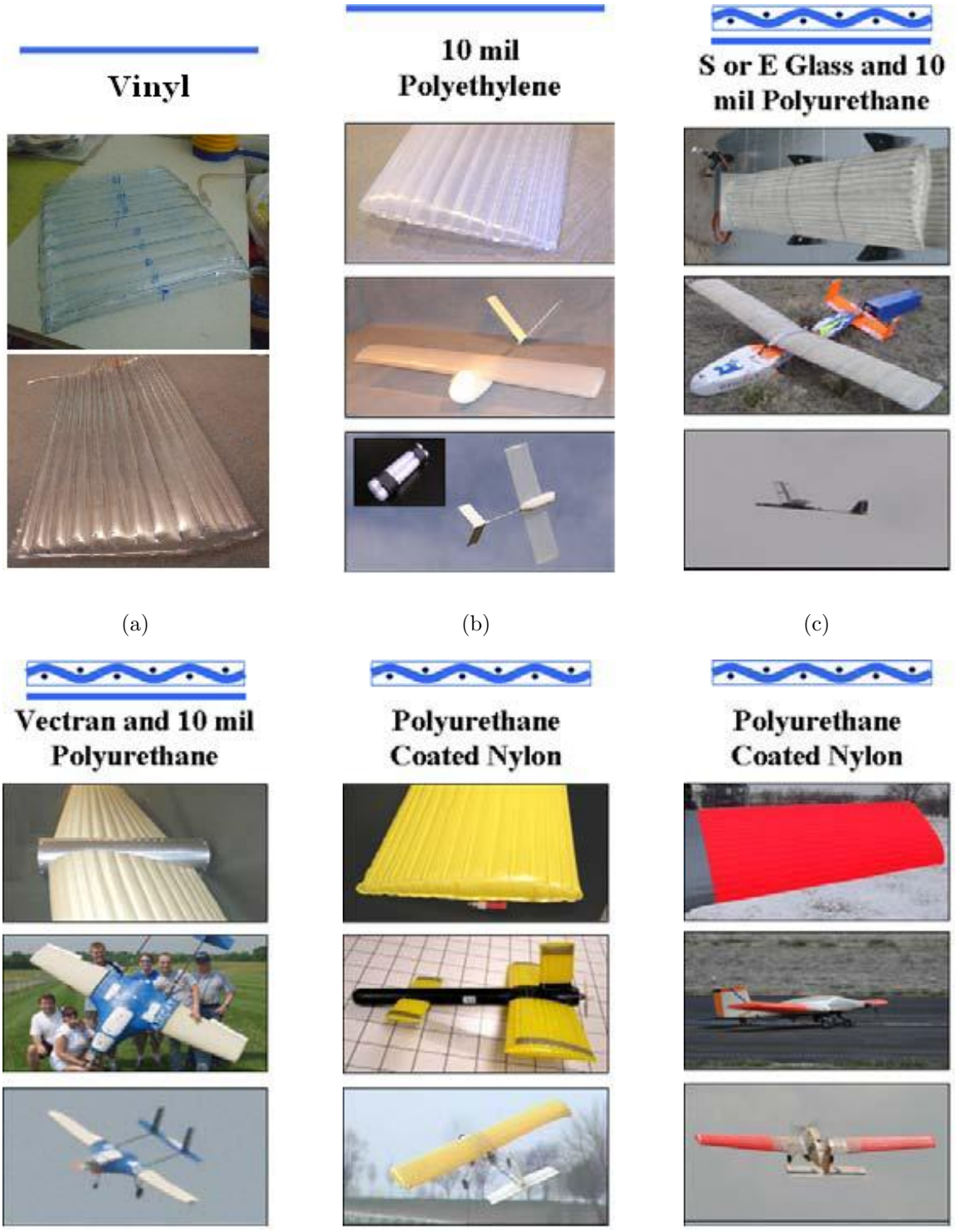

Figure 4.1: Wing material configurations [8].

Jacob [10]. This is a plus for military application. Please note that only vinyl, and polyurethane coated nylon fabricated wings were tested in this research. Cadogan *et. al* and Simpsons's dissertation have detail discussion on the pmoment3.JPGectran wing design.

The inflatable wings use a baffled wall design as proposed by ILC Dover. The distributed baffle wall design from the leading edge to the tip lower the required inflation pressure to the keep the wing rigid. According to Simpson *et. al* [9], baffled wall design helps increase the cross-sectional moment of inertia, hence bending moment. Other method to increase the allowable bending moment is by increasing the material's elastic modulus, thus depending on the material selection. These wings are not only easily produced, but are relatively light and operate at an inflation pressure of 6-8psi. The lower pressure makes these wings more applicable to wing deformation/warping methods for roll control. All the designs listed above has a low inflation pressure ranges from 5 psi to 40 psi compare with FASM wing as described in chapter 2. Simpson *et. al* also describes that the baffle design is constrained by a large airfoil thickness due to the manufacturing process a shown in fig. 4.2. Thinner airfoil profiles are advantageous for good aerodynamics. However, the increasing number of internal spars can cause manufacturing difficulties. Fig. 4.2 shows that thicker airfoil profile could match closer to the ideal airfoil shape. Detailed discussion on how the number of spars affect the wing profile can be found in Simpson's dissertation [9].

4.1.1 Packing

One of the major advantages of using inflatable wing is the compact stowage to help maximize storage capacity. Based on the bar chart in fig. 4.4, three types of wings with similar wing span of 72 inches were compared in span-wise direction. Each wing has a chord length of 19.5, 13.75 and 18 inches, respectively. Fig. 4.3 shows that the stowed wing can be folded up to 10 times smaller than its fully deployed configuration.

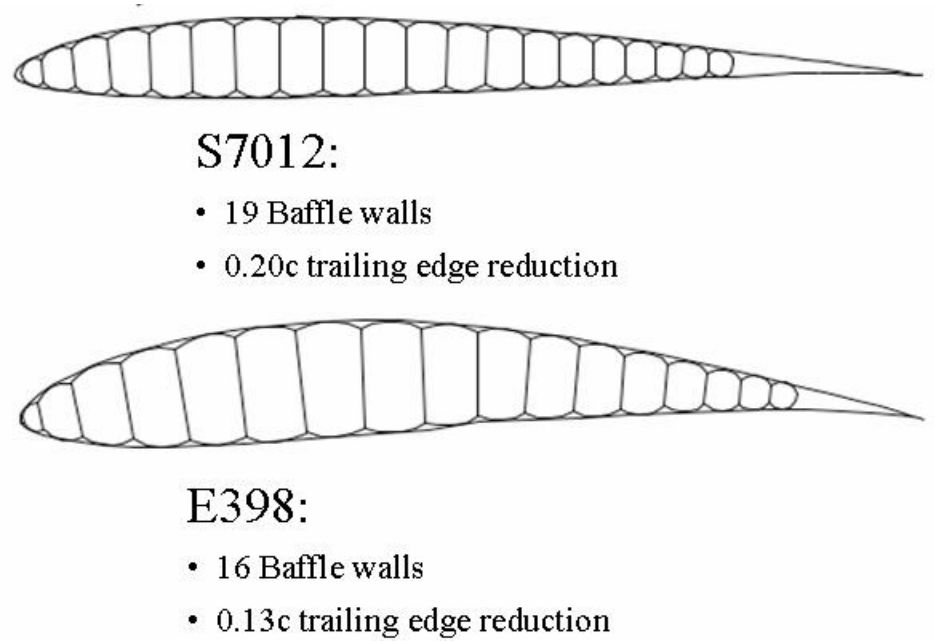

Figure 4.2: Loss in trailing edge due to manufacturing [9].

An obvious trend shows that thicker wing material, longer wing span and larger chord length increase compacted volume. In this case, Vectran has the thicker wing material and followed by orange and yellow ILC Dover wing. However, the storage volume can be 10 times or more by using yellow ILC Dover wing compared with the fully deploy configuration. With these advantages, inflatable winged aircraft can be beneficial for military operation that has limited storage space at combat zone.

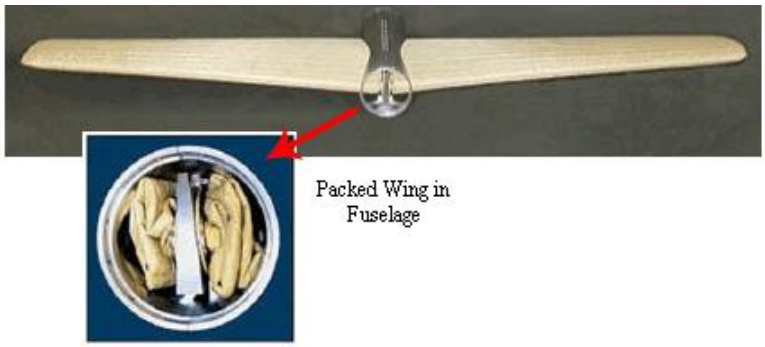

Figure 4.3: Compact storage

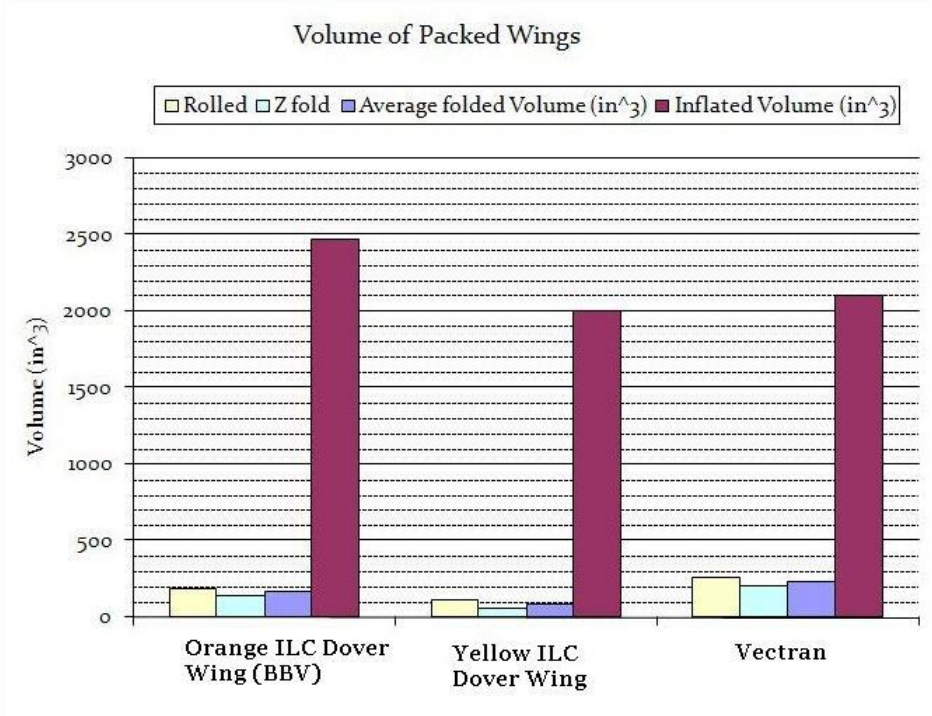

Figure 4.4: Wing volume estimation for stowed and deployed configurations.

4.1.2 Aerodynamic Performance

Due to the peculiar wing airfoil, Simpson *et. al* [9] has investigated the aerodynamic performance of an inflatable design for MARS aircraft. Wind tunnel tests combined with smoke visualization methods were conducted on rigid model of the "bumpy" profile of the inflatable-rigidizable design with that of the ideal "smooth" profile. The initial consideration was to improve the aerodynamic performance by placing a skin over the wing to reduce the perturbation of the baffles and to provide a sharper trailing edge. The test results are reviewed in fig. 4.5. At low Re case, the surface perturbation improved the flow over the wing surface. The ideal E398 airfoil performed poorly compared with inflatable profile. At AOA of 0 and Re = 25 x 10^3, flow separation occurs very close to the leading edge for the ideal wing and there is no reattachment. For the same conditions, the bumpy profile shows attached flow and the streamlines adjacent to the surface are not distinctly clear. This is due to the bumps tripping the

flow to promote transition to turbulence earlier. It can be observed that the position of the separation region is shifted further downstream of the laminar separation point, due to the additional bumps.

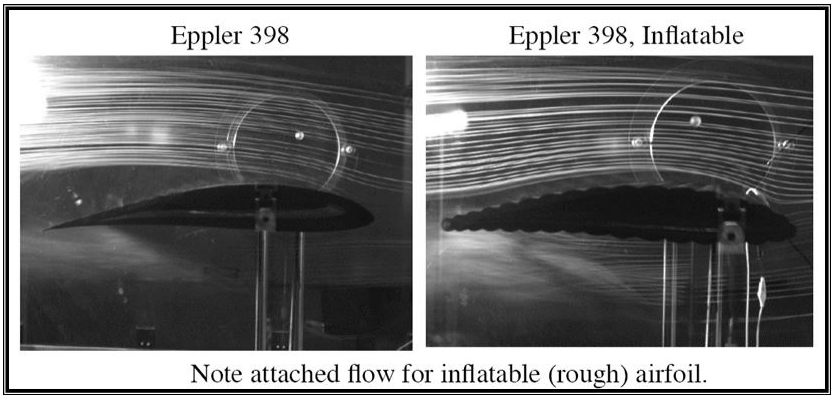

Figure 4.5: Flow separation was delayed on bumpy airfoil at low reynold number [9].

4.1.3 Reliability, Survivability and Durability

When an airplane is flown at an angle that exceeds the critical angle of attack, the airplane will stall. Excessive load factors caused by sudden maneuvers, steep banks, and wind gusts can also cause the aircraft to exceed the critical angle of attack and thus stall at any airspeed and any attitude. Just like conventional rigid wing, an inflatable wing can experience stall at critical angle of attack even pressurized to its designated pressure. For a typical conventional wing, excessive load factors could cause substantial damage to the wing integrity and even failure during flight. Fig. 4.6 is showing an in-flight buckling as a combination of pilot error at high flight speeds and wing warping. The inflatable wings survived from this serious crash have resulted in the near total destruction of the vehicle.

Impact test was conducted on a inflated wing by University of Kentucky to test its durability. 4 lb of sandbag was used and dropped on center of the inflatable wing as shown in fig. 4.7. Due to its flexibility, the wing could recover and return to its

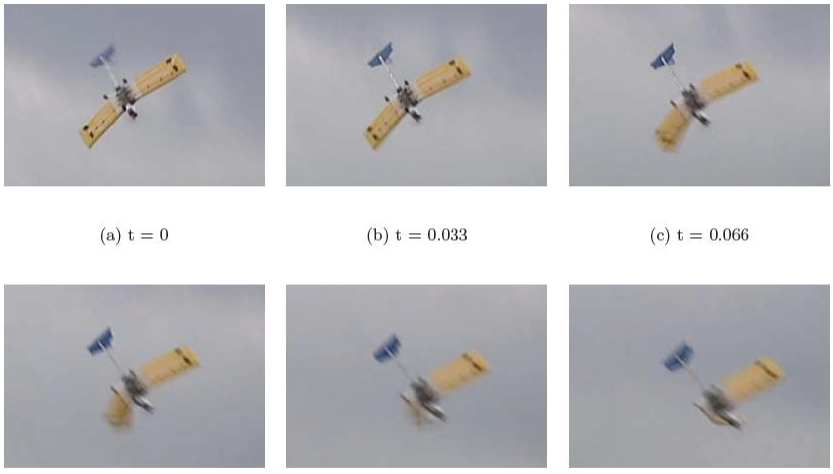

(a) t = 0 (b) t = 0.033 (c) t = 0.066

(d) t = 0.1 (e) t = 0.133. (f) t = 0.166.

Figure 4.6: In-flght wing buckling due to structural overloading [9].

original shape after a sudden deformation. This result shows that inflatable wings were extremely damage resistant. This would be a catastrophic structural failure or substantial damage to a rigid wing if a similar test was conducted. Thus, vehicles requiring high damage tolerance may benefit from such wings.

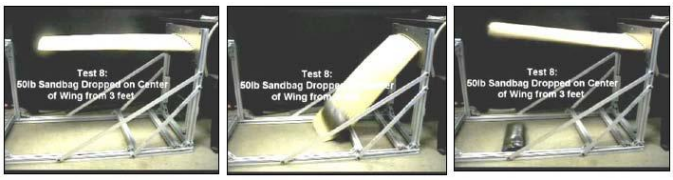

(a) Vectran wing.

(b) Nylon wing.

Figure 4.7: Dynamic impact tests [9].

One of the unforeseen benefits of the inflatable wing have been unrivaled performance in crash survivability. Fig. 4.8 shows the BBV aircraft was accidentally crashed

onto a tree after takeoff during flight test. Note that the airplane bounced back upon impact and survived. No repair was done on the wing except a replacement for the nose section and electric motor.

Figure 4.8: An inflatable winged aircraft survived a direct impact [9].

In terms of repairability, a punctured wing surface can be patched as easily as repairing a bicycle tire. This could eliminate the need of major repair on the wing. In the military operation perspective, this could be beneficial in reducing maintenance cost and could recover quickly for time sensitive mission. Fig. 4.9 shows pin-hole damage was temporarily sealed using electric tape and operates well even after the wing was fully pressurized.

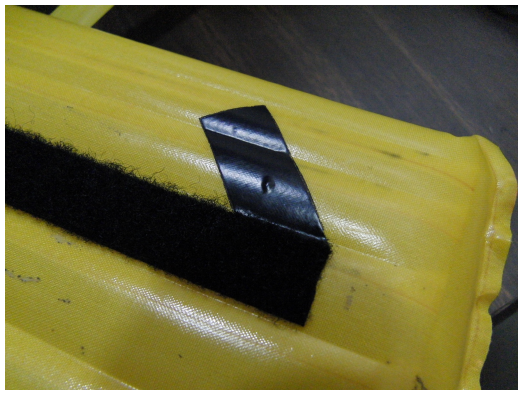

Figure 4.9: Pin-hole damage.

4.2 ILC Dover Polyurethane Coated Nylon Wing

The polyurethane coated nylon wing was manufactured by ILC Dover, Inc as shown in fig. 4.10. This is a straight rectangular wing that has a root chord of 13.75 inches

Figure 4.10: Inflatable wing in deployed and stowed configurations.

with a semi-span of 36 inches. The airfoil has an NACA 4318 profile with a one-way-flow inflation host bonded on one side of the wing; located at the quarter chord location. The inflatable wing does not have any control surfaces and is designed to support the internal pressure of 8 psi, which is sufficient for structural stiffness during flight test. The burst pressure was found to be 15 psi, which is about 53% higher than the required flight pressure. The distributed internal spars from the leading edge to the trailing edge create bumpy appearance on the wing after pressurized, as shown in fig. 4.11.

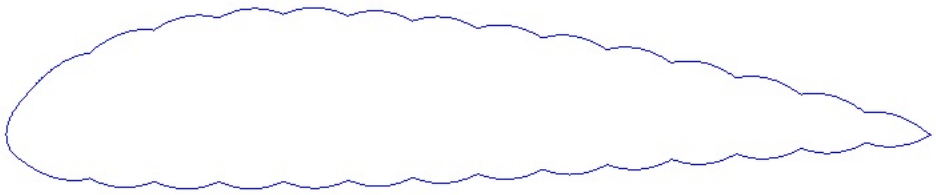

Figure 4.11: Inflatable wing airfoil profile.

4.3 Vinyl Wing

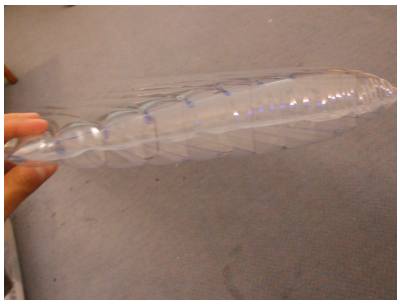

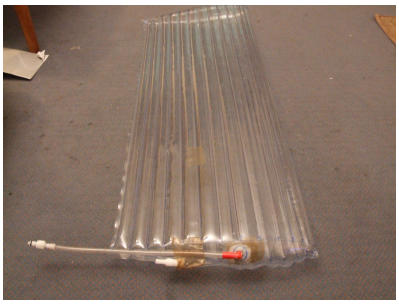

Figure 4.12: Vinyl inflatable wing.

Vinyl inflatable wings were constructed in lab based on the ILC Dover design as shown in fig. 4.12. This wing was heat sealed using a portable impulse heat sealer compared with ILC Dover that uses high-tech RF (Radio Frequency) sealer. Vinyl is a transparent, unsupported film, and can be purchased cheaply at local store. The purpose of using this material is to prove that COTS materials can be utilized and could be constructed in laboratory. If this material is chosen as inflatable wing material, the transparent characteristic allows the vinyl wing to become nearly invisible in the sky and provides low observability at low altitude flight. Therefore, this material is expected to have radar stealth characteristics similar to or better than those using composites if being used in inflatable wing construction [10]. In contrast with the ILC Dover's wing, the vinyl constructed wing has a burst pressure of about 5 psi; about one third of the ILC′s design. The burst test shows that this material is not reliable for flight testing due to the low burst pressure. However, the wing construction process has given us the opportunities to learn the manufacturing skills needed for future fabrication of inflatable wing design in laboratory. Since all inflatable wings were handmade, further developments are required to manufacture process for mass production.

4.3.1 Impulse Heat Sealer

A portable impulse heat sealer was used to manufacture inflatable wings in the laboratory. It has a 36 inch span heating strip. Different temperature settings can be adjusted with a turn of the knob ranging from 1 to 8 with 8 has the highest temperature. With this flexibility, temperatures can be adjusted according to the material heat sensitivity in order to melt and seal without accidentally burning the wing material.

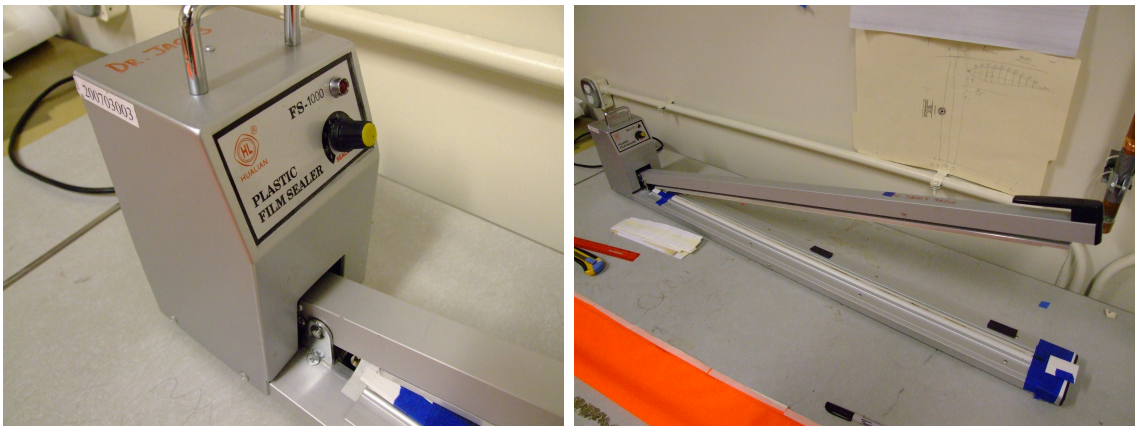

Figure 4.13: Impulse heat sealer.

4.3.2 RTV Silicone Adhesive Sealant

RTV157 as shown in fig. 4.14 is a one-component, ready-to-use, high strength silicone rubber adhesive sealant. It cures to tough, resilient silicone rubber when exposure to standard atmospheric conditions. RTV157 is a paste consistency product which can be applied to horizontal, vertical and overhead surfaces in applications requiring high strength and temperature performance. Below are the characteristics of the RTV adhesive:

- Gray colored
- High strength

Figure 4.14: RTV adhesive.

- High temperature performance
- Low temperature flexibility
- One-component
- Room temperature cure
- General primerless adhesion
- Excellent electrical insulation properties
- Excellent weatherability, ozone, and chemical resistance

In the following section, RTV adhesive paste has been proven as the best bonding solution to test the servo actuation concept. It could provide high bonding strength without damaging the nylon surface of the inflatable wing. Furthermore, no marks or stains will left behind once the dried RTV paste removed from the fabric surface of the wing.

4.4 Aeroelastic Deformation and Control

The ILC Dover's wings will deform from wing root to wing tip depending on the internal pressure, dynamic pressure and span-wise location on the wing. Thus due to

their flexibility the aeroelastic behavior of inflatable wings is of great interest. Numerous researchers have been focusing their research on the aeroelasticity phenomena of inflatable winged aircraft and their finding can be found in previous papers [21] [25]. Inflatable wing deformation measurements were measured by Simpson *et. al* using photogrammetry to find the relation between internal pressure and wing deflection. Please note that this thesis will not cover this issue in-depth. An effective studies of aero-elasticitiy of inflatable wing is presented in Simpson's PhD Dissertation, published in 2008 [9].

Extensive research has been conducted at the University of Kentucky by Jacob *et. al* and Simpson *et. al* on developing UAVs with wing warping control. The studies can be found in Simpson's dissertation [9]. Effort has been focused on actively deforming the nylon inflatable wings to provide roll control through wing warping. As the wings are entirely inflatable, they do not include traditional ailerons. Aircraft using inflatable wing in the past relied exclusively on empennage for control [11, 6]. Due to the nature of nylon inflatable wing flexibility, it was possible to manipulate the wing shape by applying external forces on the wing surface. Fig. 4.16 depicts the deformation from leading edge to trailing edge by using servo actuation. Several wing warping concepts were studied by Graham, *et. al* and Jacob *et. al* with the performance requirements in mind, including roll rate response, frequency response, low mass, low power consumption, ability to be folded and packed, and high cycle life. According to Simpson *et. al*, the approach using smart materials such as nitinol, and piezoelectric actuators as shown in fig. 4.15 have hampered flight testing due to the substantial equipment requirement for in-flight operation. In contrast, mechanical actuators such as servo motors offer reliability and simple operation, but hinder compact stowage. Unlike an aileron, the deflection is smooth so the associated drag penalty is also lower, resulting in an increase in L/D ratio.

The warping was accomplished through the use of Futaba S3003 servos deliver-

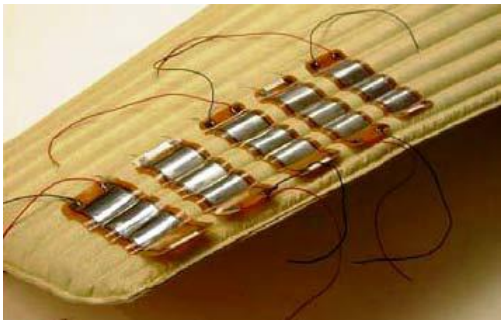

Figure 4.15: Pizoelectric [8].

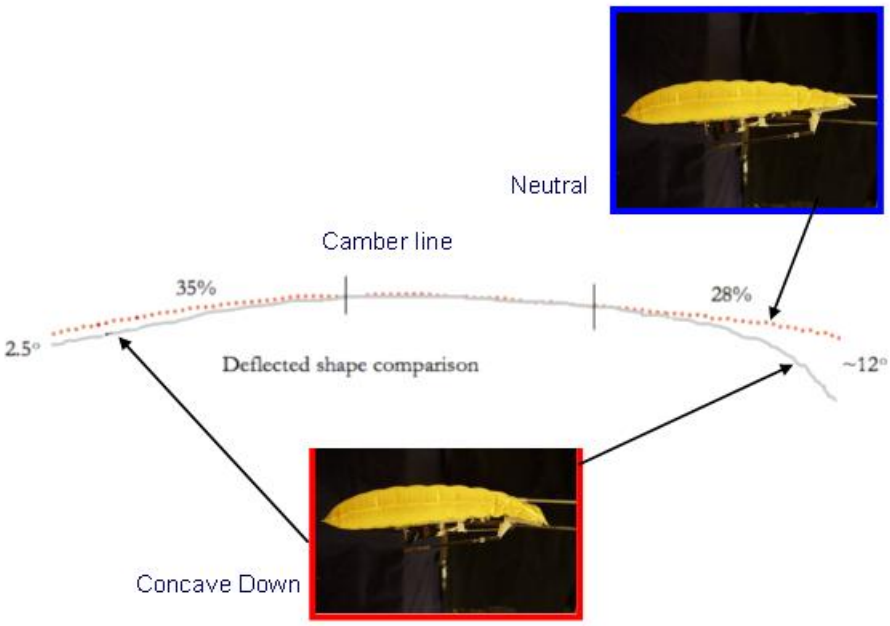

Figure 4.16: Camber outline comparison.

ing 14.4 kg.cm (200 oz.in) at 4.8 V or 4.1 kg.cm (56.8 oz-in) at 6V. As shown in fig. 4.17, the servos and control horns were attached to Acrylic plates, which were then adhered to the surface of the pressurized wing using RTV adhesive. Control horns were mounted to the plate to provide additional attachment area on the wing surface. The servos were mounted at the quarter chord of the wing and control horns were mounted on the trailing edge.

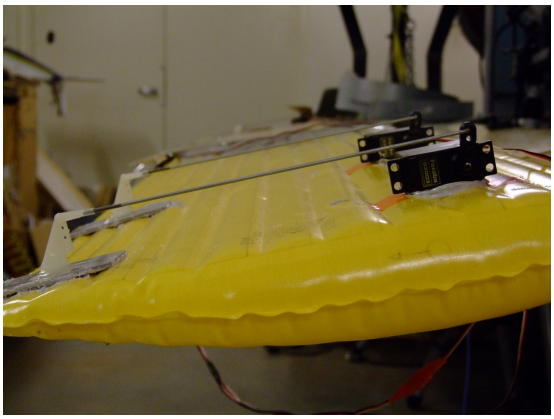

Figure 4.17: Servo attached on the wing using RTV adhesive.

In-flight testing was successfully conducted to demonstrate the feasibility of servo actuation to provide roll control. An inflatable wing with internal pressure of 8 psi was used and tested in-flight as shown in fig. **??**.

Figure 4.18: Flight testing using servo actuation.

4.5 Tape Selection

A typical conventional wing has a robust structure that allows the wing to be connected to the fuselage by means of bolts and nuts. However, semi-span inflatable wings have to be strategically designed to attach to the fuselage. Earlier ILC Dover inflatable wing designs like the FASM wing were mechanically connected to the fuselage using aluminum mounting flange. Each pair of FASM wing has keep a unique

bolt pattern at the root chord that required experimentalists to fabricate unique test fixtures for each set of wings as shown in fig. 4.19 (a). Later wing attachment designs were simplified to reduce weight by using a plastic molded sleeve and bonding by RTV adhesive as shown in fig. 4.19 (b). Fig. 4.20 is showing another version of the attachment method using acrylic plate. The plate has an ideal airfoil profile similar to the bumpy airfoil. Extra skin material was used to wrap and was chemically bonded around the root chord of the inflatable wing. The additional skin material was then sandwiched between the acrylic plates and later bolted to the fuselage.

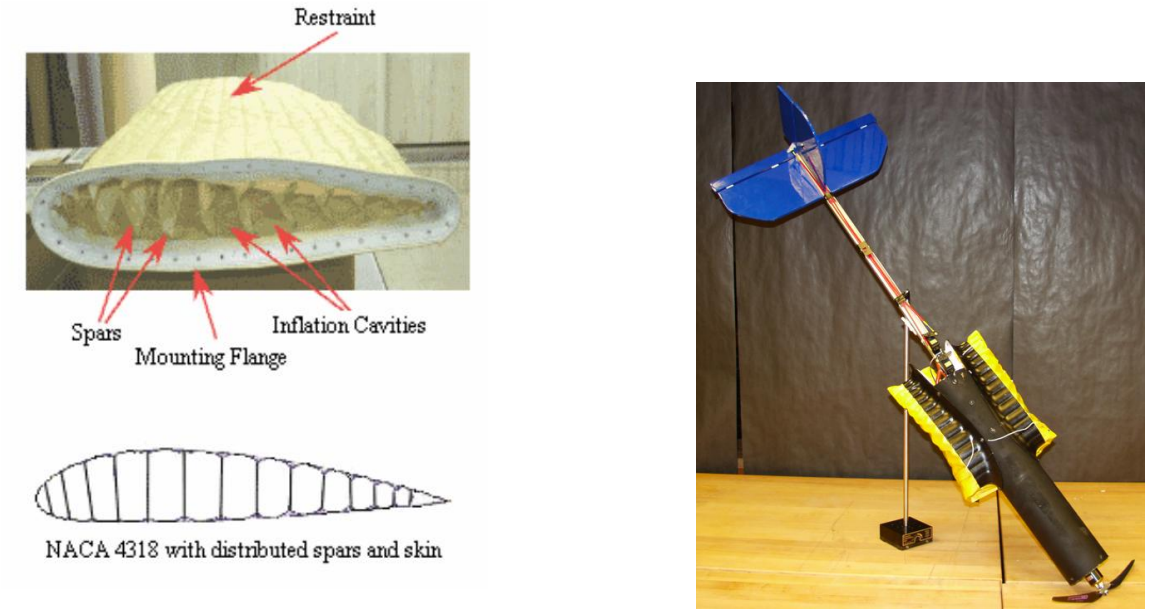

(a) FASM wing with mounting flange

(b) Plastic molded sleeve

Figure 4.19: Wing attachment method proposed by ILC Dover [10].

However, all these designs are bulky and significantly increase the aircraft weight. Therefore, OSU has proposed an alternative method using adhesive tape to optimize the weight issue on BIG BLUE V fuselage. Adhesive tape is typically stronger in the longitudinal direction and better resistant to shear load. Therefore, it was expected to perform well as bonding and load transfer medium. This method was later tested in-flight as described in chapter 6.

During flight, the wing structure is subjected to cantilever load that acting per-

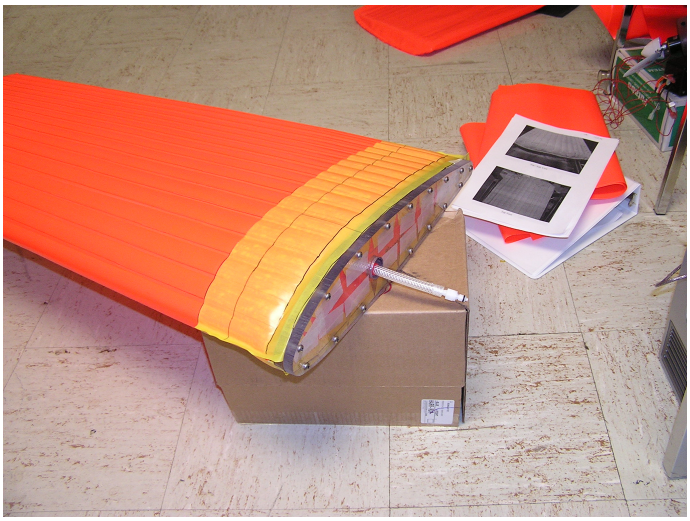

Figure 4.20: Inflatable wing attachment proposed by ILC Dover.

pendicular to the wing surface. This bending load creates skin tension on the bottom and skin compression on the top along the span wise direction. A wing sleeve similar to the molded plastic in fig. 4.19 (a) is created using adhesive tape to carry the load. The sleeve is created after multiple strips of tapes were used to wrap and bond portion of the wing root chord. With enough bonding area, the makeshift sleeve should hold the wing intact during flight. Wing tip test was conducted to justify this "taping" method at the end of this section. Furthermore, such design is relatively light-weight in comparison with the methods proposed by ILC Dover. When this design was first proposed, the biggest concern was the sensitivity of adhesive properties to temperature. To select a suitable tape for sub-zero atmospheric condition flight for the proposed MarsAircraft in BIG BLUE project or sea level flight, tensile test was conducted to determine which of tapes had the strongest adhesive, thus providing the largest margin of safety.

The way to determine the tape with the strongest adhesive was to calculate how many pounds per square inch it would take to pull a piece of tape from the inflatable wing material. Tensile test is the ideal test to decide the strength of the adhesive on each of selected tapes. Stress formula was used, $\sigma = \frac{F}{A}$, but rather than "A" signifying

the cross sectional area of the tape it is representing the area of tape applied to the wing material, thus providing us with the stress required to pull the tape from the wing material. The tape with the largest stress value would provide the largest margin of safety. Once the tape was applied to the wing material a load would be applied to the tape until the adhesive failed and the tape was pulled from the wing material. Three different tapes were selected as shown in table 4.22.

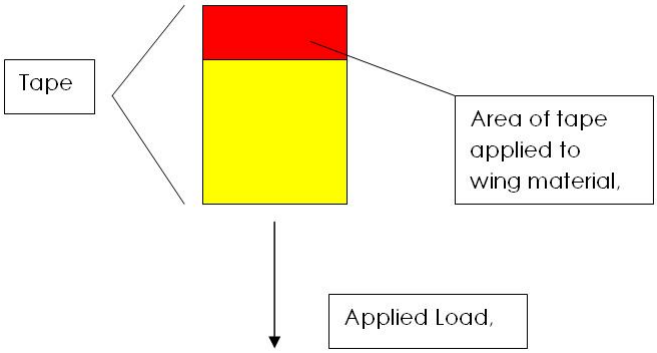

Figure 4.21: Tape test set up schematic.

Tapes	Adhesive Type	Rated Temperature		Wide, in	Weight, g/cm^2	Item number/brand
		°F	°C			
3 Mil Conf. PTFE Tape	Silicon Based	-10	-23	4	0.019	McMaster-Carr, PTFE Tape Part Number 76025A717
Silicone Coated Fiberglass	Silicon Rubber Based	-100	-70	2	0.035	McMaster-Carr, Silicon/Glass Cloth Tape Part number 791A65
Duct Tape	Rubber Based	-100	-70	1.875	0.027	Duck Brand

Figure 4.22: Material properties for each tape.

4.5.1 Room Temperature Tensile Test

A third test was performed on the duct tape and no other tape because of the inconsistencies between the first two tests. It should also be noted that the duct tape ripped in half before the adhesive gave way in tests 1 and 3.

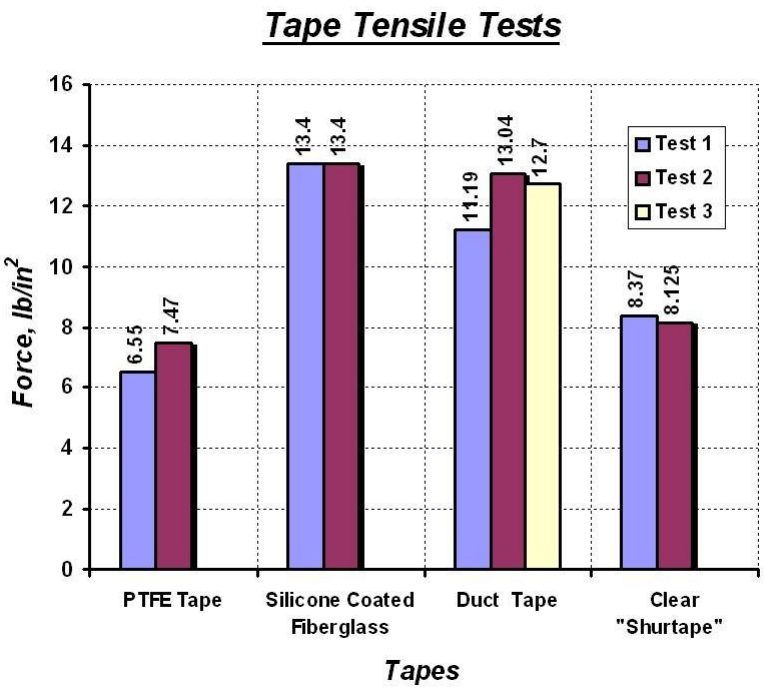

Figure 4.23: Tape tensile test results.

4.5.2 Extreme Cold Temperature Tensile Test

As represented in the room temperature test results, it is apparent that tapes 2 and 3 significantly outperformed the other two tapes. Therefore, cold temperature tensile test was conducted on tapes 2 and 3 to see how the adhesiveness of each of the tapes would perform under extreme conditions. Each tape was subjected to dry ice before the tensile test was performed.

Once the duct tape was removed from the dry ice the adhesive no longer was clinging on to the wing surface. This result was also surprising since the adhesive of the duct tape had worked successfully during our original tape test. The reason that the duct tape may have been successful in the first tape test could be due to the fact that there were many layers of the duct tape rather than a single piece of tape. In the preliminary tape test, multiple strips of duct tape were used to make a wing sleeve. The wing was then rolled and inflated while observation was made on

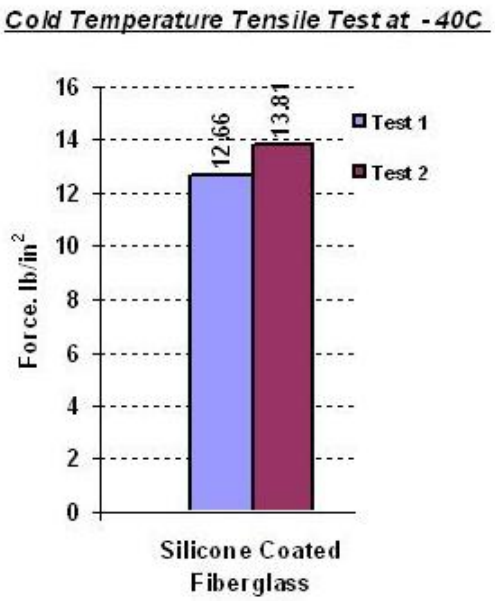

Figure 4.24: Tape tensile test results at -40 degree Celsius.

the performance of the duct tape. As for tape 2, the cold temperature had little to no effect on the adhesiveness.

4.5.3 Tensile Test at Environmental Condition

The tape tensile test was repeated across a range of environmental conditions (temperature and humidity) and shear loads. All three tapes were tested to a minimum of 17°F (-8°C) by placing the test articles outside overnight. In pure shear tests, all three tapes were subjected to a 1 lb load per 24 inch square of attached area overnight with conditions down to 17°F (-8°C) and nearly 100% humidity. Fig. 4.25 shows the results of a test of the three tapes used to attach a 36 inch span yellow inflatable wing to a composite balsa mount under cantilever loads. Tip deflections are shown on the y axis. Note that of the three tapes, the silicone/ glass tape performed the best. Tests on the MarsAircrafts fuselage have been conducted using standard duct tape. The primary concern is the transfer of the distributed wing loads to the fuse-

lage via the tape attachment to the wing mount bulkhead and skin. To ensure proper load transfer, the wings were ground tested using a distributed load test as shown in fig. 4.26 where the inverted wings were subjected to a distributed load. Results are shown in fig. 4.27. Tip deflections for a 9.09 kg (20 lb) distributed load on each wing are approximately 10 cm (4 in), or less than 5% of the total span. For a 5.9 kg (13 lb) plane, this is equivalent to a 3 g pullout. Note that though no load was applied to the wing mounts, this will provide some lift carrying capability during actual flight reducing the load on the wings.

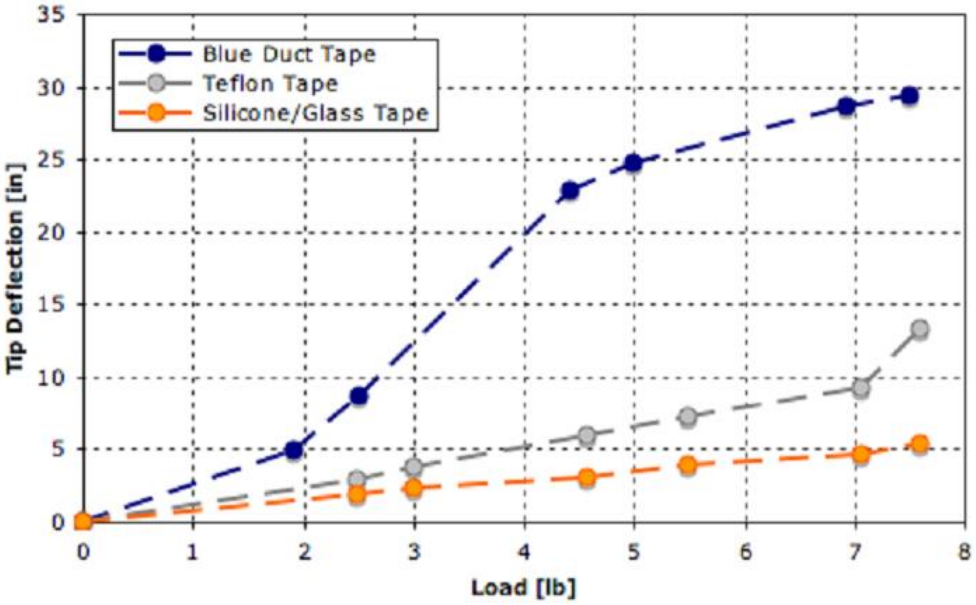

Figure 4.25: Tip deflection results for each tape with conditions down to 17F (-8C) and nearly 100% humidity.

Based on the results from the tests, it is clear that the silicone coated fiberglass tape outperformed the other three tapes. This tape will give the aircraft the largest margin of safety, and is recommended that this tape be used in flight to hold the inflatable wing onto the rigid wing. The feasibility of the method was successfully demonstrated in final flight of BLUE BIG V project as shown in fig. 4.28 (a) and (b).

Figure 4.26: Wing tip test.

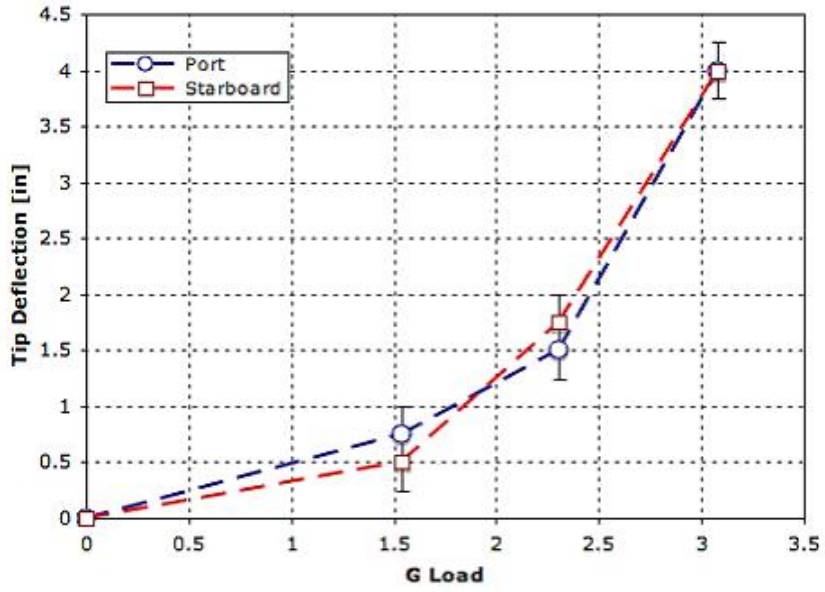

Figure 4.27: Tip deflection vs. G load.

4.6 Structural Analysis - Why Inflatable Wing Works

The bending moment along the span of the wing is of great importance to the structural integrity. This factor is normally driven by vehicle weight and the maximum

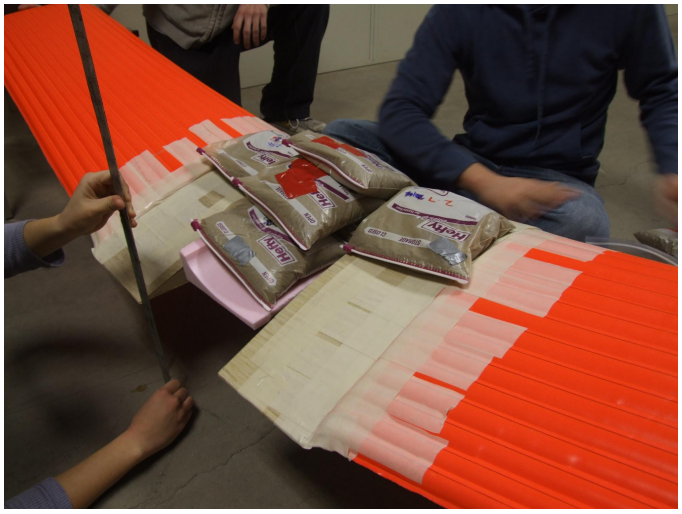

(a) Wing deflection test

(b) Fight test

Figure 4.28: Prove of concept using adhesive tape as wing attachment element.

accelerations the vehicle will undergo. Typical rigid wing requires robust design or composite material to maintain its structural integrity under operation conditions. The ILC Dover wing used in this research is made of Nylon based fabric coated with polyurethane. Fabric is a compression intolerant material. Thus, how can inflatable wing design maintain its structural rigidity against bending load or any aerodynamic load during flight?

According to Cadogan *et.al*, the strength and stiffness of the inflatable wing depends on the cross section design of the wing, inflation loads and the wings material

elastic modulus. A closer look at the ILC Dover's wing shows a series of fabric spars that run roughly perpendicular to the aircraft body, and are attached to an upper and lower fabric restraining layer. The surface of the resultant inflated structure has a bumpy appearance, as inflatable structures approximate the shape of a cylinder upon inflation.

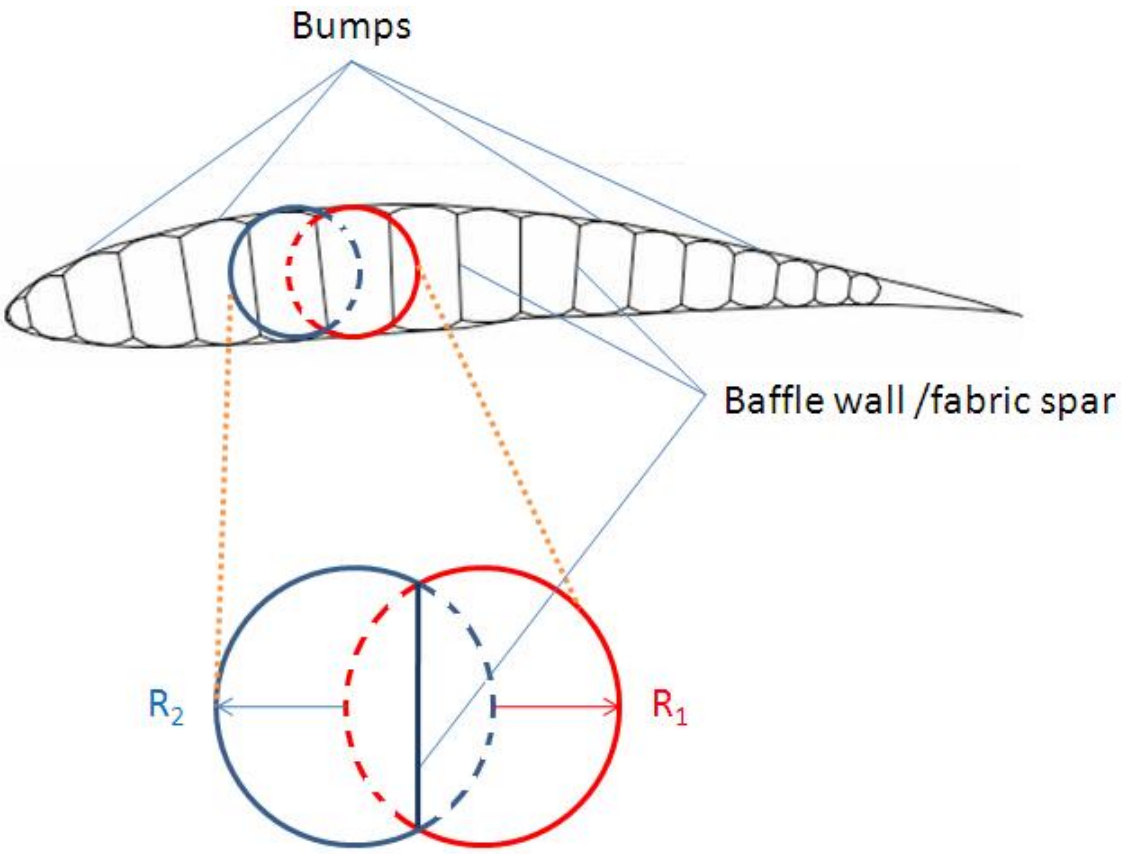

Figure 4.29: Baffle design

An example of inflatable wing cross section shown in fig. 4.29 demonstrates that the wing appears to be a series of intersecting cylinders beam with the fabric spar position in between the intersections of the cylinders. R is the radius of curvature of the tube. The inflatable beam assumed to be a straight section. In an air structure there is a property called hoop stress. The classic equation for hoop stress created by an internal pressure on a thin wall cylindrical pressure vessel is

$$\sigma = \frac{Pr}{2t} \tag{4.1}$$

where t is the wall thickness, P is the internal pressure and r is the radius. The wall is significantly thinner than the other dimensions, which implies that the difference between inner and outer radius is small. This equation shows that the bigger the diameter of the tube the greater the stress on the fabric for any given pressure. Therefore a small diameter tube can withstand greater pressure inside and still have the same amount of stress on the fabric. Now think about a long inflated tube. If the base fabric stretches, it will take more pressure inside of the tube to keep it ridged, because the fabric can stretch along the outside of the bend in the tube. This is why some inflatable structures never seem to attain the same rigidity as others.

Since the radius of curvature of the bumps decreases as one moves from the maximum wing thickness toward the trailing edge, the skin stress correspondingly drops. Cadogan et.al has shown that the Vectran wing at the operating conditions noted above shows that a nominal inflation pressure of 48 psi is required to prevent the wing from buckling under flight loads. At this inflation pressure, the hoop stress in the region of wing near the tip varies from 52 lb/in in the largest cell to 14 lb/in in the smallest cell (trailing edge). (Note that stress in a thin shell structure such as an inflatable is typically expressed in lb/in.) The derived stresses were used as the basis of development for the morphing wing actuation systems as demonstrated by Simpson *et.al* in section 4.4.

The hoop stress can be related to the bending moment using

$$\sigma = \frac{Pr}{2t} = \frac{M_0 r}{\pi r^3 t} \tag{4.2}$$

Where M_0, is the root bending moment . The fabric thickness does not play a major role since both sides of the equations are multiplied by the fabric thickness. Rewriting equation 4.2 yields:

$$P = \frac{2M_0}{\pi r^3} \tag{4.3}$$

This is shown notionally in fig. 4.30. While P is linear with M_0, doubling the tube radius reduces P by a factor of 8. Thus, larger diameter tubes are extremely beneficial when used on inflatable wings to support bending load. These explain the benefit of having a larger diameter cylindrical spar at the quarter chord to support the wing load at operating condition. Since the baffled wing consists of a series of hollowed tubes with varying radii of curvature running from the leading edge to the trailing edge, each tube acts as like an individual spar that provides additional resistance to wing bending loads.

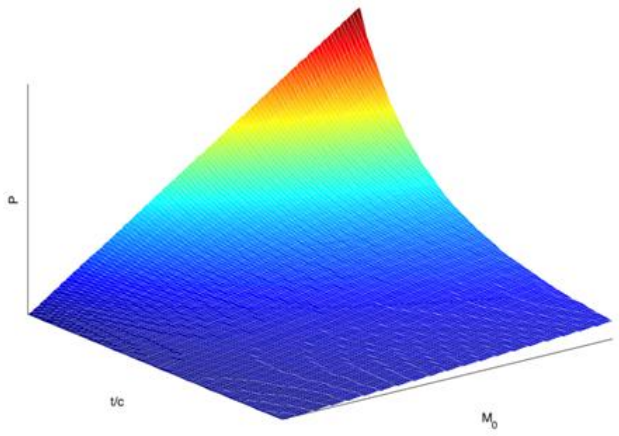

Figure 4.30: Pressure relation.

Assumption was made that wrinkling will occur when the compressive stress due to bending becomes as large as the tensile stress due to internal overpressure. The wrinkling load is always obtained when the resultant stress cancels on the upper or the lower generative of the tube as depicted in fig. 4.31. In this location, the total stress in the tube will become zero.

It is assumed that the fabric cannot sustain compressive stress and therefore, wrinkling will occur. Wrinkling can be expected at the attachment point or at location

closest to the root of the wing. Collapse load is defined when the whole resultant stress cancels on one of these generative.

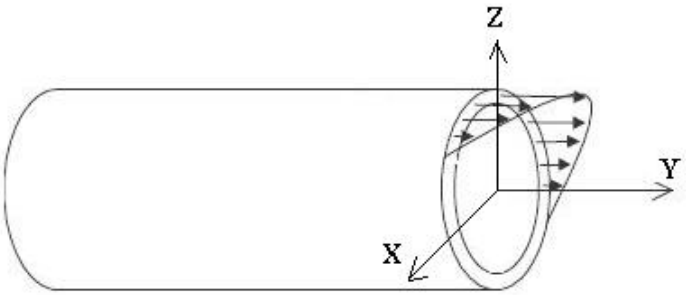

Figure 4.31: Stress distribution during bending load

The primary consideration for failure in an inflatable structure is the maximum sustainable bending moment or collapse load. To determine the load carrying capability of a simplified inflatable beam design, we begin with the Euler Bernoulli beam equation that relates the beam deflection with applied moment and applied moment and material properties on a cantilever beam [26].

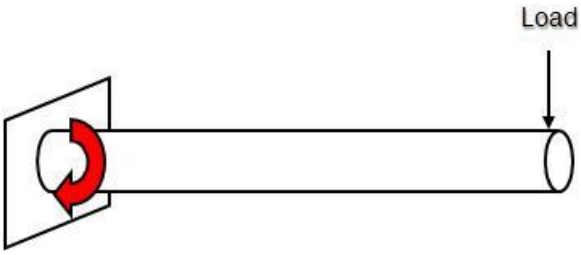

Figure 4.32: Beam under bending moment load.

$$\frac{d^2y}{dx^2} = \frac{M(x)}{E_w I} \tag{4.4}$$

E_w is the Young's modulus of the material, M is the applied moment, and I is the cross-sectional moment of inertia. According to Simpson *et. al* [9], the ILC

Dover baffle design maximizes the area moment of inertia of the cross section; thus minimizing the inflation pressure required to reduce deflection and prevent buckling. Equation 4.4 clearly shows the relations. Main *et. al* modified this with respect to an inflated fabric tube to develop a relation for the bending moment equation for a single inflated fabric spar for space based inflated structures [27, 28].

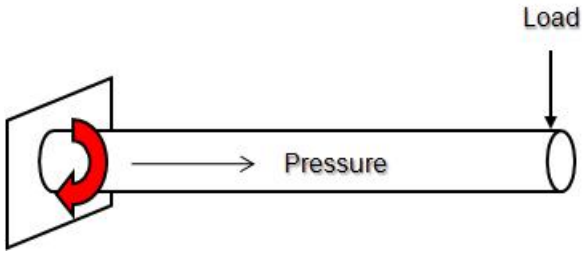

Figure 4.33: Inflatable structure under bending moment load.

$$\frac{d^2y}{dx^2} = \frac{M}{E_l \pi r^3} \text{ for } M < \frac{\pi p r^3}{2}(1 - 2\nu_t) \tag{4.5}$$

$$\frac{d^2y}{dx^2} = \frac{M - 2\nu_t p r^3 \sin\theta_0}{E_l r^3[(\pi - \theta_0) + \sin\theta_0 \cos\theta_0]} \text{ for } M > \frac{\pi p r^3}{2}(1 - 2\nu_t) \tag{4.6}$$

where M is the bending moment. E_l is the longitudinal fabric tensile modulus, r is the beam radius, and θ_0 is the wrinkle angle. The relation includes the impact of wrinkling and accounts for the biaxial stress in the beam fabric and the impact that it has on the wrinkling threshold of the beam as well as the beam's postwrinkling bending behavior. The model was well validated against experimental data of fabric beams under loads. The essential behavior of the model is presented in fig. 4.34.

As the load increases, the beam deflects in a linear manner. Once the wrinkling threshold is reached, the relation becomes non-linear. Soon after, the beam buckles. This will scale depending upon the type of structure involved. While buckling is the failure mode, the onset of wrinkling indicates the maximum design load and will be used for the design limit. It should be noted that unlike metal or composite rigid structures that will either plastically deform or crack, respectively, once the yield

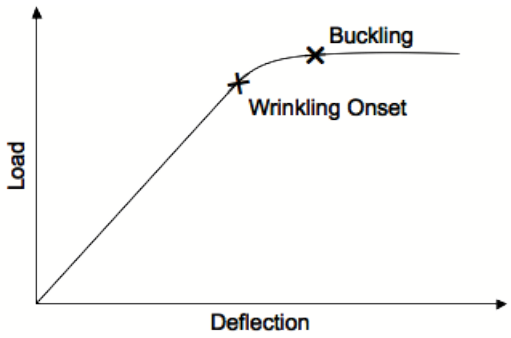

Figure 4.34: Load vs. deflection relation for inflatable beam.

stress is reached, the inflatable beam will bend, but then will return undamaged to its original state after the load is reduced or removed.

Methods to reduce the inflation pressure also being investigated by Brown *et.al* and Breuer *et.al* as shown below. Brown *at.el* has patented a design to cover the inflatable tube with braid to provide additional skin stiffness and reduce internal pressure.

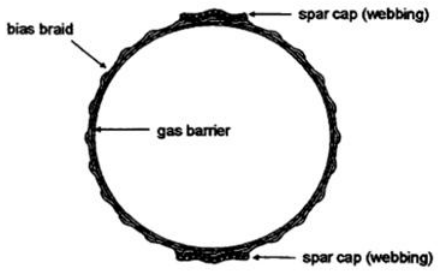

Figure 4.35: Braid

Breuer *et.al* is suggesting tensairity method by adding compression element to counter act the compression loading on the wing.

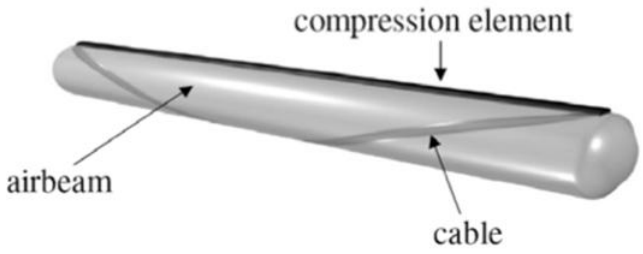

Figure 4.36: Tensairity element

Figure 4.37: High aspect ratio research aircraft.

4.7 Preliminary Morphing Concepts using inflatable wing

According to Cadogan *et. al*, the best advantages that inflatable provide over conventional structure is packaging [12]. Inflatable wings can provide low volume storage and is able to provide sufficient structural stiffness during flight after being fully pressurized to its final shape. In comparison with folding rigid wing, the overall wing structure required advanced material to maintain its structural integrity due to its increasing load as wing span increases. Advance folding design is required to overcome high dynamic load acting on the wing upon deployment. Even though the folding wing can be constructed using lighter advanced material to decrease weight as span increases, however, rigid folding wing are volume limited structures and cannot be packed into a smaller storage volume. Contrarily, the inflatable wing is mass limited

structure where weight penalties will be a dominant issue as the wing span or chord increases. For a wing design with aspect ratio of above 20 as shown in fig. 4.37, innovative wing design can be achieved by combining both inflatable wing and folding rigid wing design to provide the lowest packed volume and weight for highest deployed span.

4.7.1 Morphing Wing Concepts Using Inflatable Wing

Deployment synchronicity is improved as the rates of deployment are increased. Some control can also be achieved through specific patterns and control of the inflation path. Five preliminary morphing wing concepts have been investigated in the early stage of this research to achieve in-flight morphing. Currently, concept 1, 2 and 3 have been successfully fabricated in lab for wind tunnel and flight test. This thesis is mainly focus on testing the feasibility of these three concepts for in-fligth morphing. Concept 4 and 5 are still in concept phase and only briefly discussed here. Each concept will be introduced separately. Please note that the drag and lift issues generated by each design during the period between deployment and complete inflation still need to be addressed in future work.

Concept 1: Inflatable Wing Only

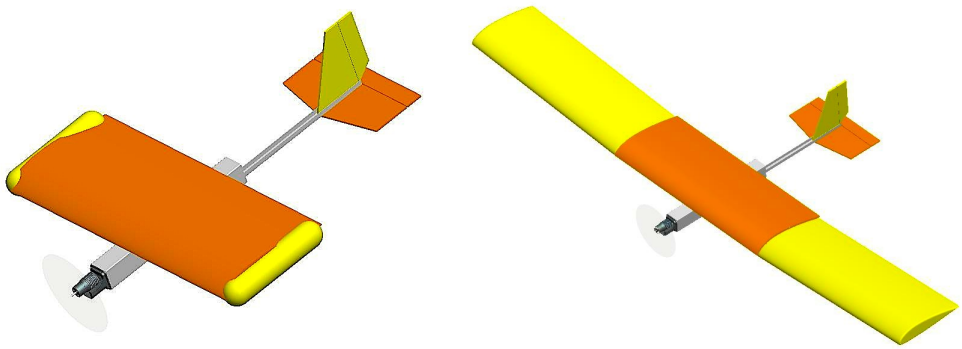

Figure 4.38: Inflatable wing attached to the rigid wing tip.

Concept 1 consists of two sections: rigid wing and inflatable wing. The rigid wing has the same airfoil profile as the inflatable wing except it has a smooth surface compared with the bumpy appearance of the inflatable wing. Aerodynamically designed lightweight-external pods are required to store the rolled up inflatable wing while reducing drag during flight. Upon deployment, the pod cover will be separated from the rigid wing. However, unsteady flight can occur upon deployment if using an onboard inflation system that produces slow flow rate. Based on our wing tunnel deployment test, we observed that the inflatable wing was pushed backward by wind loading upon deployment. The inflatable wing was folded half and landed flat on either top or bottom of the rigid wing while the inflatable wing is slowly being inflated to its final shape. Therefore, a fast inflation system that could fill the wing within fraction of a second is needed to overcome or minimize the unsteady flight issues upon deployment.

Concept 2: Reinforced Inflatable Wing

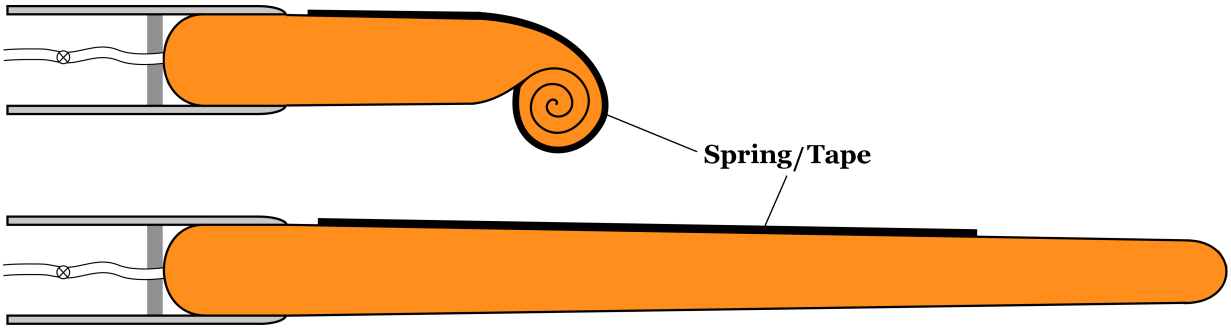

Figure 4.39: Inflatable wing with stiffener.

Concept 2 as shown in fig. 4.39 is similar to concept 1 with an additional structural support attached on top and bottom of the inflatable wing using strip(s) of self-uncoiled material, for example: strip(s) of measuring tape that have a u-shape contour. The strip of constant force spring will act like spars at the wing quarter to

give additional support to overcome high wing loading on the inflatable wing. To increase the deployment speed of the wing, we propose to investigate the use of constant force springs attached to the wing surface as shown in fig. 4.39. This was previously proposed by ILC Dover for both deployment enhancement and wing re-stowage once the internal wing pressure was removed. A bi-stable composite system is being investigated for the latter operation. Upon actuation of the wing release mechanism, the springs will completely deploy the wing and the inflation system will just fill the wing.

Concept 3: Inflatable Wing with Deployment Control Element

Based on the wind tunnel test, the flapping situation could happen under dynamic pressure if the deployment was slow due to low mass flow rate . Velcro was chosen to mitigate this issue. Velcro might help control the deployment by holding the rest of the wing temporarily while allowing pressure building up from root to tip. Velcro can also be used as alternative wing restraint compare with cat-coller. Fig. 4.40 shows the wing design with stripes of Velcro attached on both sides of the wing surface.

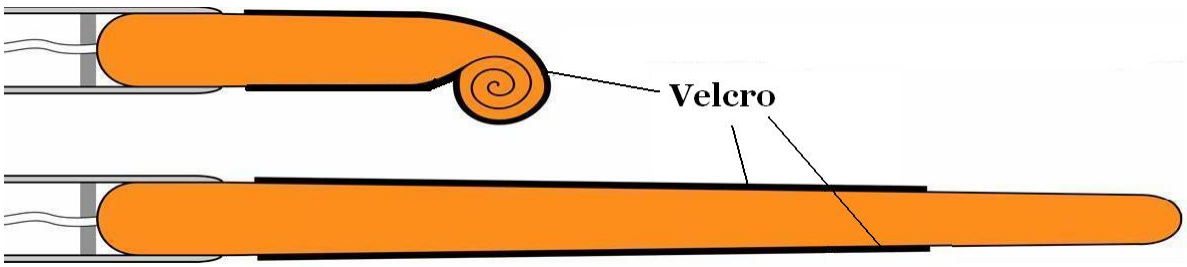

Figure 4.40: Inflatable wing with CDE.

Concept 4: Hybrid Wing with Partial Inflatable Wing Section

As shown in fig. 4.41, this hybrid wing design is a combination of three sections: leading edge foam, carbon fiber spar and inflatable wing. The spar is located at the

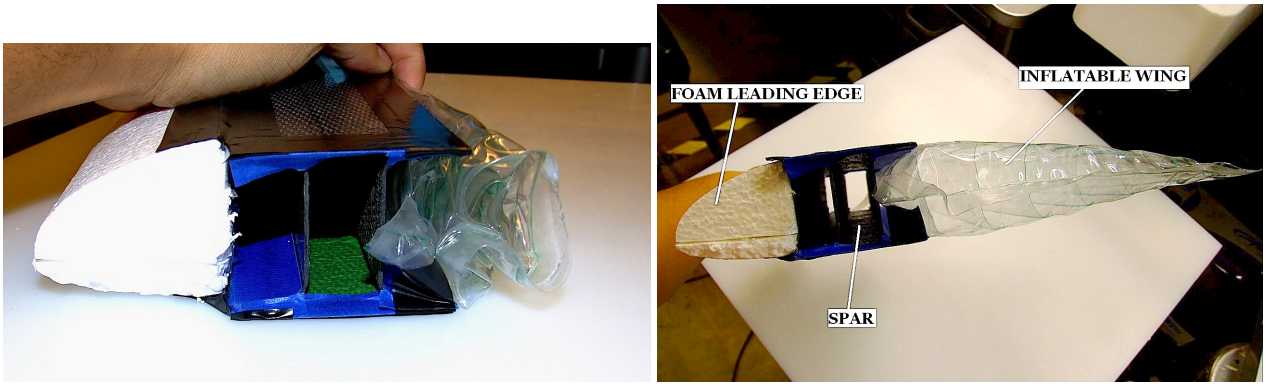

(a) Hybrid wing (b) Stowed Mode

Figure 4.41: Hybrid wing design

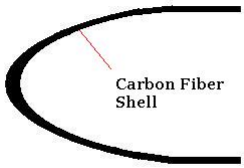

Figure 4.42: Carbon fiber shell.

quarter chord of the wing and is made of 3 layers of prepreg carbon fiber sheet for each ply. The carbon fiber spar has a I-channel shape with a hollow space in-between that allows air hoses and servo wires to go through. The spar also provides storage space to store the deflated inflatable wing as shown in fig. 4.41 (b) and the wing is temporary being secured using a release mechanism. The leading edge foam is not only lightweight but it is easy to attach to the front of the carbon fiber spar using silicon based adhesive tape or epoxy bonding. To enhance the design of this hybrid wing leading edge section, the whole foam and spar section can be made into one piece using carbon fiber sheets as shown in fig. 4.42 using molding method to shape its contour. This enhanced design can provide more storage space to store the deflated inflatable wing while maintaining its airfoil leading edge shape and providing structural strength. The inflatable wing will be attached to the rear of the spar using silicon based adhesive tape, which is a proven bonding technique used by the MARS

team to attach the inflatable wing onto the rigid wing.

4.7.2 Concept 5: Fusion of Rigid Folding Wing and Inflatable Wing

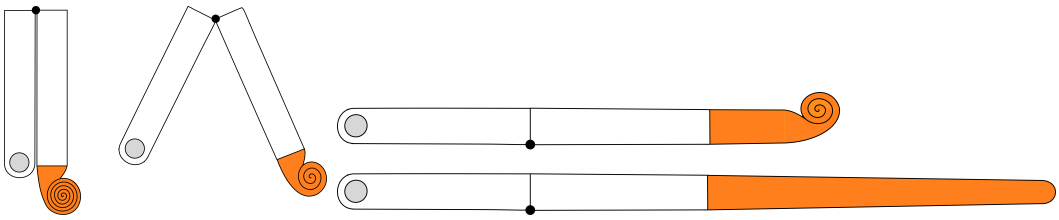

Figure 4.43: Hybrid folding rigid wing with inflatable wing section.

Concept 5 is a combination of concept 1 integrated with folding rigid wing. This method helps reduce the rigid wing span by replacing part of the wing with inflatable section. This combination helps minimize the storage volume and increase the wing span after deployment.

CHAPTER 5

Dynamic Deployment Tests

The purpose of the wind tunnel test is to investigate the deployment behavior of the inflatable wing. The finding presented will response to the speculations made in chapter 2 and justify the preliminary morphing wing concepts discussed in chapter 4. The investigation was conducted in three stages based on three different wing designs. The initial deployment test was primarily focused on the impact of dynamic pressure on the inflatable wing at low inflation rate: Wing Alone (WA). A high-speed camera was used to observe the deployment behavior and record the change in pressure. Two types of wing folding techniques were investigated. The WA results demonstrated significant instability that lead to the second deployment test: Reinforced wing using stiffener (WSE). Aerodynamic loads were measured using load cells at a constant angle of attack of 0. High-speed camera reviewed similar behavior as WA, where wing flapping and folding was seen. Therefore, deployment control element (DCE) was introduced to mitigate these problems. Wing using DCE showed significant improvement during deployment, even at a stall angle of attack. In this test, a pressure transducer was integrated to measure. Extensive static and ground deployment tests on a full-scale wing using DCE were conducted. Preliminary tests showed positive results. Please note that a total wing span (combined with rigid and inflatable wing section) of 20.8 inch was used for WA and WSE tests. The DCE test used a slightly longer wing mount, which gave a wing span of 21.5 inches. The inflatable wing section are the same in all cases with 17 inches span.

5.1 Wing Alone (WA)

Based on the predicted flight performance of IFI (as calculated in Appendix A), three sets of free-stream conditions and V_∞ were chosen to simulate the in-flight inflation. These velocities are 16, 25 and 29 m/s, which is equivalent to 0.60, 1.50 and 2.02 inches of H_20 dynamic pressure, respectively. The velocity of 16 m/s is the predicted cruise speed that keeps the flight level. Varying AOA was also an interest of investigation since the angle of attack might varying during deployment. The maximum free-stream velocity at 29 m/s is slightly higher than the maximum calculated flight speed at high aspect ratio configuration. These conditions are predicted higher than the expected flight velocity calculated by Simpson *et. al* at 15m/s using a 1 meter span inflatable wing.

For each free-stream condition, the wing was positioned at three AOA of 0, 5 and 10 degrees. Before each test began, the wing was carefully stowed using a wing-retention as shown in fig. 3.8 (b). Two types of folding method were used to investigate the impact of folding technique on the deployment rate. Pressure reading was obtained after reviewing the high-speed images at every 1 second. Plot of pressure versus time was made to investigate the changes in internal pressure during deployment. Both cameras were synchronized to trigger simultaneously once the inflation began. In each case, only five set of images presented in this paper for each deployment test. Please note that the airflow is moving from right to left. A total of four cases were investigated as listed below with their results.

Result

5.1.1 WA Case 1: V_∞ = 16 m/s at AOA of 0, 5, and 10 (Rolled)

Graph in fig. 5.1 shows the pressure history for $V_\infty = 16$ m/s at three angles of attack. Fig. 5.2, fig. 5.3 and fig. 5.4 are the image sequence at AOA of 0, 5, and 10 degrees,

respectively.

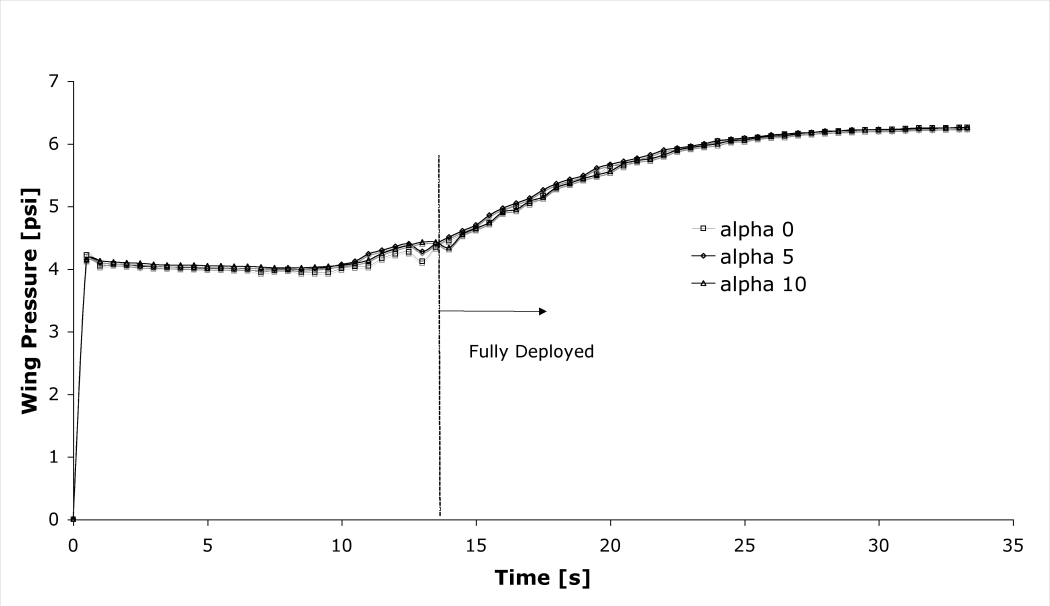

Figure 5.1: WA Case 1 : $V_\infty = 16$ m/s.

(a) t =0 s. (b) t = 0.5 s. (c) t = 6 s. (d) t = 11 s (e) t = 33.3 s

Figure 5.2: WA Case 1 : $V_\infty = 16$ m/s at AOA of 0.

(a) t =0 s. (b) t = 0.6 s. (c) t = 5 s. (d) t = 11 s (e) t = 33.3 s

Figure 5.3: WA Case 1 : $V_\infty = 16$ m/s at at AOA of 5.

(a) t =0 s. (b) t = 0.5 s. (c) t = 5 s. (d) t = 12 s (e) t = 33.3 s

Figure 5.4: WA Case 1 : $V_\infty = 16$ m/s at at AOA of 10.

5.1.2 WA Case 2 : $V_\infty = 25$ m/s at AOA of 0, 5, and 10 (Rolled))

Graph in fig. 5.5 shows the pressure history for $V_\infty = 25$ m/s at three angles of attack. Fig. 5.6, fig. 5.7 and fig. 5.8 are the image sequences at AOA of 0, 5, and 10 degrees, respectively.

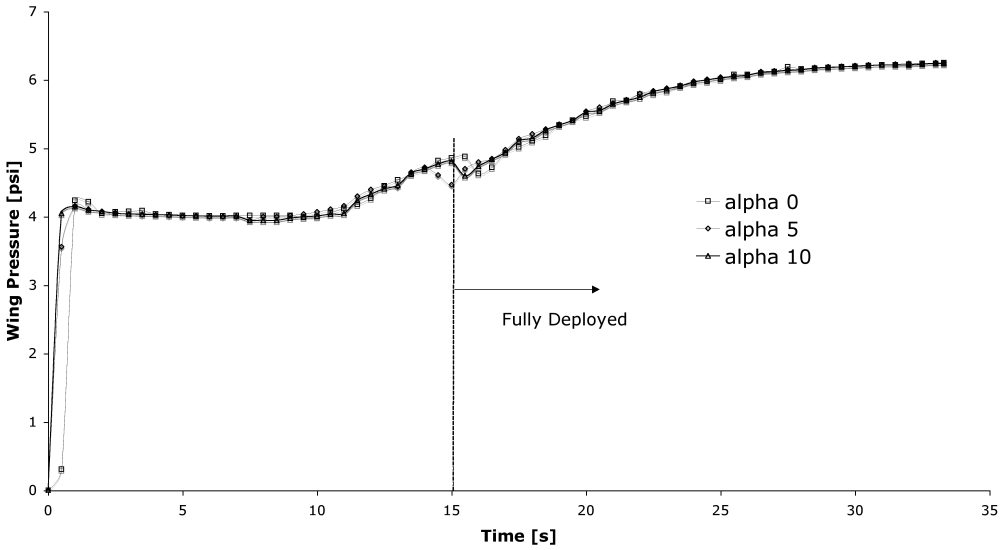

Figure 5.5: WA Case 2 : $V_\infty = 25$ m/s.

(a) t =0 s. (b) t = 1.1s. (c) t = 5 s. (d) t = 12 s (e) t = 33.3 s

Figure 5.6: WA Case 2 :$V_\infty = 25$ m/s at at AOA of 0.

(a) t =0 s. (b) t = 0.7 s. (c) t = 5 s. (d) t = 12 s (e) t = 33.3 s

Figure 5.7: WA Case 2 : $V_\infty = 25$ m/s at at AOA of 5.

(a) t =0 s. (b) t = 0.7 s. (c) t = 5 s. (d) t = 12 s (e) t = 33.3 s

Figure 5.8: WA Case 2 : $V_\infty = 25$ m/s at at AOA of 10.

5.1.3 WA Case 3: Constant AOA of 0 at $V_\infty = 16$, 25, an 29 m/s (Z-fold)

Graph in fig. 5.9 shows the pressure history for fixed AOA of 0 degree at three V_∞. Fig. 5.10, fig. 5.11 and fig. 5.12 are the image sequence at $V_\infty = 16$, 25, and 29 m/s , respectively.

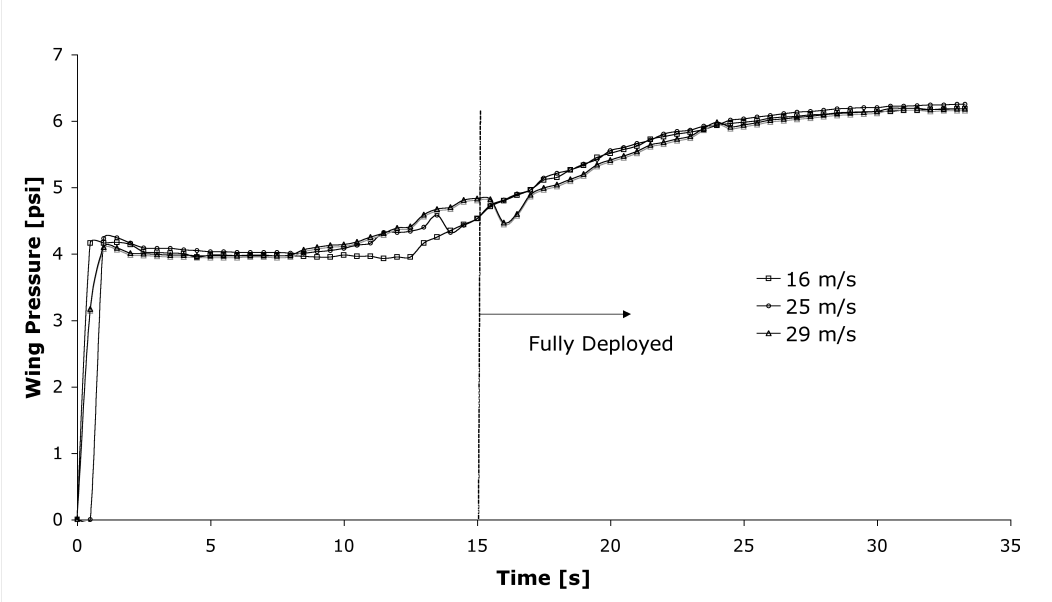

Figure 5.9: WA Case 3 : AOA of 0 at 16, 25 and 29 m/s.

(a) t =0 s. (b) t = 0.7 s. (c) t = 5 s. (d) t = 12 s (e) t = 33.3 s

Figure 5.10: WA Case 3 : V_∞ = 16 m/s at AOA of 0.

(a) t =0 s. (b) t = 0.7 s. (c) t = 5 s. (d) t = 12 s (e) t = 33.3 s

Figure 5.11: WA Case 3 : V_∞ = 25 m/s at AOA of 0.

(a) t =0 s. (b) t = 0.7 s. (c) t = 5 s. (d) t = 12 s (e) t = 33.3 s

Figure 5.12: WA Case 4 : V_∞ = 29 m/s at AOA of 0.

5.1.4 WA Case 4 : Z-folding vs. Rolled

Graph in fig. 5.5 shows the pressure history for V_∞ = 25 m/s at three angles of attack. Fig. 5.6, fig. 5.7 and fig. 5.8 are the image sequences at AOA of 0, 5, and 10 degrees, respectively. Both fig. 5.14 and fig. 5.15 show the deployment at 16 m/s. Both fig. 5.16 and fig. 5.17 show the deployment at V_∞25 m/s. An observation on the pictures shows that Z-folding method allows the inflatable wing to be deployed and achieve its final shape faster (at t =12 s). Both results on pressure history a similar trend as previous cases (shown in fig. 5.13).

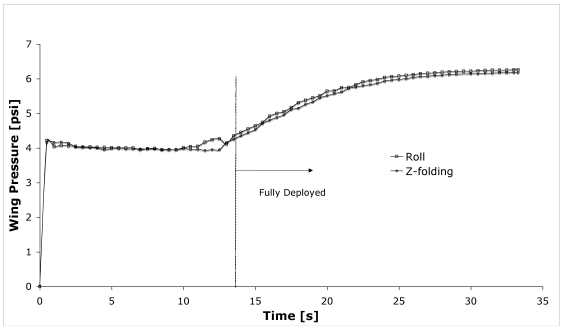

(a) $V_\infty = 16$ m/s at 0 alpha.

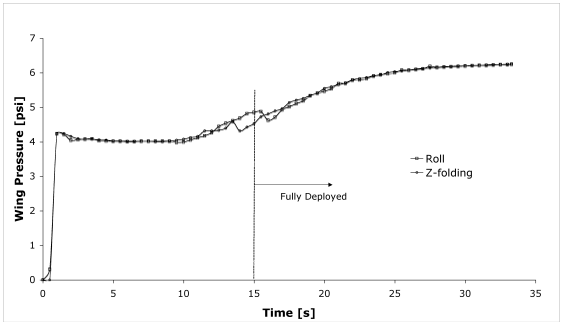

(b) $V_\infty = 25$ m/s at 0 alpha.

Figure 5.13: WA Case 4 : Z-folding vs. Rolled pressure history.

(a) t =0 s. (b) t = 0.5 s. (c) t = 6 s. (d) t = 11 s (e) t = 33.3 s

Figure 5.14: WA Case 4 : (Rolled Method) $V_\infty = 16$ m/s at AOA of 0.

(a) t =0 s. (b) t = 0.7 s. (c) t = 5 s. (d) t = 12 s (e) t = 33.3 s

Figure 5.15: WA Case 4 : (Z-Folding Method) $V_\infty = 16$ m/s at AOA of 0.

(a) t =0 s. (b) t = 1.1s. (c) t = 5 s. (d) t = 12 s (e) t = 33.3 s

Figure 5.16: WA Case 4 : (Rolled Method) $V_\infty = 25$ m/s at AOA of 0.

Discussion

In all cases, inflatable wing under free-stream loading were found folded in a similar behavior upon released. Instead, in some, wing flapping was observed. All cases experienced constant pressure expansion at about 4 psi as the wing volume gradually

(a) t =0 s. (b) t = 0.7 s. (c) t = 5 s. (d) t = 12 s (e) t = 33.3 s

Figure 5.17: WA Case 4 : (Z-Folding Method) V_∞ = 25 m/s at AOA of 0.

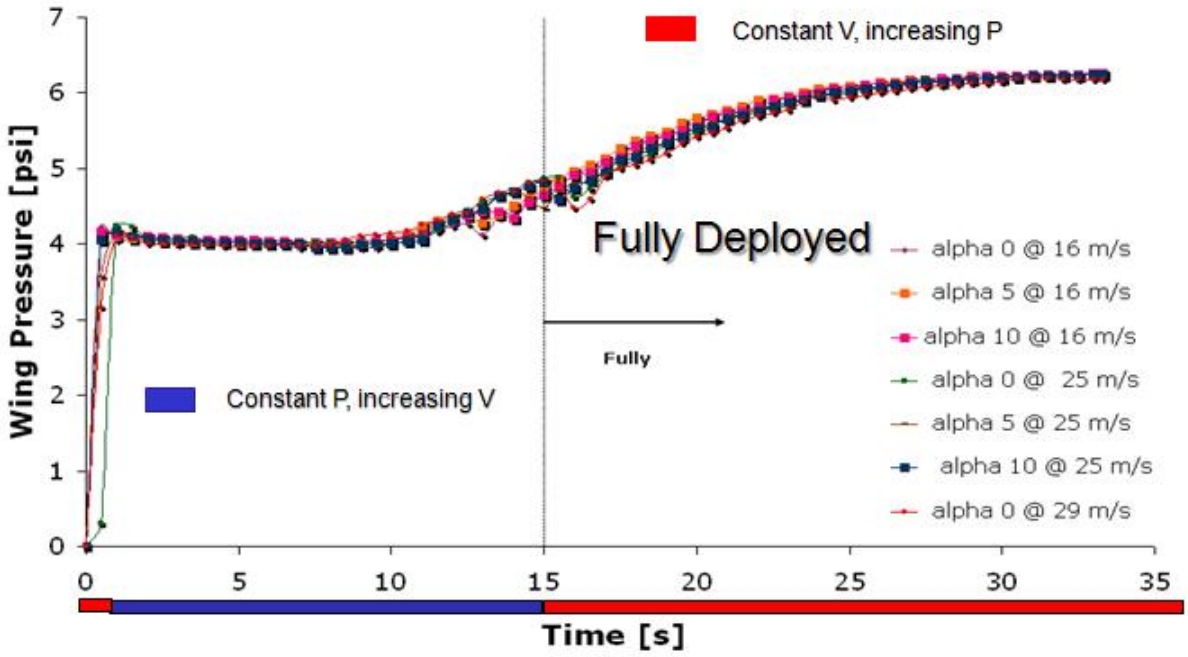

Figure 5.18: WA: Pressure History

increased. A small peak of pressure drop was observed momentarily, followed by constant volume expansion as the pressure gradually increased in time. Boyle laws describes the relationship between pressure and volume at constant temperature. Boyle laws states that at constant temperature, as the pressure increased the volume decreases. In other words, the volume of a gas is inversely proportional to the pressure applied on it. The wing deployment clearly showing the Boyles relations. Based on fig. 5.13 (b), the deployment sequence exhibited three stages of expansion until the wing was fully pressurized: (1) Constant volume, (2) Constant pressure then (3) Constant volume expansion.

(1) Constant Volume Expansion:

Closer look at the p-t curve shows that the stowed wing experienced a sharp increase in pressure once the air valve was opened. Before deployment, the stowed wing had a fix wing volume (minimum wing volume). The initial wing volume was quickly filled up due to the sudden expansion in pressure. The wing volume expanded as the wing was released from the stowed configuration as the pressure continued to build up. Combined with the dynamic pressure, the wing was seen to be folded and kinked thus separate the wing into two sections.

(2) Constant Pressure Expansion:

The first portion of the wing experienced a constant pressure expansion at 4 psi while the wing was being filled up with air. The air pressure stabilized for about 11 seconds as the air filledup the wing volume.

(3) Constant Volume Expansion:

After 11 s, the wing pressure filled up the first half of the wing volume and followed by an increase in pressure. The pressure increased for about 3 seconds as the second portion of the wing slowly unfolded itself. Based on the pressure-time curve result, a sudden drop of pressure was observed at 15 seconds. At this moment, the wing was straightened from the kinked section and experienced a sudden expansion in wing volume. This lead to a sudden drop in wing pressure as stated in Boyle Laws. This momentary drop in pressure was followed by an increase in pressure. The pressure was gradually increased to fill up the wing volume until it reached the regulated pressure at 6psi that rigidized the wing.

Regardless of which folding method was chosen, a variety of dynamic pressures or angles of attack, wind tunnel deployment tests exhibited a similar trend where the wing was still able to be deployed at slow inflation rates to achieve its final

wing shape. However, the wing-flapping issue had to be mitigated using some sort of reinforcement. The chosen material had to provide additional stiffness and still provide flexibility to enable it to rolled along the wing. Additional reinforcement was expected to help avoid the kinked behavior. Therefore, a stiffener, like measuring tape, was used to improve the deployment behavior. Spring metal with a thickness of 0.005 inch was considered but it stiffness was too high to be coiled up tightly as the wing rolled up.

5.2 Wing with Stiffener Elements (WSE)

Based on the results obtained from WA, the combined behavior of folding and flapping upon deployment had to be mitigated. Stiffener of flexible metal stripes was considered, like the measuring tape. As shown in fig. 5.19, the U shape contour of the tape has an identical shape as that of the curve of the bumpy surface. The attached tape can be perfectly covered after being attached to the wing surface using silicon tape as shown in fig. 5.19 (a). Its flexibility also allows it to be rolled tightly and stowed along the wing , without damaging the wing surface. The length of the tape is about 16 inches.

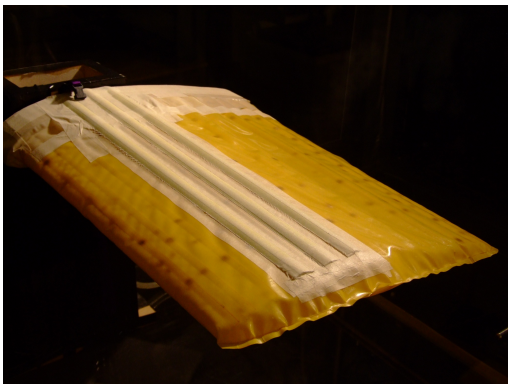

(a) Reinforced Inflatable wing

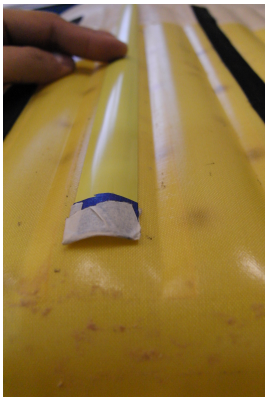

(b) U Shape contour

Figure 5.19: WSE : Three stripes of flexible tapes attached on the wing at the quarter chord

Figure 5.20: WSE : Numbered baffel.

Load cell was available in this test to measure the dynamic load during the deployment. However, unlike the previous test, pressure history was not recorded. This test was mainly focused on mitigating the combined issue of wing folding and flapping behavior. Furthermore, the preliminarily test using stiffness showed similar deployment behavior as demonstrated in fig. 5.21. Thus, an assumption was made that pressure history was not the primary objective in this test.

(a) Inflatable wing only

(b) Inflatable wing with reinforcement elements.

Figure 5.21: WSE : Deployment sequence of inflatable wing at 16 m/s.

A total of 5 different wing designs were tested at airspeed of 0.6 in H20 (16 m/s)

and 1.5 in H20 (25 m/s) at constant AOA of 0 degree. The velocity of 29m/s was ignored to prevent the load cell from overload due to high dynamic load and wing flapping as observed in the previous test. Each design is different in terms of the tape placement on the wing as shown in fig. 5.20. The wing has a total of 14 bumps chord-wise. Bumps number 6, starting from the leading edge, is the wing quarter chord. Please note that the tape placement for each of this design was not optimized to improve aerodynamic efficiency but was expected to aid the deployment behavior. Each case was tested at 16 m/s and 25 m/s except case 3. Case 5 has an additional strip of tape on one side of the wing. All tests demonstrated similar deployment behavior and only one series of images are display in this thesis (shown in fig. 5.21). The direction of the airflow is from right to left in the picture. The lift and drag coefficient for each case was plotted, where a solid red line indicated the drag value and solid blue line indicated the lift value.

Results

5.2.1 WSE Case 1 : Baseline

Wind tunnel tests using only inflatable wing were repeated and will be used as a baseline for comparison. A representation of the dynamic loading from the previous tests is shown in section 5.1 at AOA of 0 degree. At 16 m/s , the wing deployed, followed by a strong drag dominate vibration for about 2 s. The wing immediately folded backward upon release. Lift was dominant for about 5 seconds as the wing was still in a kinked position, with a folded half. As the folded wing pressure gradually increased, the lift decreases before the wing straightened out to achieve its final shape. Based on the observation at $V_\infty = 25$ m/s, the wing deployment had experienced continuous vibration released due to wing flapping. The vibration lasted about 5 seconds . The drag was dominance throughout the deployment.

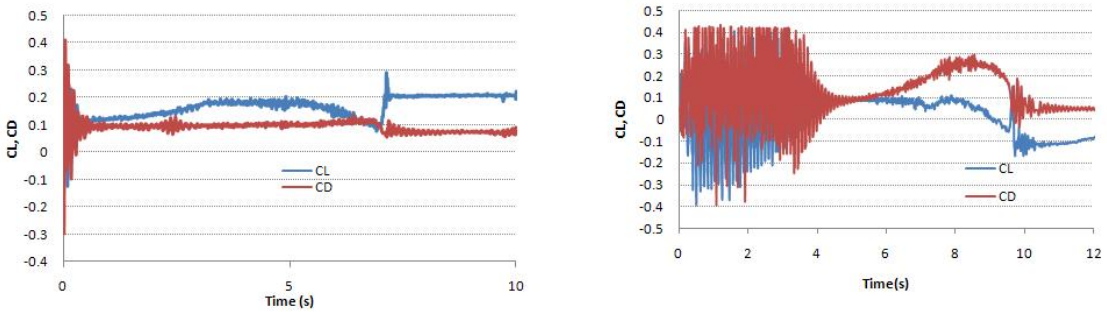

(a) 16 m/s. (b) 25 m/s.

Figure 5.22: WSE Case 1.

5.2.2 WSE Case 2 : Reinforcement at the Quarter Chord

Tapes were attached at the quarter chord on both side of the wing, on bumps number 5, 6, and 7. At $V_\infty = 25$ m/s, the drag was dominant upon deployment, compared with the deployment at 16 m/s.

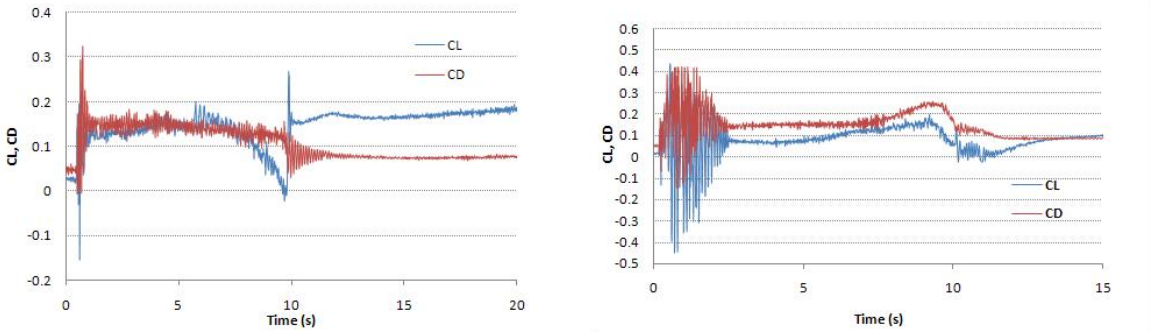

(a) 16 m/s. (b) 25 m/s.

Figure 5.23: WSE Case 2.

5.2.3 WSE Case 3 : Slow vs. Fast Inflation Comparison for Case 2

Slow vs. fast inflation comparison for case 2 at 16 m/s. At slow inflation rate, wing flapping was observed 10 s after deployment. Drag was dominant.

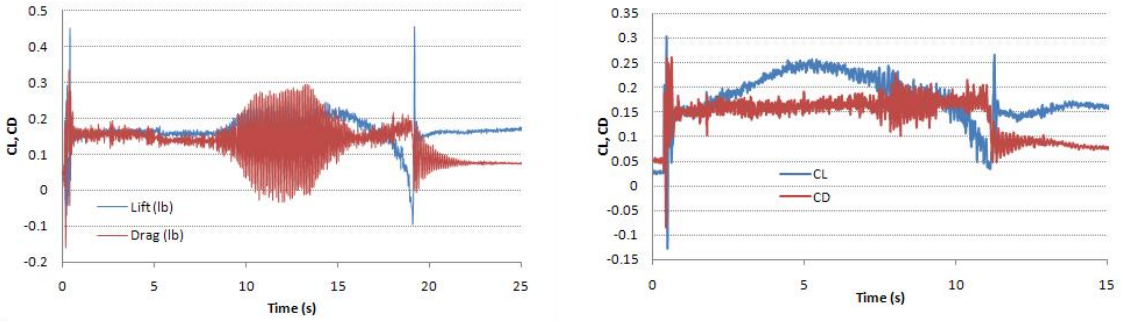

(a) Slow inflation rate.

(b) Fast inflation rate.

Figure 5.24: WSE Case 3.

5.2.4 WSE Case 4 : Reinforcement at Bottom Surface

Reinforcement at bottom surface, only at bump 5,6 and 7. No wing flapping was observed after deployment.

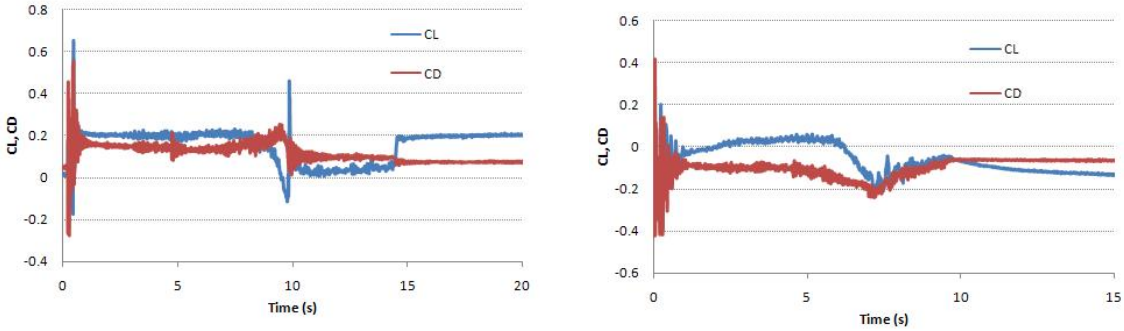

(a) 16 m/s.

(b) 25 m/s..

Figure 5.25: WSE Case 4.

5.2.5 WSE Case 5 : Tapes on both Quarter Chord and Leading Edge

Tapes were attached on bumps number 5, 6, and 7, on both sides of the wing, plus one strip on top of bumps, number 3 from the leading edge. This extra strip of tape was expected to straighten the wing leading edge upon deployment. In comparison, both drag and lift force was doubled at $V_\infty = 25$ m/s and showed similar trend as inflation progress in time.

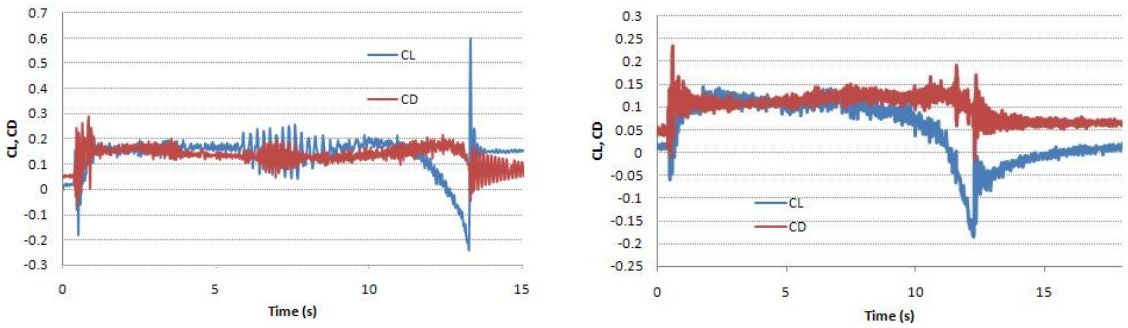

(a) 16 m/s. (b) 25 m/s.

Figure 5.26: WSE Case 5.

Discussions

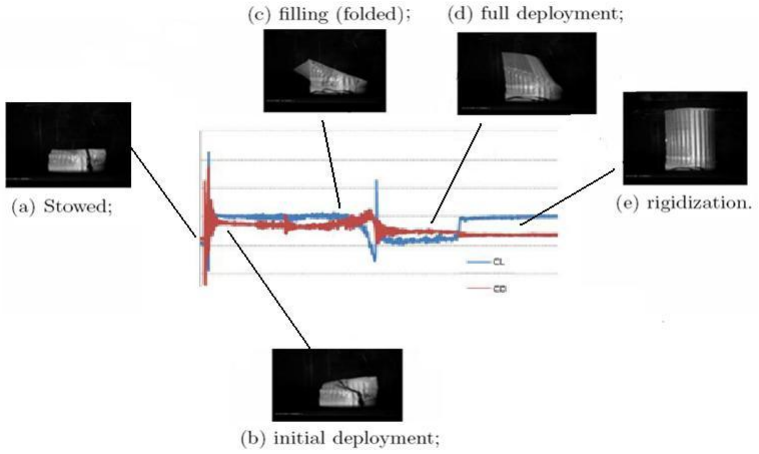

Figure 5.27: WSE : Transient lift and drag variation with wing stages. (a) Stowed; (b) initial deployment; (c) filling (folded); (d) full deployment; (e) rigidization.

A significant vibration was observed immediately upon release. This might be a contribution from the spring load tape as it was pre-loaded during stow configuration. Whether the strong vibrations upon release would cause serious instability during flight is still an open question. After deployment, the wing was kinked as the unpressurized wing portion was blown backward by the airflow. It was later followed by vibration or flapping as the wing unfolded itself as pressure increased. In some cases like case 3 (a), the wing experienced flapping when it was in folding position.

The last peak was an indication of final deployment for the rest of the wing. It was a result of the unfolding of the wing from the kinked position as pressure increased to its final pressure. Overall, all tests demonstrated a similar behavior as seen in the WA tests and wing flapping issue still required attention. Therefore, this issue lead to the use of Velcro as an innovative design to mitigate the deployment behaviors.

5.3 Wing with Deployment Control Elements (DCE)

For the past four decades, Velcro USA Inc. has manufactured an extensive line of fastener systems for applications ranging from aerospace to deep sea and between. However, in the research herein, VELCRO brand hook and loop fastener was only being used as a restraint mechanism for internal subsystem of the IFI or BIG BLUE. It was never brought into attention as a solution to control the deployment behavior of the inflatable wing. This method was later applied in this research due to creative thinking and application. This fastener was expected to outperform the spring tape and help alleviate the dual behavior of wing flapping and folding as demonstrated in previous tests. The Velcro strip was made of but precision woven of 100% polyester yarn and can be easily integrated onto the surface of the inflatable wing with reliable holding power. Preliminarily test showed that the Velcro allowed the inflatable wing to be stowed tightly even tested under highest predicted flight velocity of 29m/s (67 mph). It was also more reliable then to previously restraint mechanism used in BIG BLUE project. Initially, there were only a total of 4 cases investigated, until an interesting observation was found and presented as Case 5. Preliminary test was conducted using full-scale semi span wing to verify this unconventional method.

All cases were tested in the wind tunnel at 16 m/s (36 mph). The first three cases had similar Velcro placement on both side of the wing. Fig. 5.28 shows that Velcro strips were attached on the 4th and 8th bumps on both sides of the wing. The impact of mass flow rate on deployment behavior was also being investigated. Comparison

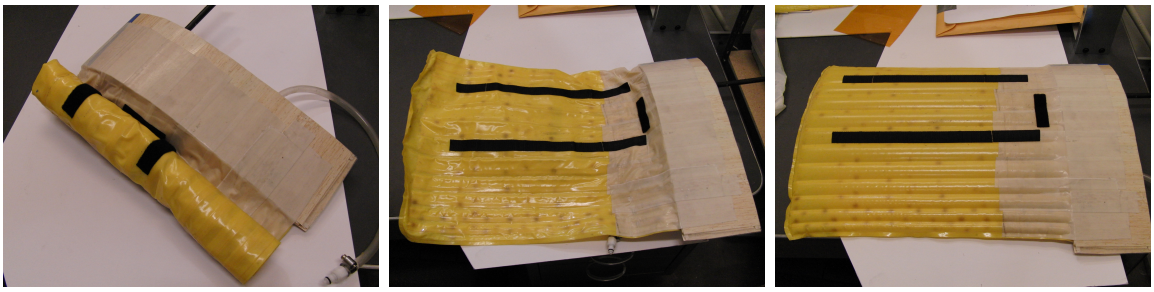

(a) stowed (b) fully unfolded (c) fully inflated

Figure 5.28: DCE : Small scale wing with DCE.

was made between the use of electric air pump and lab air hose. The results were presented as case 2 and 3. Later investigation on case 4 showed that extended Velcro length until the wing tip significantly improved the deployment behavior, even at a stall angle of attack at 12 degree. Lastly, case 5 presents the results of the relationship between lift coefficient and change in internal pressure.

Results

5.3.1 DCE Case 1: Wing Alone (WA) vs. Wing with DCE at AOA of 0 degree

Graph in fig. 5.29 shows a significant changes in lift coefficient between two wing configurations. For the WA configuration, the wing experienced both flapping and folding behavior upon release. On the other hand, the wing with DCE had a stable and gradually increasing lift force and eliminated the adverse behaviors. Fig. 5.30 showing the instant state of the wing 5 second after the deployment. This shows that the wing with DCE did not demonstrate an abrupt change in lift during deployment. Both achieve the final pressure close to 5 psi as shown in fig. 5.30. The Velcro's rough surface affected the wing aerodynamics. The result also shows that the lift generation was reduced by about 9 percent with the use of Velcro. The airflow is moving from top to down in the picture.

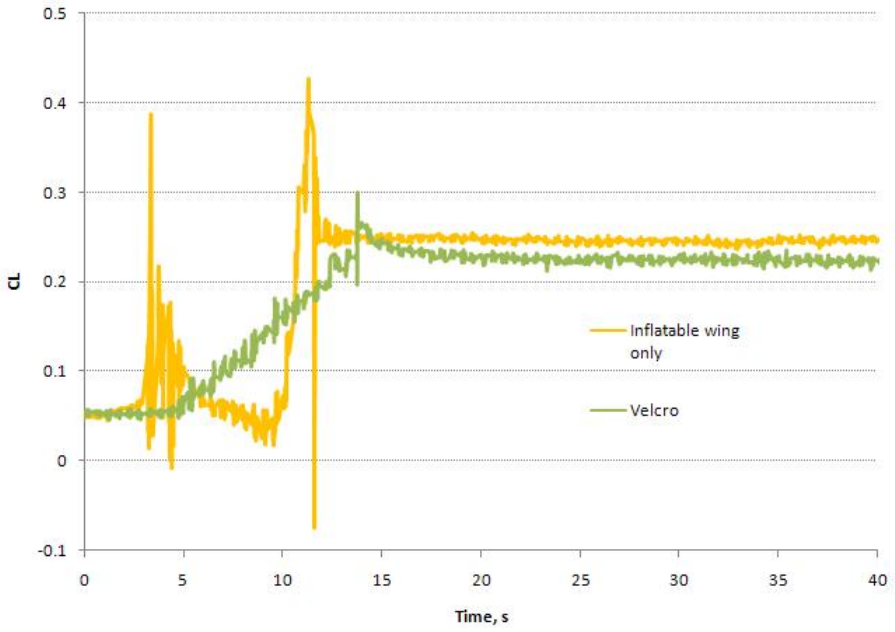

Figure 5.29: DCE Case 1 : Lift coefficient in comparison with inflatable wing only.

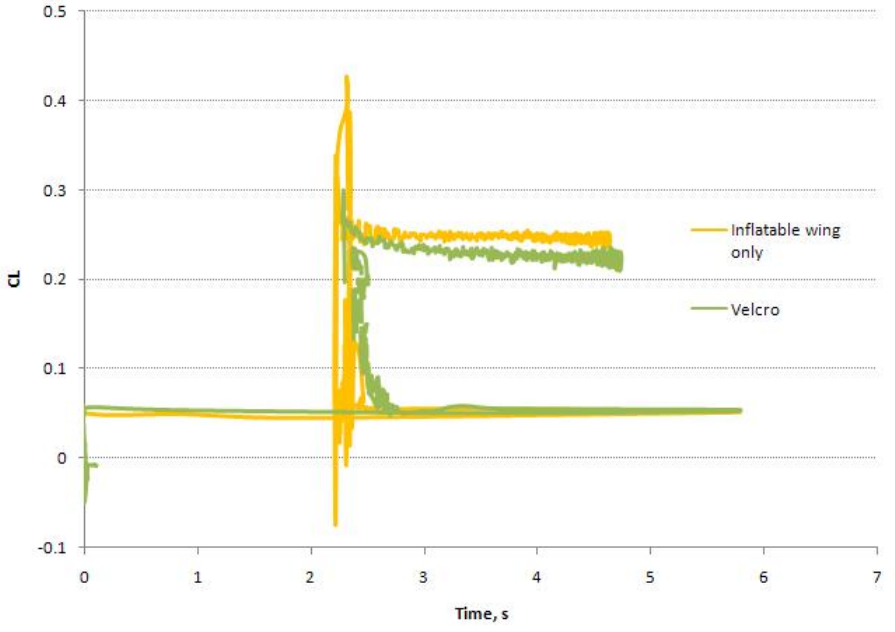

Figure 5.30: DCE Case 1 : Lift coefficient with respect to pressure.

5.3.2 DCE Case 2 : Various AOA from 0 to 12 using Electric Air Compressor

Based on the observation made from DCE case 1 result, the wing with DCE was systematically tested at AOA of 0 to high angle of attack. The lift coefficient, drag coefficient, and pressure, with respect to time, were measured using lab-view. Both flapping and folding behaviors were successfully mitigated at AOA 0, 4 and 8 with minor vibrations as indicated in the graph. This might have been the contribution of the Velcro as it gently separated during wing deployment. The full deployment time was took about 15 seconds, and is considered slow. Lift increased as the AOA increased from 0 to 12, as the wing span increased. However, wing root bending was observed for wing deployment at AOA of 12. A valley was observed in the graph as the wing bent upward before plunging downward to straighten itself as pressure increased. Since the wing was at the stall angle, wing vibration due to flow separation was clearly seen in the change in amplitude after the wing was fully deployed at AOA of 8 and 12. Please note that the gradual decrease in lift for AOA of 8 and 12 was due to the decreasing of airflow after the wind tunnel was turned off. Fig. 5.36 showed that the Velcro could be released at low wing pressure of about 1 psi. However, a significant change in pressure was observed at AOA of 12 as the wing bent upward. Fig. 5.36 also shows slight increase of pressure at 15 second. The airflow is moving from top to down in the picture.

(a) t =0 (b) t = 4 (c) t = 12 (d) t = 15

Figure 5.31: DCE Case 2 : AOA = 0.

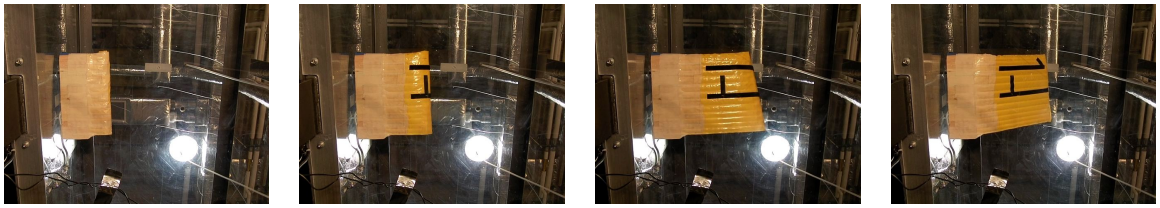

(a) t =0 (b) t = 4 (c) t = 12 (d) t = 15

Figure 5.32: DCE Case 2 : AOA = 8.

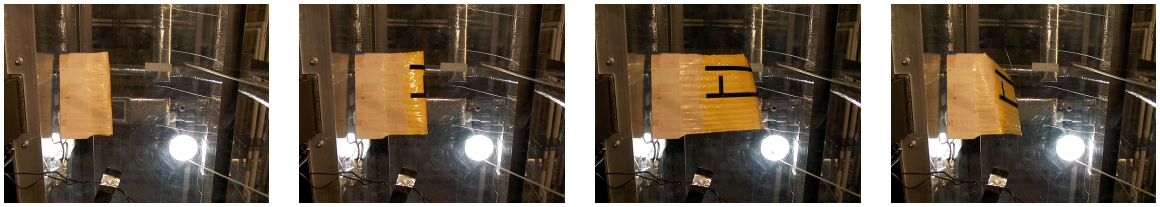

(a) t = 0 (b) t = 4 (c) t = 12 (d) t = 15

Figure 5.33: DCE Case 2 : AOA = 12.

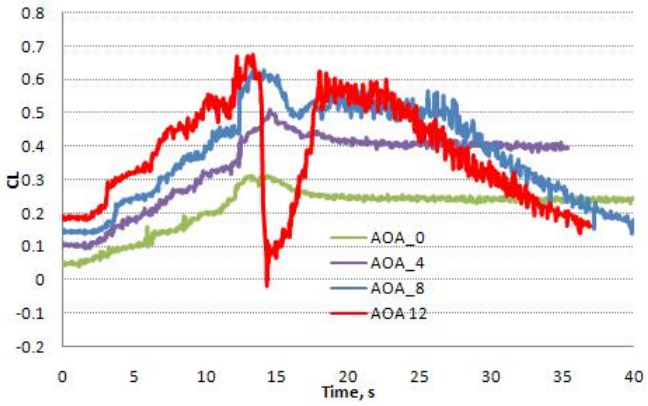

Figure 5.34: DCE Case 2 : Lift coefficient with respect to time from AOA 0 to 12.

5.3.3 DCE Case 3 : Varying AOA from 0 to 12 using Regulated Compressed Air

Case 3 is similar to case 2 but was using regulated air pressure. The Velcro strips was extended till the tip of the wing as compared to Case 2. Fig. 5.38 shows the different Velcro settings. The mass flow rate from the regulated air hose was higher compared to case 2 and shortened the deployment time. Case 2 took about 16 seconds for the wing to fully deployed and case 3 took about 9 seconds. Furthermore, a high-

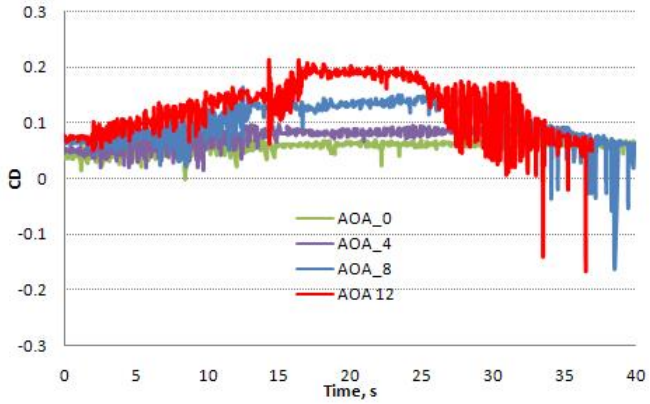

Figure 5.35: DCE Case 2 : Drag coefficient with respect to time.

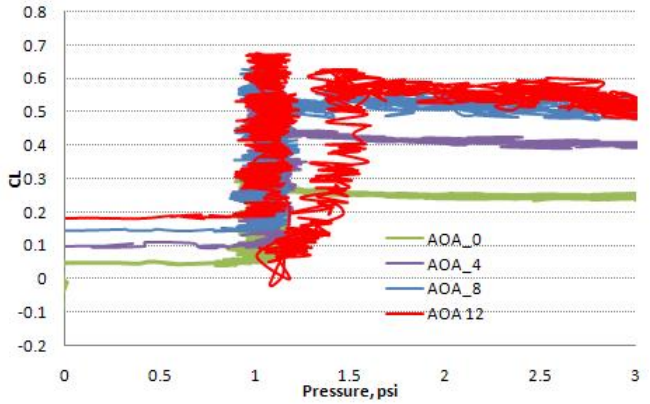

Figure 5.36: DCE Case 2 : Lift coefficient with respect to pressure.

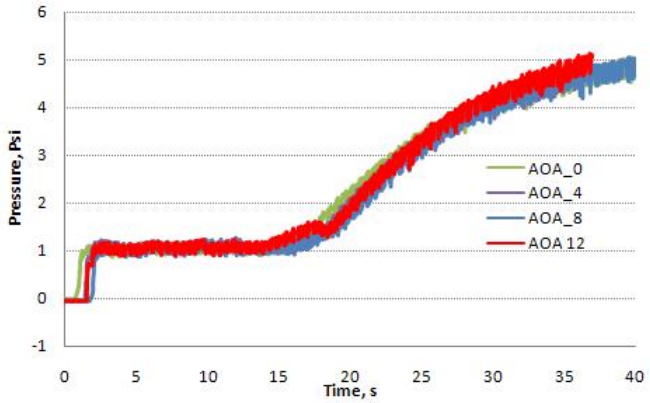

Figure 5.37: DCE Case 2 : Pressure history.

pressure spike was observed. Fig 5.48 shows that the spike marks the beginning of the deployment after the air valve was opened and experience a suddenly change in pressure. The wing experienced constant pressure expansion at 2.5 psi before it was fully extended. Once the wing was fully extended, the pressure gradually increased until it reached 5 psi. Fig. 5.46 shows the comparison in terms of lift versus time. The changes made on the Velcro setting showed a significant improvement where the deployment was complete controlled even at stall AOA of 12 degrees. The results should be compared to fig. 5.34 in case 2. Careful observation shows a sharp decrease in lift after the wing was fully expanded and reaches a peak in lift. Fig. 5.46 shows the peak value of lift coefficient for each AOA in comparison with both stowed and fully deployed configurations. Therefore, we decided to investigate these phenomena that lead to the sudden 30% increase in lift. The result was presented in DCE case 5. The airflow is moving from top to down in the picture.

(a) t = 0 (b) t = 2 (c) t = 5 (d) t =9

Figure 5.38: DCE Case 3 : AOA = 0.

(a) t = 0 (b) t = 2 (c) t = 5 (d) t = 9

Figure 5.39: DCE Case 3 : AOA = 4.

(a) t = 0 (b) t = 2 (c) t = 5 (d) t = 9

Figure 5.40: DCE Case 3 : AOA = 8.

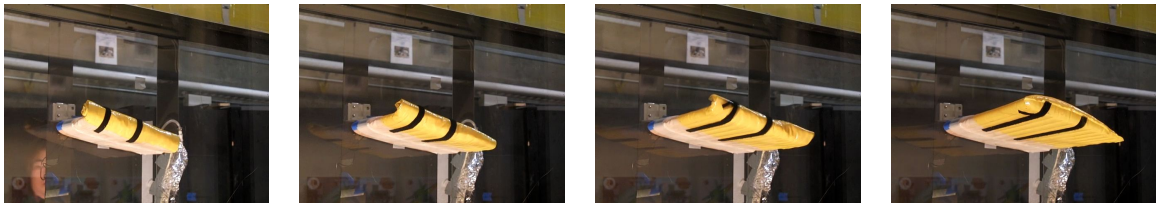

(a) t =0 (b) t = 2 (c) t = 5 (d) t = 9

Figure 5.41: DCE Case 3 : AOA = 12.

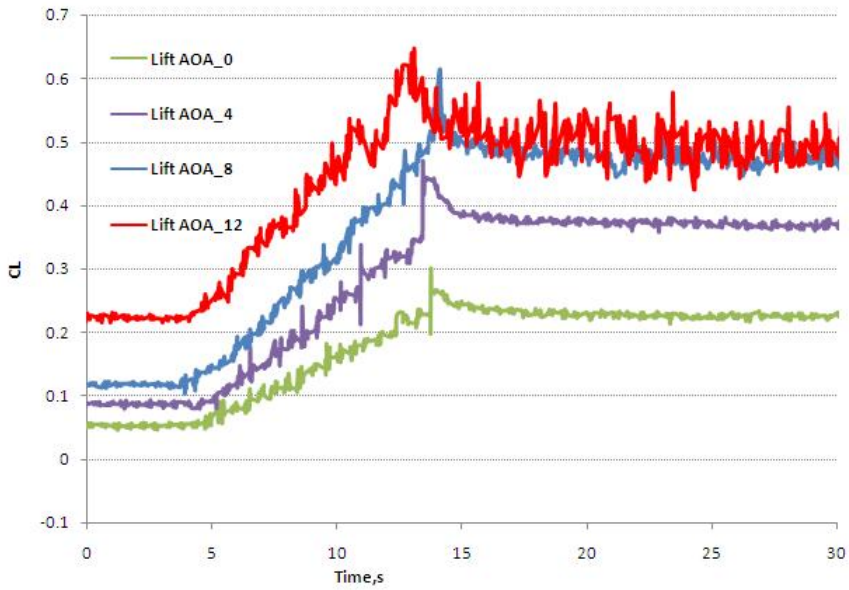

Figure 5.42: DCE Case 3 : Lift coefficient with respect to time.

5.3.4 DCE Case 4: Impact of Velcro Setting on Deployment Behavior at Stall AOA

Based on the improvement observed at stall AOA in Case 3, Case 4 presents the results for comparing different Velcro setting. Wind tunnel test was repeated at AOA

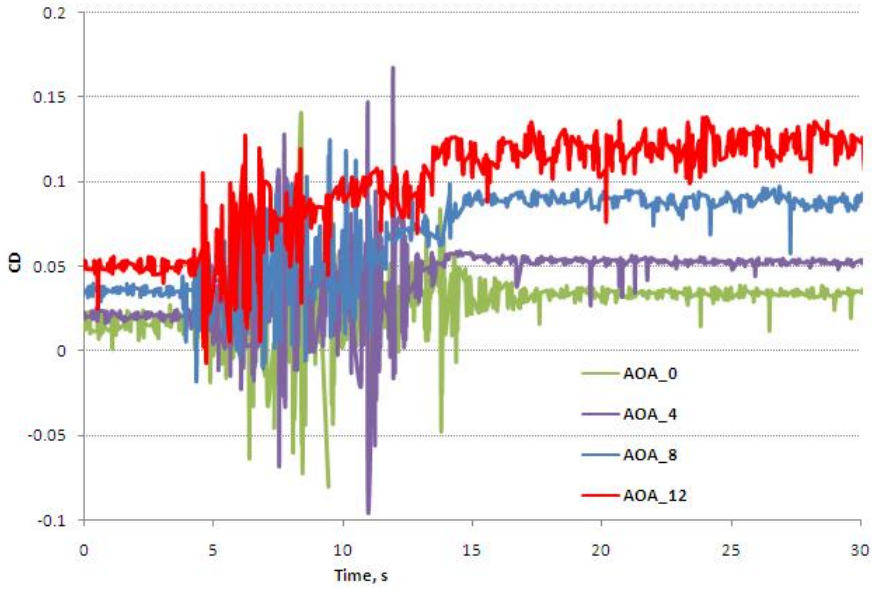

Figure 5.43: DCE Case 3 : Drag coefficient with respect to time.

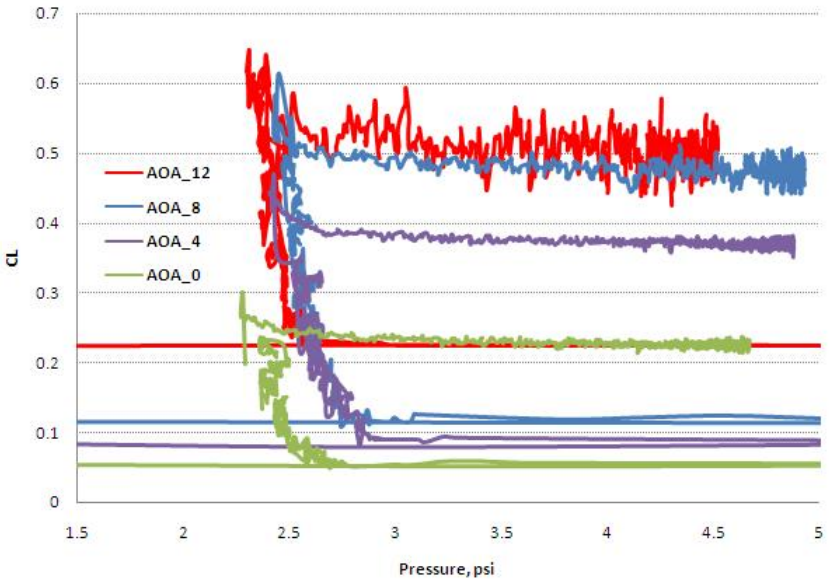

Figure 5.44: DCE Case 3 : Lift coefficient with respect to pressure.

of 12 to verify the impact of Velcro setting on the deployment behavior. Fig. 5.49 shows the 4 different Velcro configurations on the wing and its relative results in later

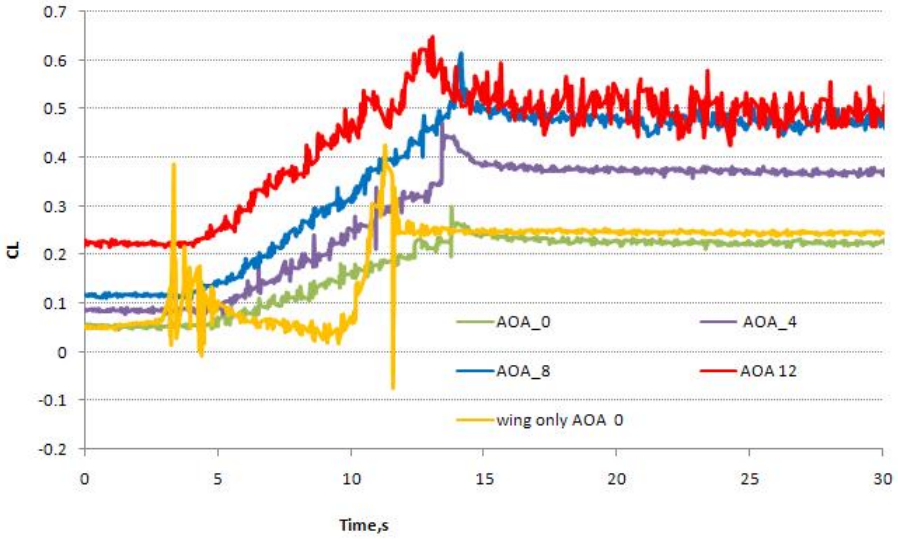

Figure 5.45: DCE Case 3 : Lift coefficient with respect to time compare with only inflatable wing.

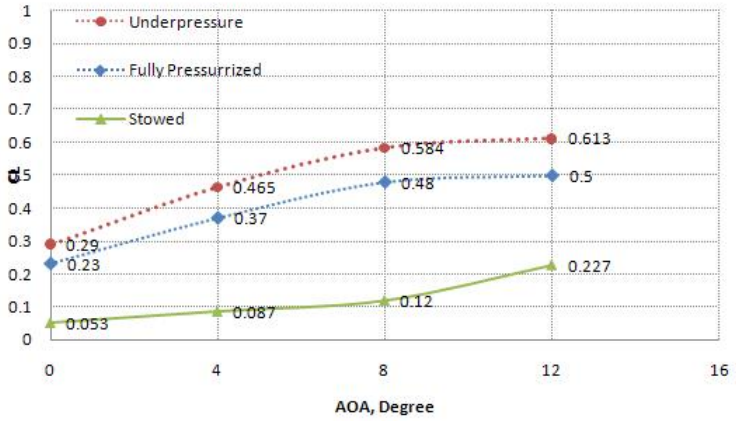

Figure 5.46: DCE Case 3 : Lift coefficient vs. angle of attack.

graphs. Different width of Velcro was also used to make the comparison. Note that the airflow was reduced for Set 1 after it was fully deployed, and therefore a clear reduction in lift after 20 seconds. The airflow is moving from top to down in the picture.

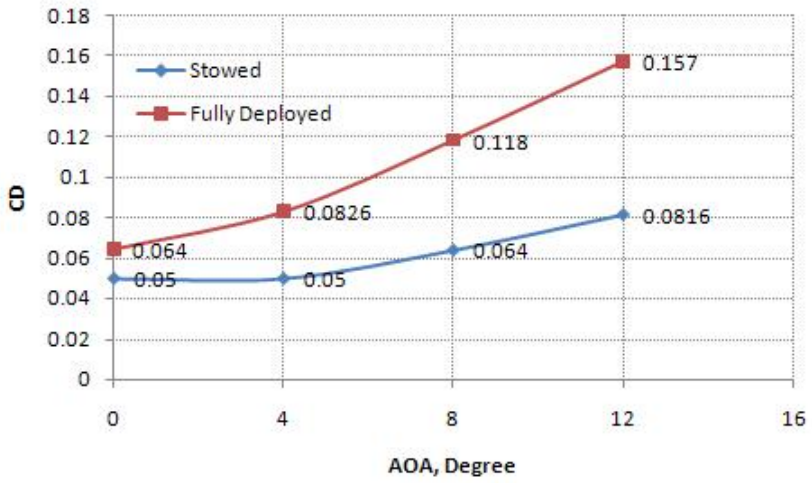

Figure 5.47: Drag coefficient vs. angle of attack.

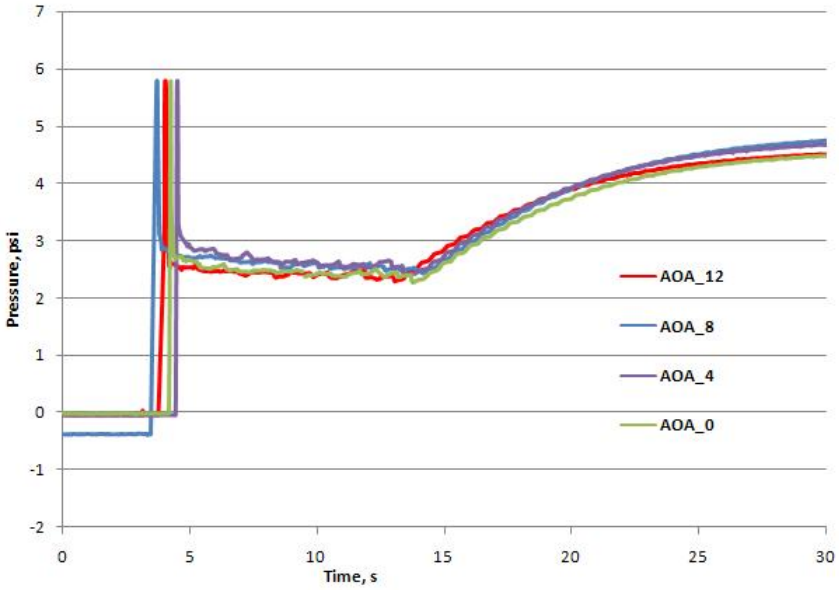

Figure 5.48: DCE Case 3 : Pressure history from AOA 0 to 12.

The results clearly show that the additional length of Velcro start from the wing tip result in a stable deployment. Without Velcro at the tip of the wing, both high and low mass flow rate (set 1 and 4) experienced wing bending and thus lead to a sudden drop in pressure and lift at the same AOA. This lead to the conclusion that

(a) velco set 1 (low pressure) and set 4 (high pressure) : 0.75 inch width (b) velcro set 2 : 0.75 inch width (c) velcro set 3 : 2.0 inch width

Figure 5.49: DCE Case 4 : Different velcro attachments.

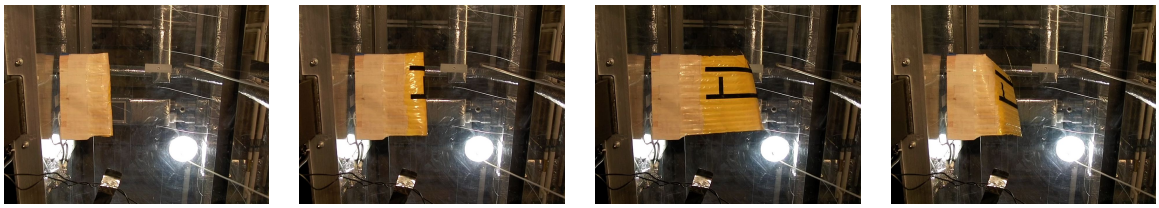

(a) t = 0 (b) t = 4 (c) t = 12 (d) t = 15

Figure 5.50: DCE Case 4 : Set 1.

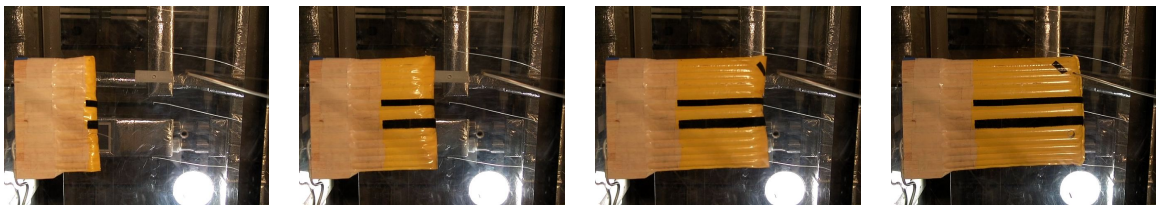

(a) t = 0 (b) t = 4 (c) t = 7 (d) t =10

Figure 5.51: DCE Case 4 : Set 2.

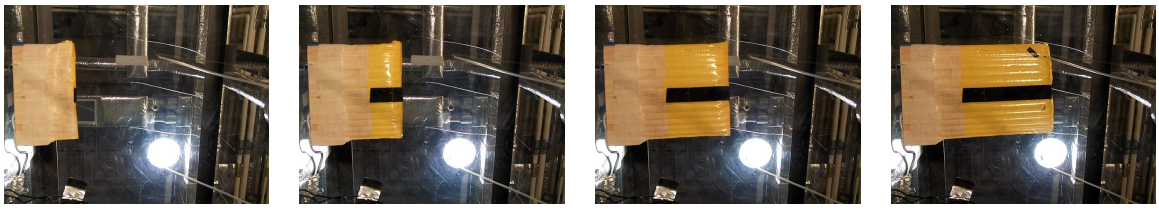

(a) t = 0 (b) t = 4 (c) t = 7 (d) t =10

Figure 5.52: DCE Case 4 : Set 3.

constant pressure expansion can be achieved by attaching the Velcro from the wing tip. In addition, the strength of the Velcro also has slight impact on the deployment

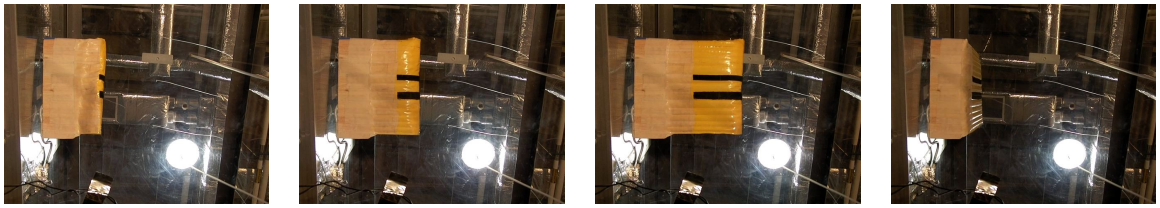

(a) t = 0 (b) t = 4 (c) t = 7 (d) t =10

Figure 5.53: DCE Case 4 : Set 4.

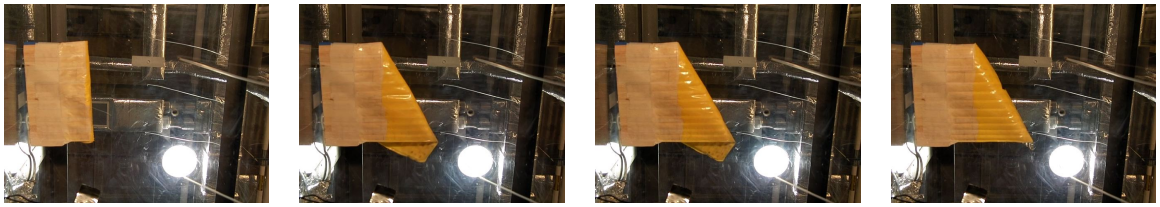

(a) t = 0 (b) t = 4 (c) t = 7 (d) t =10

Figure 5.54: DCE Case 4 : Set 5.

dynamic. The use of 2 in Velcro strip (set 3) has caused a momentarily increase in pressure for about 1 second after 34 second upon deployment. This shows that higher pressure is required to overcome the Velcro bonding strength, due to larger surface area.

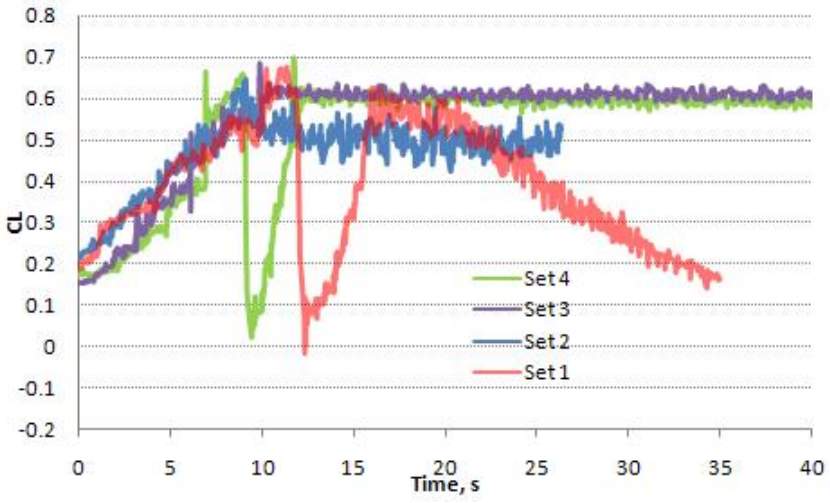

Figure 5.55: DCE Case 4 : Lift coefficient with respect to time.

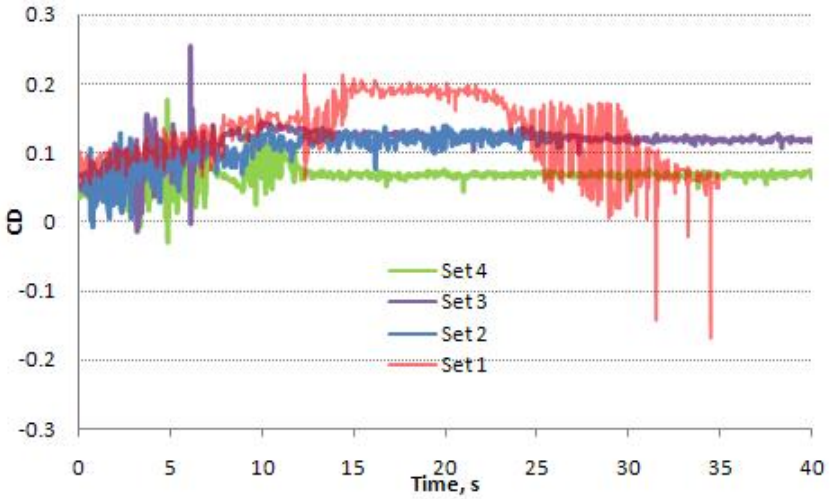

Figure 5.56: DCE Case 4 : Drag coefficient with respect to time.

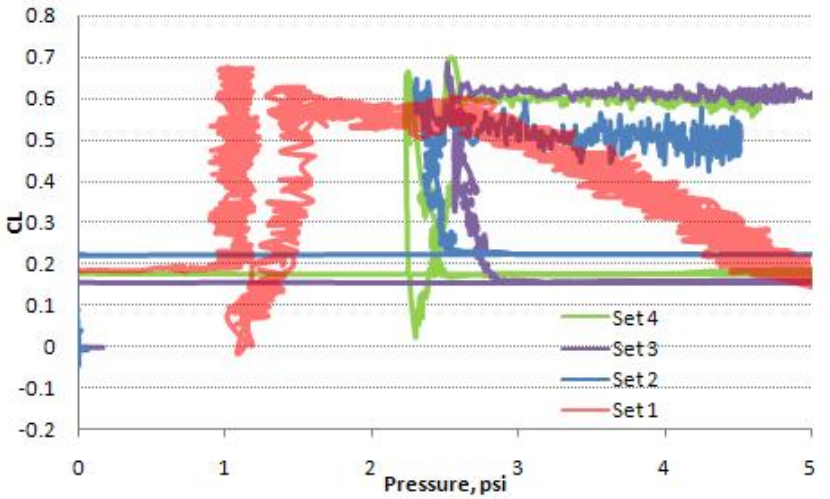

Figure 5.57: DCE Case 4 : Lift coefficient with respect to pressure.

5.3.5 DCE Case 5 : Impact of Partially Inflated Wing on Lift Generation

A delayed inflation test was conducted and was compared with the rapid deployment in DCE case 2 at AOA of 0 degree. Air hose was manually adjusted to slow down the deployment rate as the wing approached its final expansion. The air hose was completely shut off to maintain the wing pressure and measure the change in lift as shown in fig. 5.60. Please note, that the black dash line is shows the internal pressure

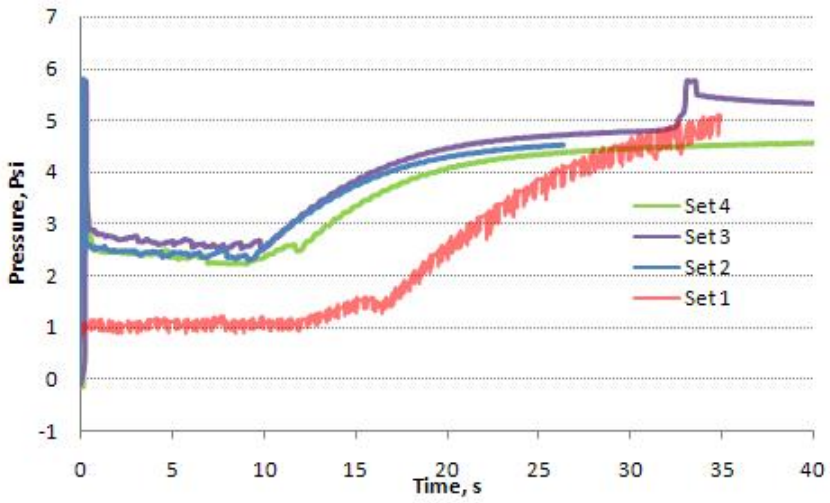

Figure 5.58: DCE Case 4 : Pressure history.

of the wing, even though the graph shows a zero pressure reading. The air mass flow rate was ceased as soon as the valve was shut off. The air hose was opened after 10 seconds and a noticeable drop in CL was observed as shown in fig. 5.61. When comparison was made with baseline inflatable wing, similar trend was noticed. It was clearly shows that the partial inflation at constant provided higher lift compared to the fully inflated wing. The constant value of lift coefficient is matched with the lift peak, right before a sharp drop occurred for the rapid deployment case. Close examination on the wing surface showed that the bumps on the inflatable wing was flattened when wing is under-pressure as shown in fig. 5.59. At this period, dynamic pressure was higher than the wing internal pressure even though the wing was rigid enough to prevent bending moment. We conclude that as the bumps around the inflatable wing were flattening due to under pressure; the airfoil shape was close to an ideal airfoil, thus a "smoother" surface to promote an increase in lift. The airflow is moving from top to down in the picture.

(a) Underpressure (b) Fully pressurized

Figure 5.59: DCE Case 5 : Bumps deformation due to dynamic pressure.

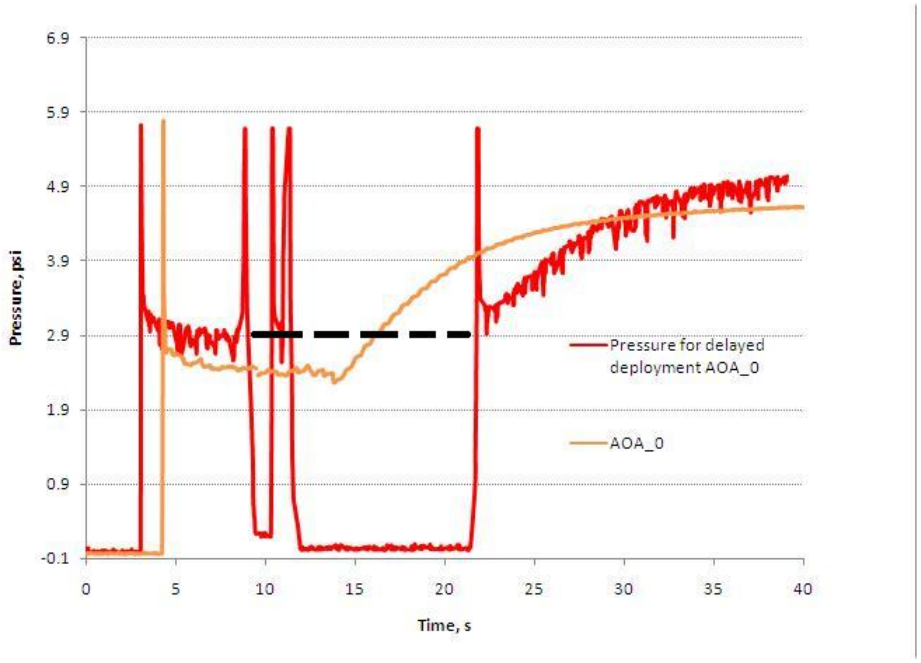

Figure 5.60: DCE Case 5 : Pressure history comparison.

5.3.6 Full Scale Preliminary Test

Based on the full-scale-truck-test result, strategically placed Velcro strip improve the deployment by eliminating the flapping and folding behaviors at wind speed up to 16 m/s (36 mph). This behavior was similar to the wind tunnel test results. The Velcro helps keep the wing rigid as the wing gradually expanded from root to tip.

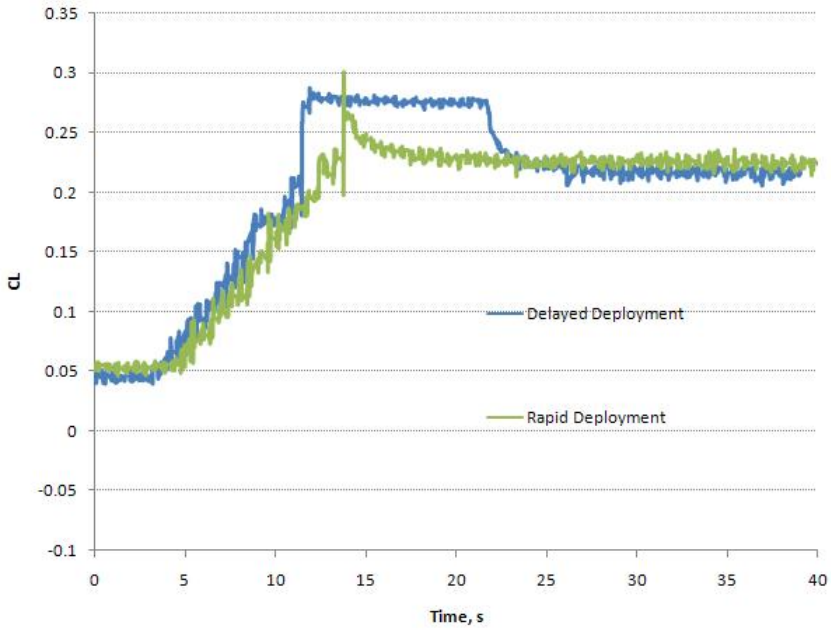

Figure 5.61: DCE Case 5 : Lift coefficient with respect to deployment time.

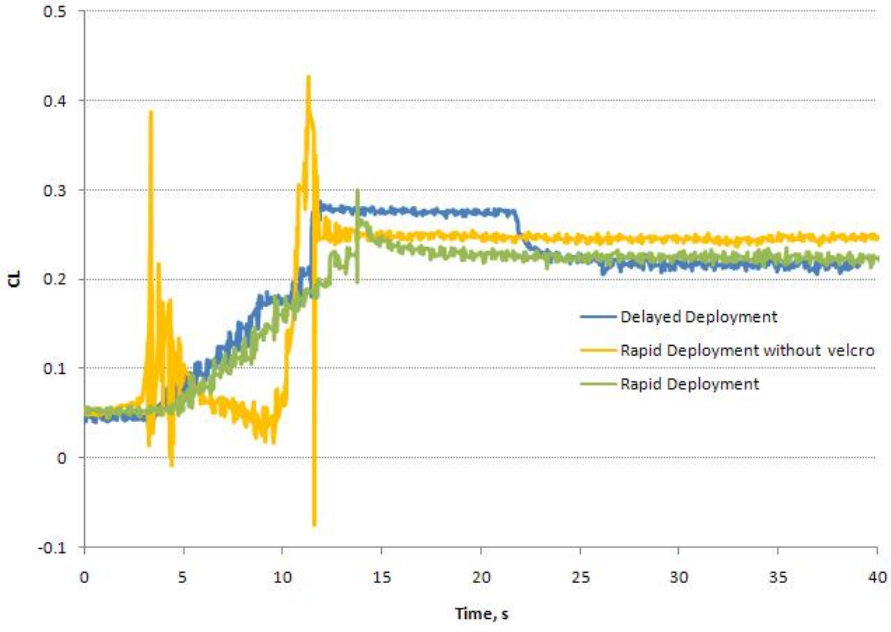

Figure 5.62: DCE Case 5 : Comparison with baseline inflatable wing deployment.

This created enough resistant to bending moment and thus prevented the flapping or folding behavior. This method provides constant volume expansion thru out the inflation process since the wing volume slowly expanded without any kinked section. The semi-span wing was inflated by using the inflation system connected to CO2 canister. The air valve was manually controlled. The wing volume took about 33 gram of CO2 to achieve it final shape at 6 psi. In addition, the Velcro could be replaced the cat-collar as stowage restraint prior to deployment. All unprecedented preliminary tests have been successfully demonstrated using Velcro.

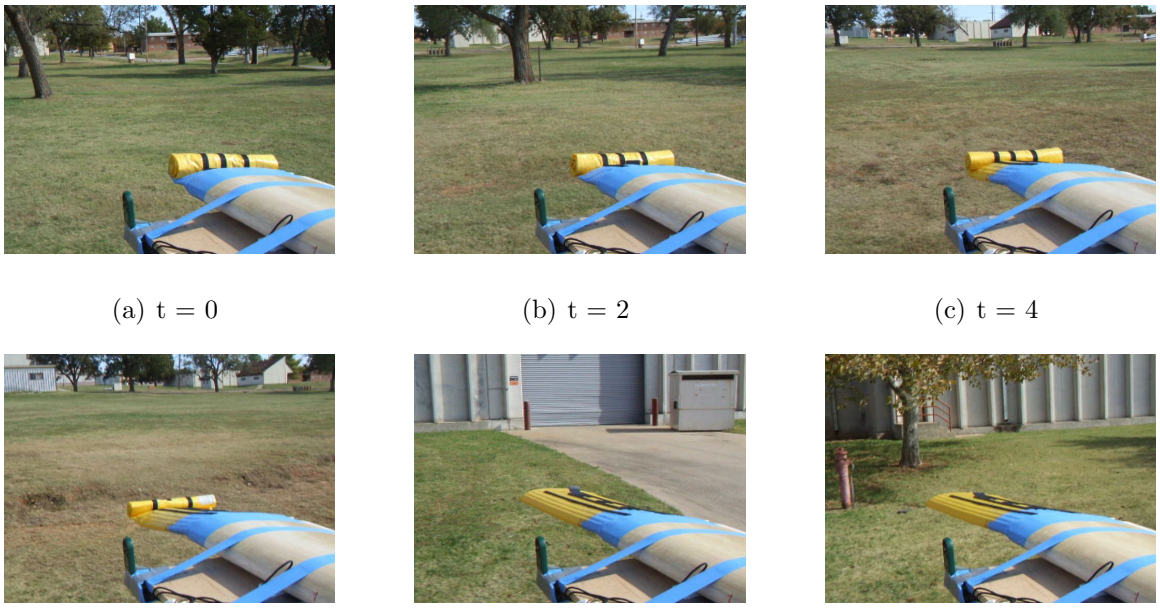

(a) t = 0 (b) t = 2 (c) t = 4

(d) t = 6 (e) t = 9 (f) t = 11

Figure 5.63: DCE : Full-scale-truck test.

5.3.7 Symmetric Deployment Test

Another stability issue was also needed to be tackled for the morphing wing concept: adverse roll due to unbalance wing span expansion during deployment. Symmetric deployment was required to achieve balance in flight. If one wing deployed faster than the other, that might lead to an adverse roll on the aircraft in flight. In addition, air pressure from the air tank needed to be equally distributed to both wings. Each wing

was connected to the hose with equal lengths, to avoid inflation delay since the air flow was affected by the hose length and diameter. Most importantly, this test was to see whether the Velcro strips could be separated easily and synchronized on both wing during deployment. Three static deployments tests were repeated to check the deployment synchronization and the total inflation time took about 10 second. All tests showed a similar behavior, thus only one test result is shown here in fig. 5.64 (a) to (f).

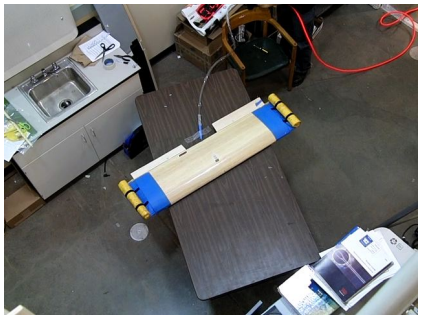

(a) t = 0

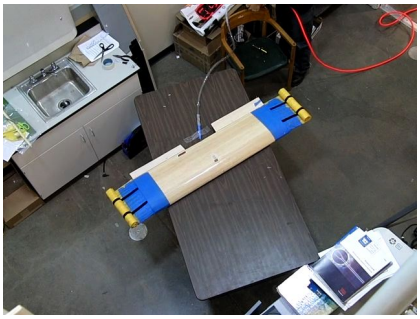

(b) t = 2

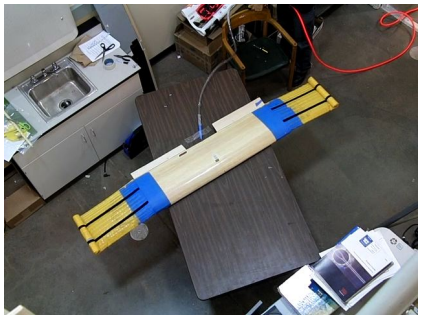

(c) t = 4

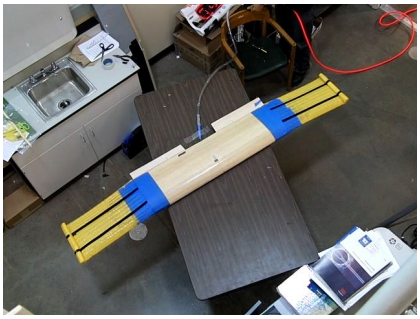

(d) t = 6

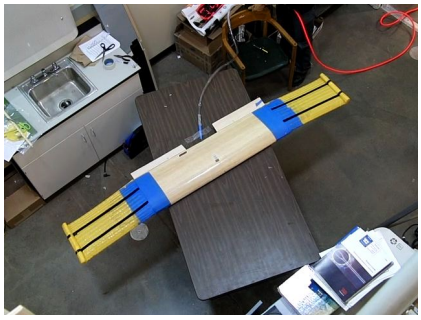

(e) t = 8

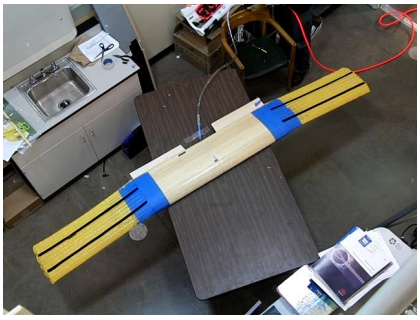

(f) t = 10

Figure 5.64: Static symmetric deployment test.

5.3.8 Gimbal Static Deployment Test

The gimbal tests measures the motion of the symmetric deployment for both WA and DCE cases. In comparison with WA deployment, DCE deployment exhibited a distributed vibration throughout the expansion period. Only two significant peaks were recorded on WA deployment. The deployment sequences are shown in fig. 5.68 and fig. 5.69. These images show that the distributed vibrations were mainly due to the separation motion of the Velcro strips as the wing pressure gradually increased. For WA configuration, both wings just dropped down symmetrically upon release and remained static in motion as the pressure slowly built up from time t = 2 seconds to t = 8 seconds. The final peak was recorded as the wing straightened it once it reaches a critical pressure. In contrast the wing with DCE remained rigid as the wing section slowly expanded.

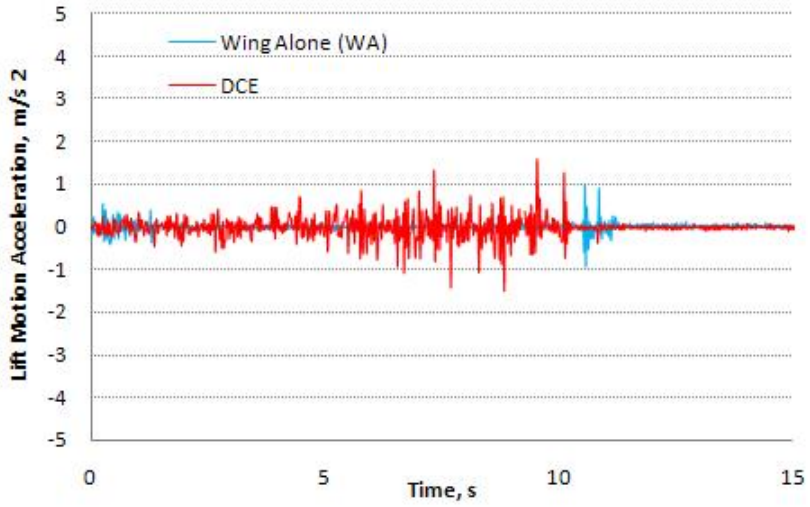

Figure 5.65: Vertical motion.

Discussion

The inflatable wing was successfully deployed using the Velcro as the control element. With the proper placement of Velcro, wing folding, due to dynamic pressure could

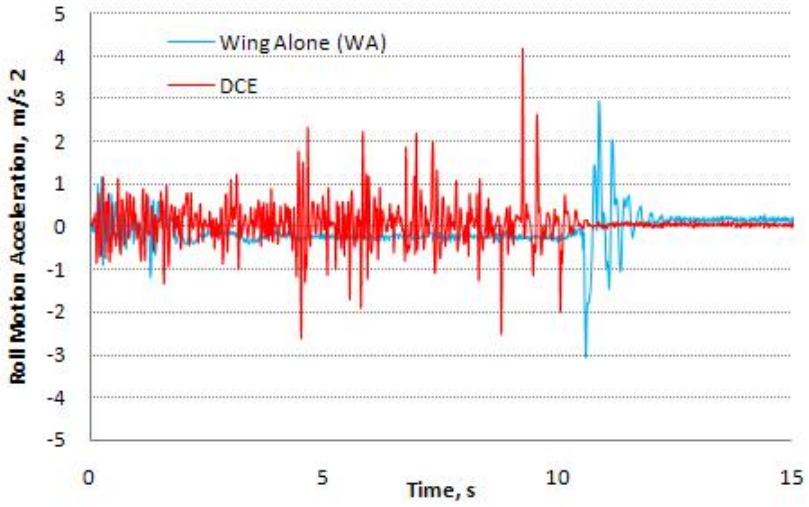

Figure 5.66: Roll motion.

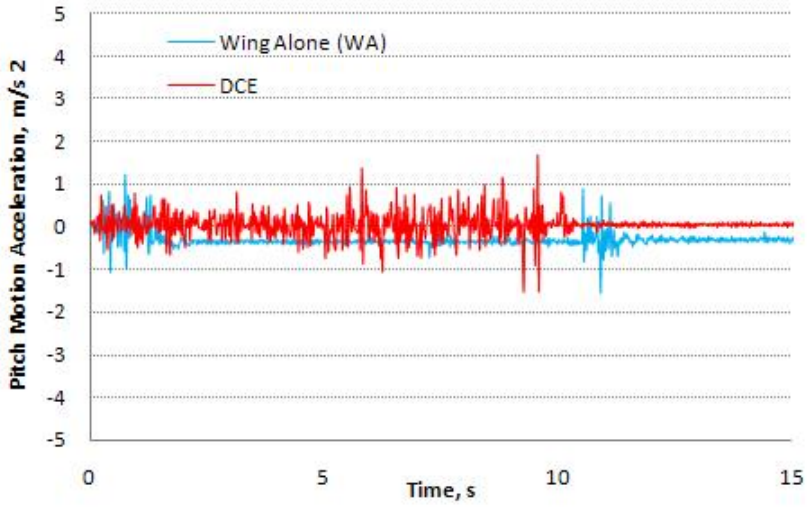

Figure 5.67: Pitch motion.

(a) t = 0 (b) t = 2 (c) t = 8 (d) t = 11

Figure 5.68: Static deployment for wing alone (WA).

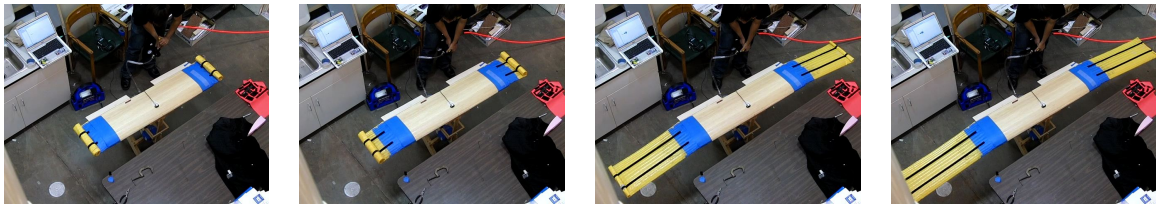

(a) t = 0 (b) t = 2 (c) t = 8 (d) t = 11

Figure 5.69: Static deployment for wing with DCE.

be eliminated, compared to the earlier investigation using inflatable wings only and stiffener. The flapping behavior was completely minimized and only minor vibrations were observed at stall AOA of 8 and 12. Furthermore, the deployment test showed that partially inflated wing could manipulate the lift by reducing the pressure to produce a smoother airfoil shape. Since inflatable wing has been successfully demonstrated in flights as conducted like the NASA I2000, BIG BLUE Project and AIRCAT, these results can lead to new control system by using pressure difference between the two wings to provide roll control. Roll control could be achieved without deforming the camber using servo actuator as described by Simpson *et. al* in chapter 4.

CHAPTER 6

Test Vehicle and Performance Predictions

This section introduces the research aircrafts and the inflation system designs for the morphing wing aircraft concept. Two research aircrafts are presented here: IFI-A and IFI-B. IFI-A was successfully tested in flight at both low and high configuration using pre-inflated wings. The purpose of the pre-inflated flight test is to verify that the polyurethane coated nylon wings can sustain high bending moments in flight. The flight test was successful and the flight was documented by The Discovery Channel crew in June 2007. IFI-B was later constructed to integrate with an onboard inflation system for in-flight morphing. However, this aircraft is still under construction. For the inflation system design, weight and mass flow rates were the two main criteria that needed to be factored into the onboard inflation system design. Two types of inflation systems are also introduced here that use a COTS air tank. One is by using an aluminum tank widely used by RC aircraft hobbyists. The second one is by employing a CO2 canister. An aluminum tank was pressurized at pressure ranging from 90 to 115 using a laboratory compressed air hose. The static deployment test was conducted on this system to investigate the deployment rate and the change of pressure as the wings were slowly inflated. To provide similar wing air volume, the aluminum tank is a low pressure, lightweight and high occupancy volume storage (multiple tanks are needed) while the CO2 is the contrary. Regardless of which system is chosen, both designs can still provide enough air volume to pressurize the inflatable wing. This chapter discuses the characteristic of the research aircrafts and the inflation system developed in this research. Flight stability and control during

deployment are also discussed at the end of this chapter.

6.1 IFI-A Aircraft

In-Flight-Inflatable (IFI) as shown in fig. 6.1 was constructed to test the feasibility of the morphing concept using the low pressure wing. Silicon tape was used as a bonding medium to attach both wings. Multiple stripes of silicon tape were wrapped around the rigid wing tip and the root of the inflatable wing to create a makeshift wing sleeve. During flight, this concept allows the aerodynamic loads to be transferred evenly from the inflatable wing to the balsa skins of the rigid wing skin. The flight test from BBV has justified the feasibility of this method. The combined inflatable wings and rigid wing section give a span of 120 inches from tip to tip, and has a surface area of 1680 square inches, which gives an aspect ratio of 8.5. The tip test was conducted with the pre-inflated wings test with the structural integrity at 2.5 G a load. IFI has a tractor configuration using a brushless Electricstar HCAG 3129 and a 13x6 fixed propeller. The electric motor is powered by two packs of 7.5V NiMH batteries with a 5100 mAh capacity. Rubber bands were used to secure the rigid wing on top of the fuselage. Two flight configurations were investigated:

- Dash configuration using the rigid wing only
- Loiter mode with the inflatable wing pre-inflated to 6 psi

The IFI has an estimated weight of 10lb excluding the onboard inflatable system resulting in a wing loading, W/S, of 0.86 and 2.16 lb/ft2 for high and low aspect ratio configurations, respectively.

IFI-A's aerodynamic performance was calculated and presented in appendix A for each wing configuration. The estimated characteristics were summarized in the graph as shown in fig. 6.2. The proof of flight is shown in fig. 6.3 (a) and (b). No significant in-flight divergence was observed during the flight.

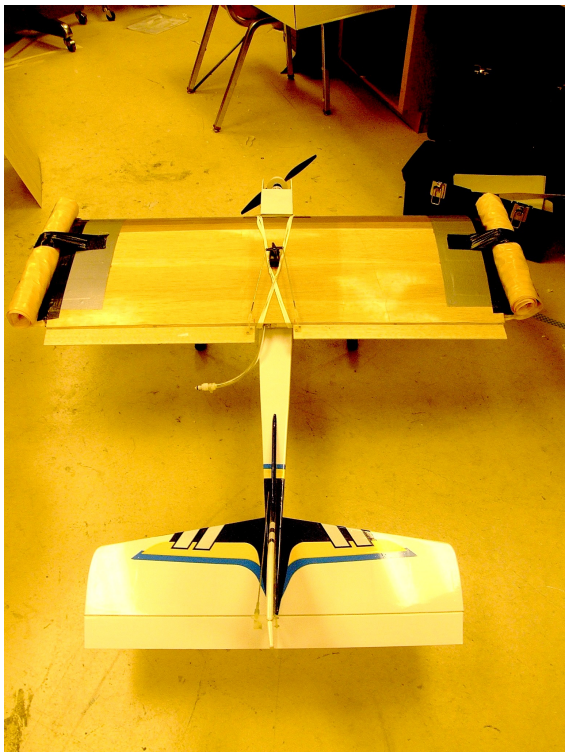

(a) Low Aspect Ratio - rigid wing only

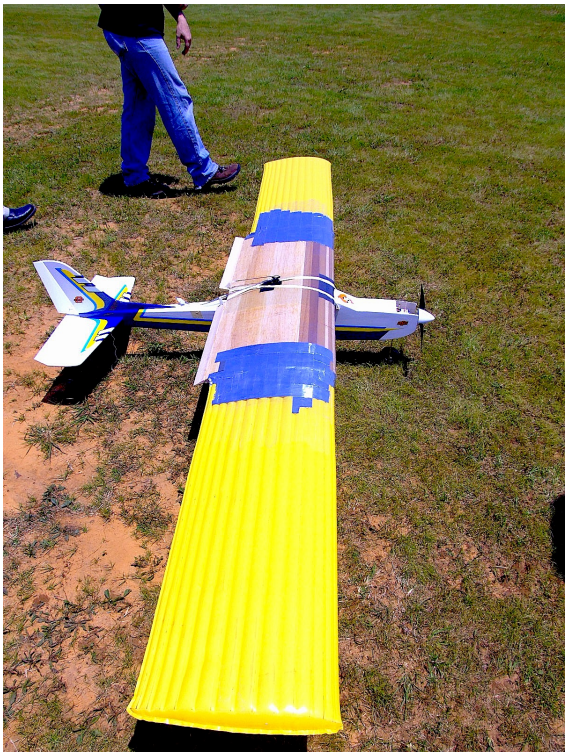

(b) High Aspect Ratio - pre-inflated configuration

Figure 6.1: IFI (In-Fight Inflatable)

6.2 Low Flow Rate Onboard Inflation System and Testing

The design of the inflation system is based on the results of the static structural characteristic and the volume of the inflatable wing. Small COTS aluminum air tanks were tested as the onboard inflation source tank. Each aluminum tank weighs about 0.19 lb and has a length of 9.75 inches and diameter of 2.6 inches. The aluminum tank is designed to be filled up to a maximum of 150 psi based on the manufacturer specification. However, the inflation system can only be filled up to 115 psi by using compressed air. The set up schematic of the static test is shown in fig. 6.4. This system provides a much slower inflation rate in comparison to the unpowered inflatable wing aircraft tested by the NASA Dryden Flight Research Center [6]. Their regulated high-pressure inflation system was designed for rapid deployment. Furthermore, our system

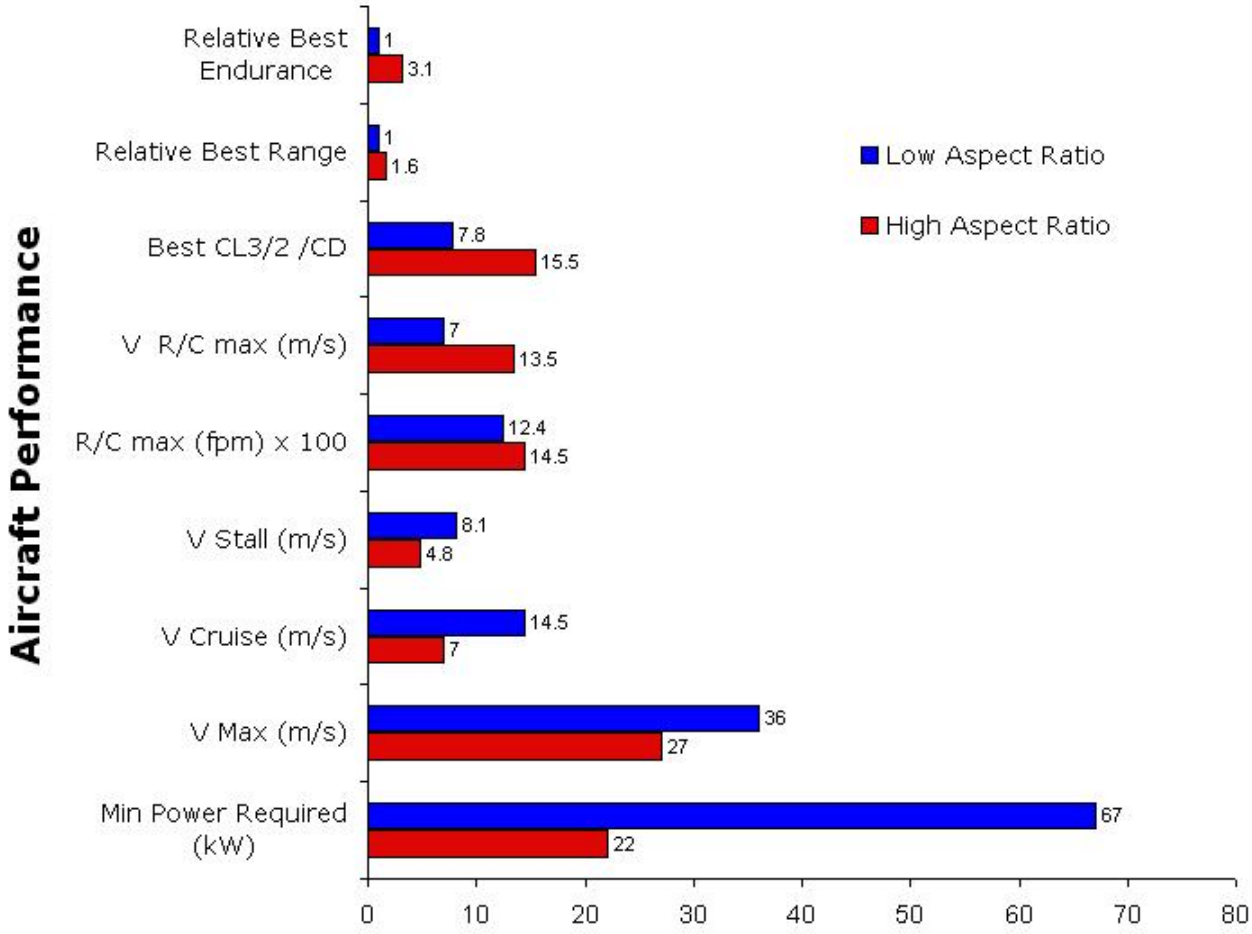

Figure 6.2: IFI's performance at both high and low AR .

(a) Low Aspect Ratio

(b) High Aspect Ratio

Figure 6.3: Prove of flight

also required more fuselage storage volumes to attach several air tanks to achieve full deployment. However, the advantages of the usage of the light-weight/high volume inflation system with the slower inflation rate can significantly reduce the structural weight and strength that is needed (on the fuselage or the rigid wing) to overcome the high dynamic loading during unfolding in flight. No regulator is needed to regulate the air tank pressure flow, thus reducing the overall aircraft weight and complexity. The major concern of using this system is the impact of the in-flight dynamic pressure on the slowly inflated wing. Therefore, wind tunnel deployment tests were conducted to verify this behavior using an air pump to simulate the slow inflation rate.

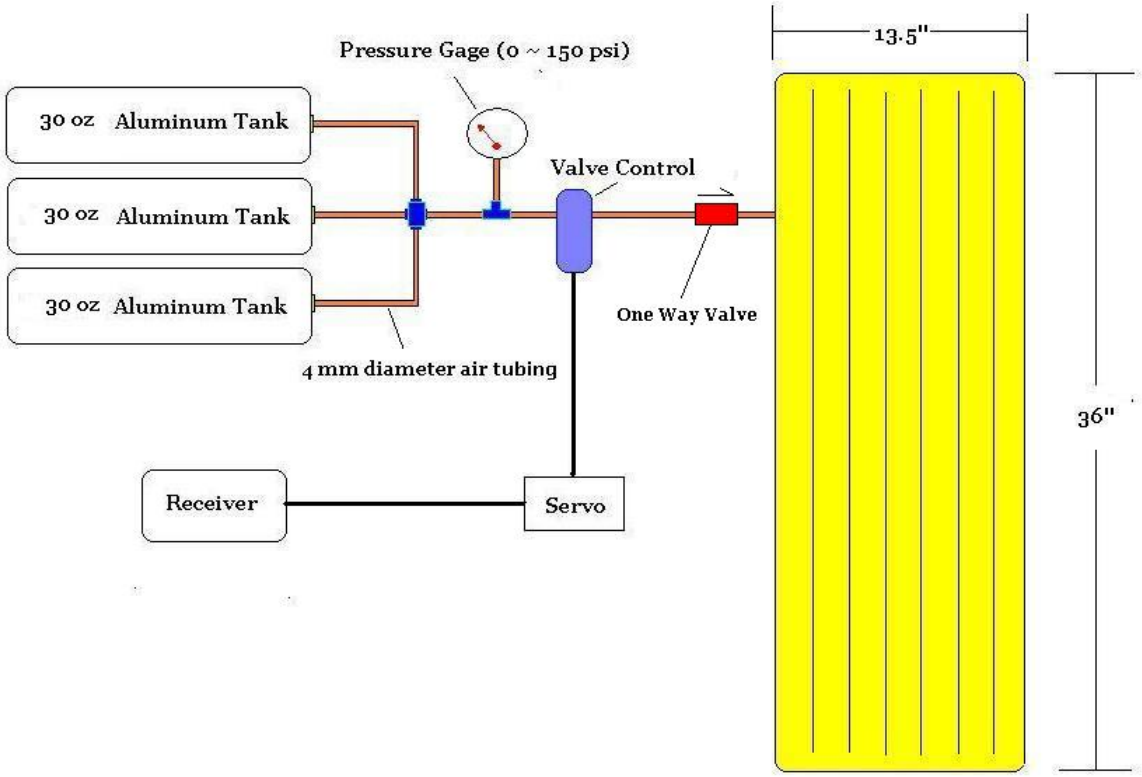

Figure 6.4: Low flow rate on-board inflation schematic

Static inflation deployment was conducted to fill up a 36 inch span inflatable wing by using three 30 oz. aluminum air tanks, as shown in fig. 6.5. Each tank was filled

up to 4 different pressures that ranged from 100 to 115 psi. No regulator was used in the system since the mass flow rate was relatively low. The pressure was recorded at 10 second intervals for 150 seconds once the valve was opened. A one way valve was used to regulate back pressure.

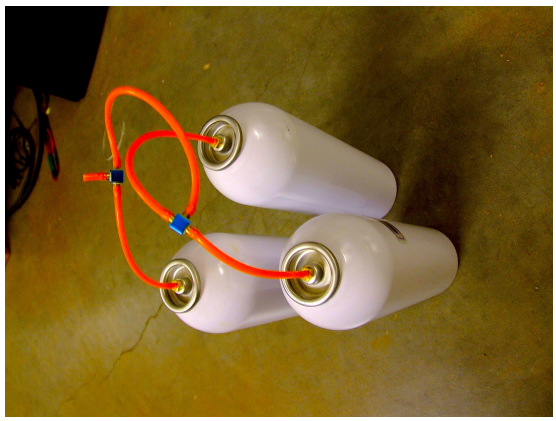

Figure 6.5: Three 30 oz. aluminum air tank

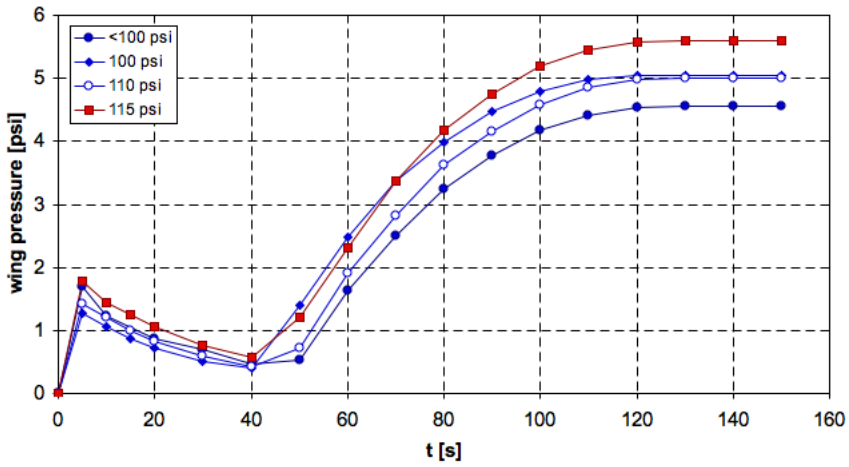

Figure 6.6: Quiescent inflation pressure history for various reservoir pressures.

Based on the static deployment test results shown in fig. 6.6., all 4 test results showed similar trends during the inflation. Each inflation test shows a rapid inflation rate from 0 to 5 seconds after the valve was fully opened. During this period, the air flow is experiences a constant volume expansion while the rest of the wing is still

rolled up. The pressure was rapidly increased to push the rolled up wing at the root section until it reached a constant pressure expansion state at 5 seconds. Once the wing is released from the restraint and rolled out, the wing volume increases and the pressure decreases. The pressure gradually decreases for about 32 seconds as the volume of the wing slowly increases to form the airfoil shape. In 40 seconds, the air tank still has enough pressure to keep the inflation going and the wing volume is still expanding. At this time both pressure and volume are increasing until the wing pressure is equal to the air tank pressure. The volume also reaches a steady state when it reaches the maximum allowable wing volume at 120 seconds. As a result, the 115 psi gives the fastest inflation rate to provide enough structural stiffness for the 36 inch span inflatable wing in 120 seconds. Inflation time can be reduced if each aluminum tank is filled up with pressures at more than 115 psi and less than 150 psi to achieve the required minimum pressure of 6 psi for an in-flight test.

6.3 High Flow Rate Onboard Inflation System and Testing

A higher mass flow rate would be an ideal case for onboard inflation system even though a slow inflation rate still allows the wing to be fully inflated with the help of Velcro. To construct a high flow rate onboard inflation system, a COTS CO2 canister was used.

A Blue Rhino CO2 canister as shown in fig. 6.7 was used as an air source for onboard inflation system. The cannister provides 72 oz of compressed liquid CO2 at 900 psi, about 500% higher than the aluminum tank thus decreasing the inflation time. The selected tank can be purchased at a local hardware store. The full tank weighs about 630 grams and an empty tank weighs about 410 grams. However, this system is much heavier, and thus yields more weight onto the aircraft's overall weight. Since our lab does not have a proper pressure transducer to test the fast inflation system, no static deployment was made to observe the change in pressure as the wing unfolds

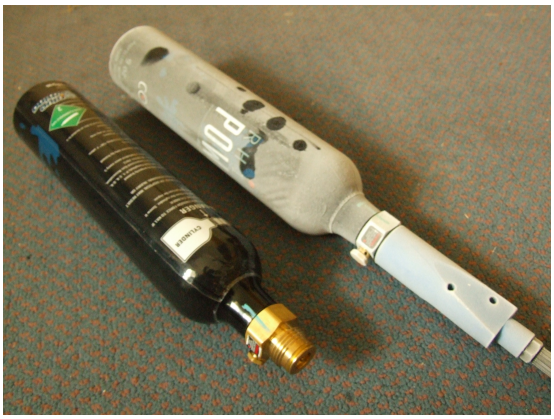

Figure 6.7: CO2 Canister

itself.

Fig. 6.8 (a) shows the schematic of this system using a manually controlled ball type valve. To remotely control the deployment, a solenoid valve is suggested to replace the ball type valve. Currently, a solenoid valve as shown in fig. 6.8 (b) is being investigated before being fully integrated into the IFIB. This small scale solenoid valve was designed specifically for paint-ball gun's trigger control system.

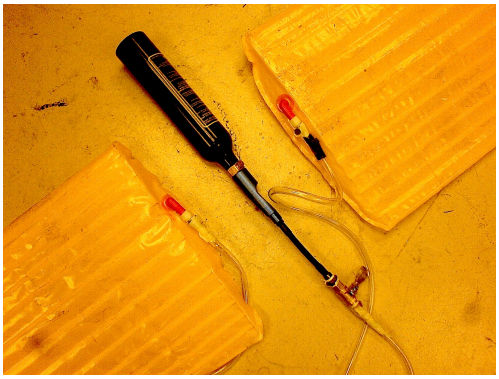

(a) CO2 canister with ball valve

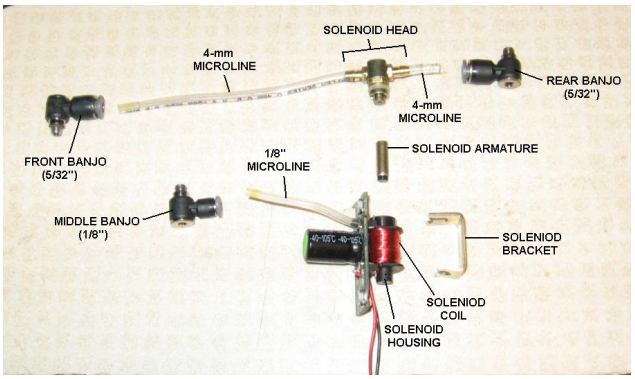

(b) Solenoid valve

Figure 6.8: High mass flow rate system subcomponents

Flight test will not be available until the solenoid valve is successfully tested for our application. Since the anticipated flight test is expected to be a short flight, no excess air is required to make up the air loss from the system. This leads to the usage of a light-weight relief valve instead of a regulator. The relief valve can be pre-

set which allows excess high pressure air to escape from the system until the overall system reaches the preset pressure value. The air tank is expected to be completely opened upon deployment until the whole system reaches 6 psi; assuming no leakage anywhere in the air hose.

Even though the automatic system is not ready for an in-flight test, a full scale inflation test was carried on by manually controlling the valve. This test was detailed in section 5 with the inflatable wings attached to the back of a moving truck.

6.4 IFI-B Aircraft

To install the chosen onboard inflation system for in flight deployment, an aircraft with larger storage volume is needed. Additional power is also required to overcome the aircraft weight gained from the onboard inflation system. Therefore, a high power version of IFI was constructed as shown in fig. 6.10. Currently, this research aircraft is still under-construction and the first flight is not expected until the beginning of spring of 2008. A new rigid wing with a longer wing span is constructed to increase the lift to overcome the weight of the aircraft and onboard system. The total wing span is 70 inches with a chord length of 14 inch. Flight control is achieved via the tail control. The combined semi span ILC Dover's inflatable wings and rigid wing gives a span of 142 inches from tip to tip, and has a surface area of 1988 square inches, which gives an aspect ratio of 10.14. IFI version B has a tractor configuration using a AXI 5320/28 model brushless motor using an 20x8 fixed propeller. The electric motor is powered by 4 packs of LiPo batteries. The CO2 canister is attached at the belly of the aircraft as shown in fig. 6.9 and separated from other subsystem due to safety reasons. No aerodynamic analysis was conducted for IFI version B yet.

Figure 6.9: CO2 canister attached to the fuselage

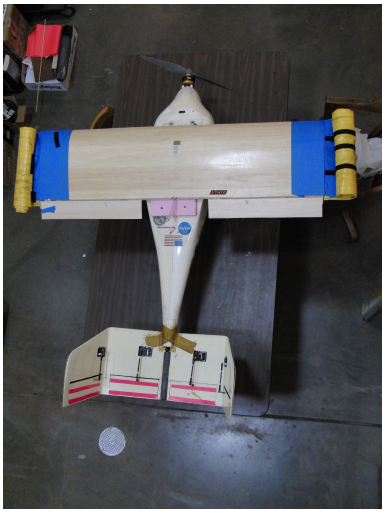

(a) Low Aspect Ratio.

(b) High Aspect Ratio.

Figure 6.10: IFI version B (In-Fight Inflatable).

6.4.1 In-flight Deployment and Stability Control

The static deployment test demonstrated that symmetric deployment is possible using DCE. However, asymmetric deployment could happen during flight if one wing deployed faster than the other under dynamic load. These might cause adverse roll

during deployment and might required significant control authority to regain stability in-flight. In the pre-inflated test flight for IFI-A, tail control was the sole control used to provide roll authority for the aircraft. Sufficient tail volume is needed for the aircraft during the transition from low aspect to high aspect ratio configuration. Servo actuation is suggested for roll control but it is not considered in the IFI-B design because of its hindering the compact stowage. However, the IFI-B rigid wing section is integrated with aileron to achieve short moment arm roll. The aileron control might be minimized at high aspect ratio, but is mainly used when the aircraft mode is on low aspect ratio configuration. One anticipated benefit is to assist roll correction and reduce the burden on tail control during deployment transition. Once the wing is completely inflated, the research aircraft will be fully controlled using the tail and limited ailerons control.

Furthermore, the power curve in fig. 6.11 shows that the transition from low to high aspect ratio configuration required the reduction in flight speed. Thus, the flight speed will be reduced gradually by the pilot during wing deployment. Flight speed will be adjusted accordingly once the inflation is completed. The power curve also shows that the power required at cruise flight is lower and thus conserved power for endurance flight at high aspect ratio.

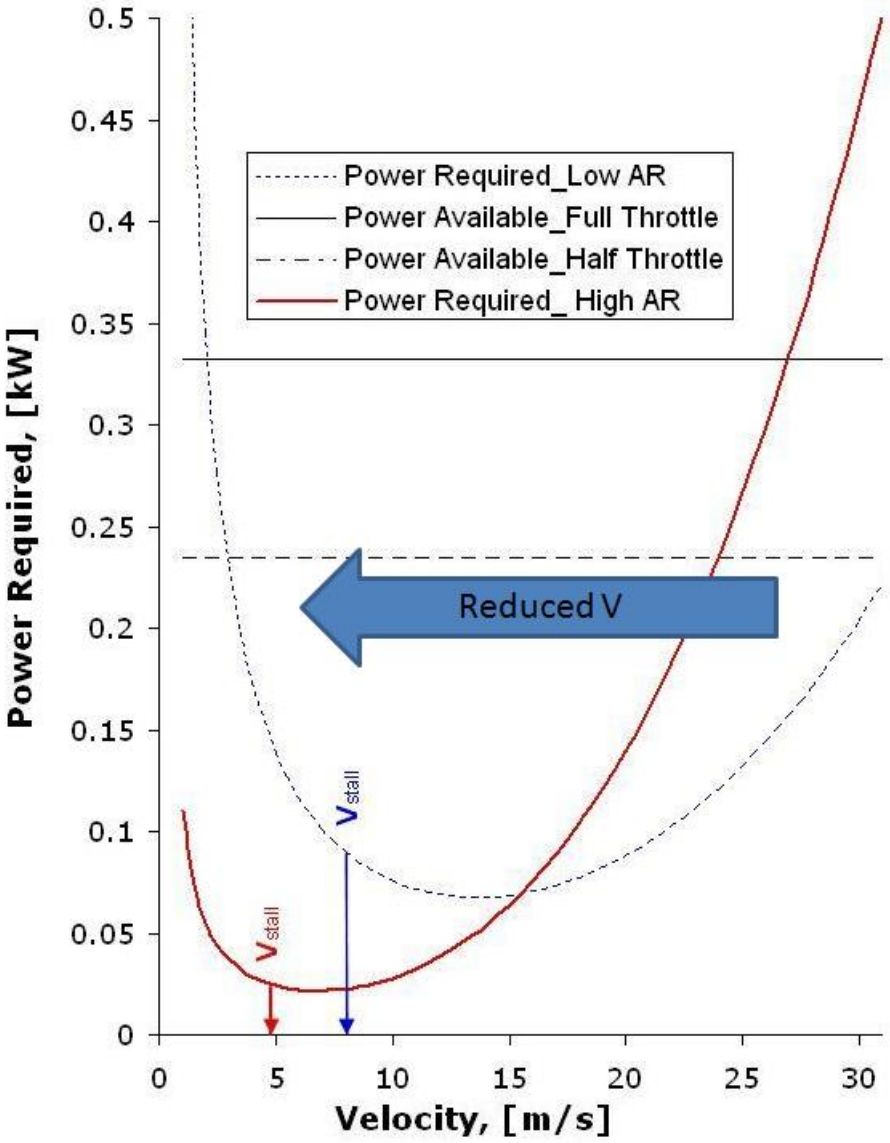

Figure 6.11: Power Curve

CHAPTER 7

Conclusions and Future Work

7.1 Conclusions

The purpose of this research is to control the deployment behavior and achieve a stable in-flight morphing capability using inflatable wings. Experiments were conducted on different wing deployment designs with various constraints, and the following points describe the main features resulting from the study of dynamic deployment of inflatable wings.

- Transient wing deployment of an inflatable wing can be separated into two stages: a constant pressure-increasing volume stage in which the wing fills followed by a constant volume-increasing pressure stage during which the filled wing increases its structural strength by increasing pressure. The wing will be unable to sustain aerodynamic loads during flight in the first stage. One can by bypass this by making the deployment very rapid (< 1 s), but that will increase the inflation system penalty. The other approach is to control the first stage and restrict the wing volume, where the wing volume only increases once the critical pressure needed to maintain structural integrity is reached, thereby ensuring that the deployment is steady.

- The current study shows that hook and loop fasteners (Velcro) mounted to the wing surface can be used as an ideal restraint and control deployment method for in-flight deployment of inflatable wings. It has been successfully demonstrated in the wind tunnel at velocities ranging from 16 m/s to 29 m/s. Velcro strips

kept the deployment controlled and no significantly instabilities were observed even though the deployment was conducted at a stall angle of attack at 12 degrees.

- Inflatable wings have shown to be very resilient to damage from sudden deflections and return to their original shape after the load is removed or reduced. In this way they can expand the flight envelope by surviving gust loads encountered in rough weather or off-nominal flight conditions. Unexpected crash events have shown a 100% survivability rate using inflatable wings. The inflatable wing can be seen deforming and absorbing the impact. Inflatable wings also have efficient packing capability where the wing can be compacted up to 10 times or more than in full span for flight. Inflatable wings have high durability and the inflatable wing used in this research has been repeatedly tested since 2004. Only a pinhole damage has occurred and can be repaired easier than patching a bicycle tire such using electric tape as a temporarily solution.

- Wing sleeve construction using silicon tape is a reliable technique for mounting. In comparison with previous designs proposed by ILC Dover, this method is a straight forward and light weight method to attach the semi-span inflatable wings to the rigid wing. Material tensile tests and flight tests have verified this method and been further applied in this research study via wind tunnel tests.

- The wing expansion during deployment shows an increase in lift as the wing extends span-wise. The lift can be maximized by using an inflation pressure less than the design pressure. At lower inflation pressures, the airfoil cross-section assumes a more streamlined shape.

- A flight test vehicle (in-flight inflatable, or IFI) was constructed and tested successfully in-flight using a low aspect ratio rigid wing and pre-inflated high aspect ratio wing. IFI version B was constructed to provide additional power

to overcome the aircraft weight gained from the installation of the onboard inflation system using the NASA 729 Kitty Hawk 3 platform. This version also provides additional storage volume for inflation system and telemetry.

- Two onboard inflation systems were investigated using COTS air tanks. Each system is suitable for onboard inflation in-flight depending on the inflation speed, aircraft storage volume, and allowable aircraft weight.

7.2 Future Work

7.2.1 In-Flight Testing

Full scale in-flight inflation test will be conducted using the IFI-B to verify the feasibility of morphing capability using inflatable wings. A high mass flow rate onboard inflation system using CO2 canister will be integrated into the aircraft to reduce the deployment time. Since this study only focuses on the deployment dynamics, aerodynamic optimization needs to be addressed to improve the flight efficiency.

7.2.2 Roll Control using Differential Pressure

Since ILC Dover's inflatable wing has been successfully demonstrated in-flight as conducted in both BIG BLUE and AIRCAT, the lift increase from a partially inflated wing can lead to an alternative roll control system. Roll control could be achieved without deforming the camber using servo actuators as described by Simpson [9]. Thus, one suggestion for future work is to provide an active pressure differential control between the two wings to control the wing lift and roll pneumatically.

7.2.3 Aerodynamic Performance

Unskinned inflatable wing designs have a drag penalty due to the inflatable baffles. Furthermore, the wind tunnel results show a 9 percent reduction in lift generation at

AOA 0 using Velcro. Further study is needed to explore the drag issue and improve the impact of on the inflatable wing aerodynamic characteristics.

APPENDIX A

Aerodynamic Predictions - Pre-inflated IFI version A

A.1 Lift Coefficient

All calculation conducted below are based on the theories and analysis tools obtain from Anderson et. al. Determination of lift coefficient of IFI was made using X-foil [cite] and finite wing corrections. Using the middle range of the expected flight velocity, calculations were performed on the baseline NACA 4318 profile at Reynolds numbers of $3.0 \cdot 10^5$. For an incompressible high-aspect-ratio straight finite wing $>$ 4 , Prandtl's lifting line theory is used to estimate the lift slope $a = \frac{dC_L}{d\alpha}$ for a finite wing in terms of the lift slope of the airfoil section $a_0 = \frac{dc_l}{d\alpha}$ as

$$a = \frac{a_0}{1 + a_0/(\pi e_1 AR)} \tag{A.1}$$

where a and a_0 are the lift slope per radian and e_1 is a factor that depends on the geometric shape of the wing, including the aspect ratio and taper ratio, respectively. e_1 was estimated as 0.95.

For an incompressible straight finite wing at AR < 4, Prandlt's lifting line theory yields poorer results as the aspect ratio is reduced. Therefore, lifting surface theory is used to predict the lift slope for low aspect ratio wing. An approximate relation was obtained by H.B. Helmbold in Germany in 1942 based on a lifting surface solution for a elliptic wings and is given by

$$a = \frac{a_0}{\sqrt{1 + (a_0/\pi AR)^2} + a_0/(\pi AR)} \tag{A.2}$$

where a and a_0 are the lift slope per radian. By applying Eq. A.1 and Eq. A.2 for

both 7.8 and 2.5 aspect ratio configurations, respectively, the lift coefficient, C_L vs. angles of attack, α for the inflatable morphing wing can be generated by using

$$C_L = a(\alpha - \alpha_{L=0}) \tag{A.3}$$

where α and $\alpha_{L=0}$ are in degrees. Note that the AOA with zero lift generation is denoted by $\alpha_{L=0}$, which is -3.92 degrees for the NACA 4318 airfoil.

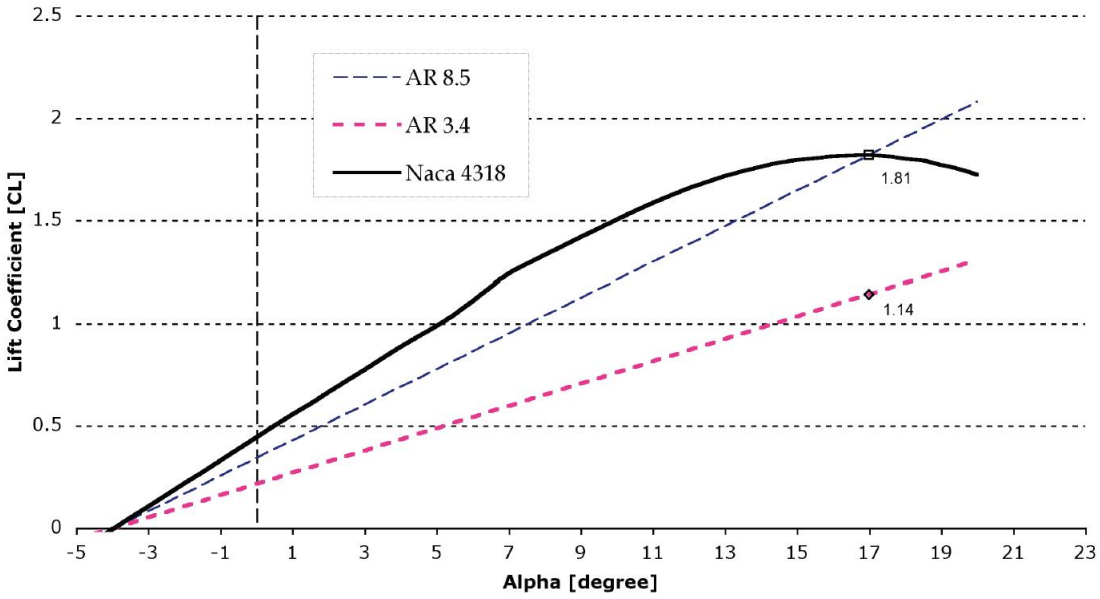

Figure A.1: Predicted lift coefficient for both low and high aspect ratio wing

Fig. A.1 shows the calculated lift coefficient for both finite wings compared to the baseline 2D NACA 4318 prediction. The lift slope for each low and high aspect ratio is 0.056 per degree and 0.088 per degree respectively, about a 58% increase in lift coefficient after both inflatable wings were deployed.

A.2 Drag Polar

The drag polar for the airplane is given by

$$C_D = C_{Do} + KC_L^2 \tag{A.4}$$

where $K = \pi eAR$ and $C_{Do} = 0.025$ and $K = 0.04$ are assumed here. Because of this assumption, the drag polar used in this calculation is only an approximation for IFI, and hence the computed result are only a representation of the performance of the vehicle as shown in Fig. A.2 as opposed to a precisely accurate result for the real airplane. For a chosen free-stream velocity, V_∞ and density, ρ_∞ at 50 ft above sea level, the lift coefficient, C_L is calculated from

$$C_L = \frac{2W}{\rho_\infty {V_\infty}^2 S} \tag{A.5}$$

This is substituted in Eq. A.5 to Eq. A.4 to construct the drag polar graph as shown in Fig.A.2.

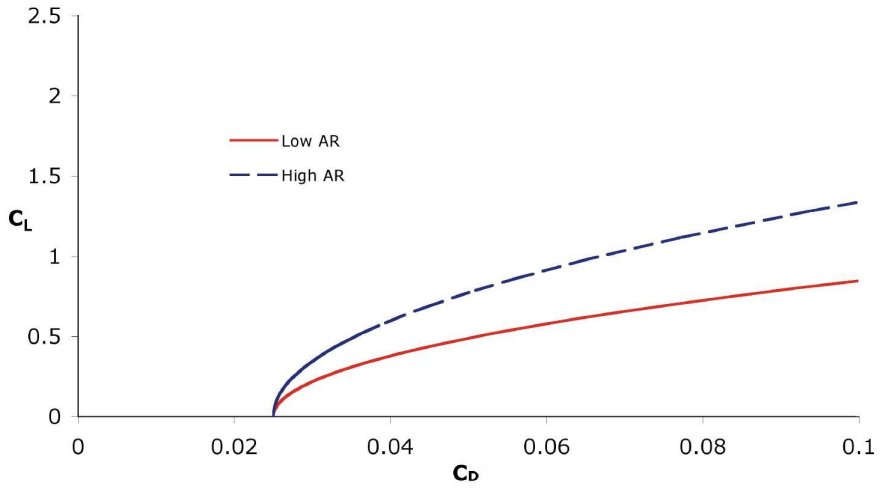

Figure A.2: Drag polar comparison between high and low AR configuration.

A.3 Thrust and Power

The Thrust Required, T_R, from

$$T_R = D = \frac{1}{2}\rho_\infty {V_\infty}^2 S C_D \tag{A.6}$$

is simply equal to the drag of the airplane and is dependent on the free-stream velocity, V_∞, air density, ρ_∞ and the surface area of the wing, S. Since the thrust required is

proportional to the wing planform area S, two graphs are generated in respect to each aspect ratio of 3.4 and 8.5 in Fig. A.3.

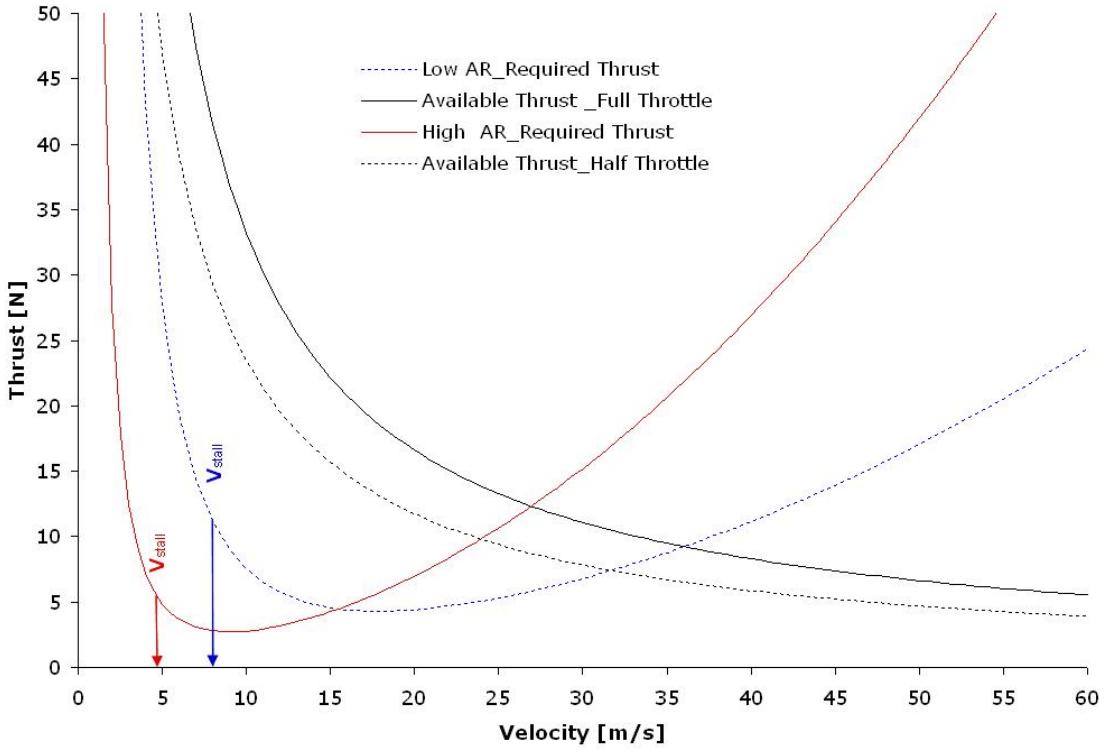

Figure A.3: Thrust available.

The typical take off thrust is at maximum throttle. As seen from Fig. A.3 and Fig. A.4, the maximum airspeed is governed by the power and thrust available from the propulsion system. Based on a wattmeter reading, the power available at full throttle is 0.33 kW and half throttle provides about 0.24 kW. The calculation of power and thrust available was made based on the assumption that both propeller and motor efficiency is only 90%. An examination of the thrust versus airspeed graph shows that the maximum speed at full throttle is 37 m/s and 28 m/s, for low and high aspect ratios, respectively; about 25% different. At half throttle, the maximum speed is 31.5 m/s and 24 m/s for low and high aspect ratios, respectively; about 24% different. Therefore, for a 10 lb IFI, the takeoff thrust at maximum speed is 12.38 N

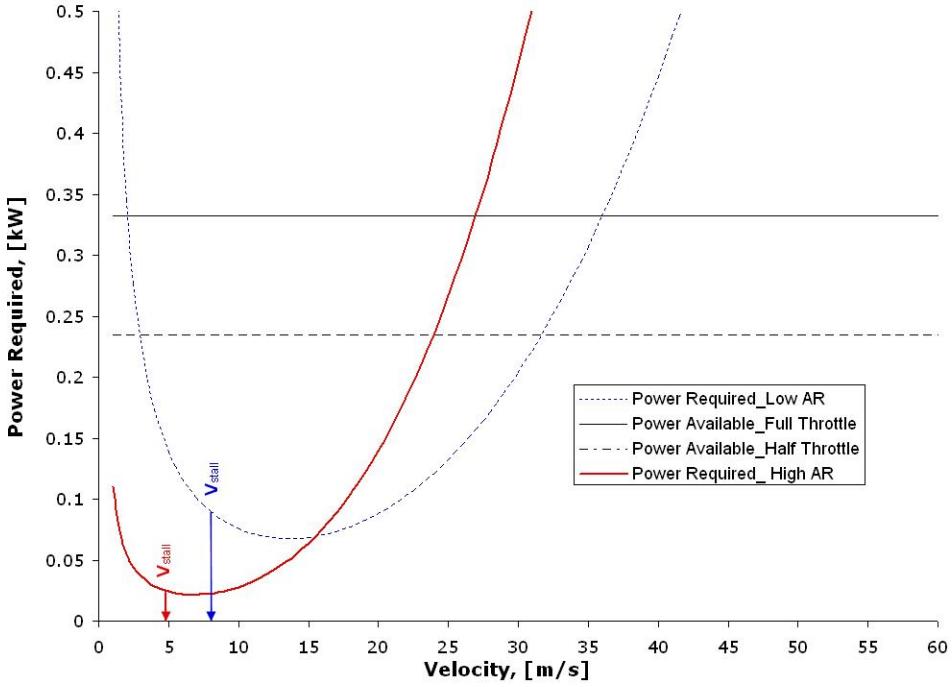

Figure A.4: Power available.

for high aspect ratio configuration and is 9.23 N for low aspect ratio configuration. The thrust difference between the two aspect ratios is also 25%.

A.4 Cruising Flight

Since drag is equal to thrust in Eq. A.6, the thrust versus airspeed plot is used to determine the airspeed that minimizes drag forces and the airspeed that requires the least power to over come drag. To find each point, a balance must be reached for level flight where parasite drag increases as speed increases, while induced drag decreases as speed increases.

As can be seen from Fig. A.3, the total drag force for the high aspect ratio configuration is minimized at an airspeed of about 9 m/s , while power is minimized at about 7 m/s. Between 7 and 9 m/s, then, is a good estimate of most efficient cruise velocities for high aspect ratio flight.

As for the low aspect ratio configuration, the total drag force is minimum at an airspeed of about 18 m/s, while the power is minimized at about 14.5 m/s. Between 14.5 and 18 m/s, then, is a good estimate of most efficient cruise velocities for high aspect ratio flight.

A.5 Stall Velocity

Stalling speed, V_{stall} for each wing configuration is also calculated using the following equation:

$$V_{stall} = \sqrt{\frac{2W}{\rho_\infty S C_{L_{max}}}} \tag{A.7}$$

Based on the calculation using Eq. A.7, the stall velocities at full throttle for low aspect ratio and high aspect ratio are 8.1 m/s and 4.8 m/s respectively, about 69% difference.

A.6 Rate of Climb

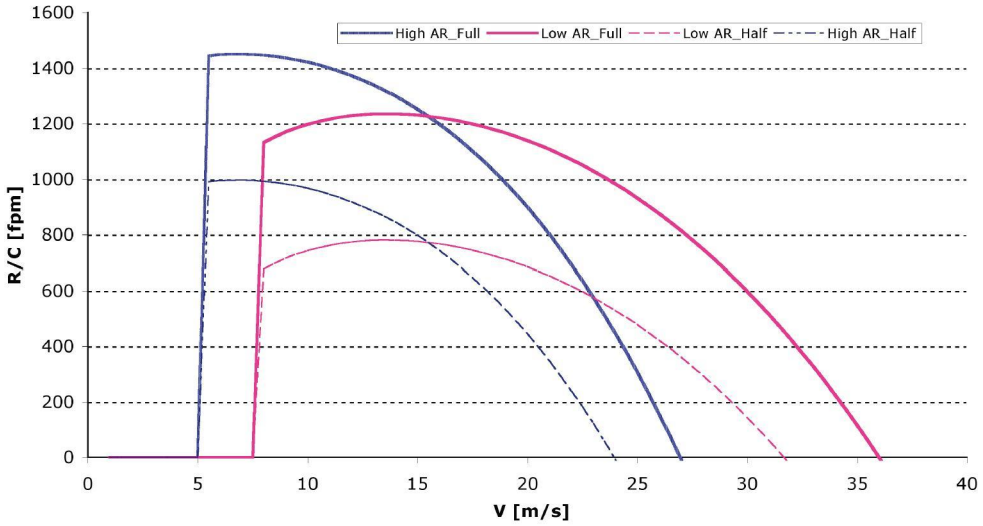

Figure A.5: Rate of climb comparison for both high and low aspect ratio configuration

The difference between the thrust and drag is the excess power available because it is the extra thrust available after the aircraft's drag is overcome. Dividing this excess power by the weight of the aircraft will provide the rate of climb at a given velocity. Calculating the rate of climb depends on the type of thrust provided by the aircraft using Eq. A.8:

$$RC = \frac{V_\infty (T - D)}{W} \tag{A.8}$$

where V_∞ is the free-stream velocity, T is the thrust available at full throttle, D is the drag and W is the total weight of the aircraft, assumed at 10 lb. As shown in Fig. A.5, the calculated maximum rate of climb at 50 ft altitude for high aspect ratio is 16% higher than the low aspect ratio with 6.3 and 7.3 meter per second (1240 and 1450 feet per minute) respectively. The respective speed at max rate of climb is 7 m/s and 13.5 m/s; both speeds are slightly lower than the estimated cruising speed. The relative best range and endurance depend on the battery capacity. Based on an estimation made using two 7.5 V NiMh batteries with 5100 mAh capacity each, the 8.5 aspect ratio has a relative best range with 58% greater than the 3.4 aspect ratio. As for the relative best endurance comparison, the 8.5 aspect ratio is 214% higher than the 3.4 aspect ratio configuration.

BIBLIOGRAPHY

[1] . . . USPTO United States Patent, Patent 1

[2] . . . USPTO United States Patent, Patent 3

[3] . . . USPTO United States Patent, Patent 3

[4] . . . USPTO United States Patent, Patent 4

[5] . Website: http://marsairplane.larc.nasa.gov/science.html, Nov 3th

[6] J. Murray, J. Pahle, S. Thornton, T. Frackowiak, J. Mello, and B. Norton, "Ground and flight evaluation of a small-scale inflatable winged aircraft," AIAA Paper 2002-0820, 40th AIAA Aerospace Sciences Meeting and Exhibit, Reno, NV, Jan. 2002.

[7] D. Neal, M. G. andC.O. Johnston, H. Robertshaw, W. Mason, and D. Inman, "Design and wind-tunnel analysis of a fully adaptive aircraft configuration," AIAA Paper 2004–1727, AIAA Aerospace Sciences Meeting, 2004.

[8] A. Simpson, S. Smith, and J. D. Jacob, "Aeroelastic behavior of inflatable wings: Wind tunnel and flight testing," AIAA Paper 2007-1069, 45th AIAA Aerospace Sciences Meeting & Exhibit, Reno, NV, Jan. 2007.

[9] A. Simpson, "Design and evaluation of inflatable wings for uavs," ph.d dissertation, University of Kentucky, Lexington, 2008.

[10] S. Smith, J. D. Jacob, D. Cadogan, and S. Scarborough, "Expanding the small uav design space with inflatable wings," SAE Paper 07atc-217, Society of Automotive Engineer, 2007.

[11] J. Chandler and J. Jacob, "Design and flight testing of a mars aircraft prototype using inflatable wings," AIAA Paper 2007-1069, 58th International Astronautical Congress, Hyderabad, India, 2007.

[12] D. Cadogan, W. Graham, and T. Smith, "Inflatable and rigidizable wings for unmanned aeriel vehicle," AIAA Paper 2003–6630, 2nd AIAA "Unmanned Unliimited" Systems, San Diego, CA, 2003.

[13] R.Guiler and W. Huebsch, "Development and testing of a wing morphing mechanism for the control of a swept wing tailess aircraft," AIAA Paper 2005-01-3391, 2005 SAE International, 2005.

[14] B.Roth, P.Chris, and W. Crossley, "Aircraft sizing with morphing as an independent variable: Motivation, strategies and investigations," AIAA Paper 2002-5840, 2002 AIAA, 2002.

[15] R. Armando, "Morphing aircraft technology survey," AIAA Paper 2007-1258, 45th AIAA Aerospace Sciences Meeting and Exhibit, Reno, NV, Jan. 2007.

[16] S. Ashley, "Flying on flexible wings," *Scientific-America*, vol. 289, pp. 74–83, Nov. 2003.

[17] C. Marty, "Nasa active aeroelastic wing fact sheet fs-061-dfrc," nasa dryden flight research center, http://www.nasa.gov/centers/dryden/news/FactSheets/FS-061-DFRC.html, Feb. 2005.

[18] J. Bondeau, J. Richeson, and D. Pines, "Design, development and testing of a morphing aspect ration with using an inflatable telescope spar," AIAA Paper 2003-1718, 44th AIAA/ASME/ASCE/AHS Structure, Structural Dynamics, and Materials Conferences, Norfolk, VA, Apr. 2003.

[19] N. N. Service, "The next 100 years of flight - part two," *Reed Business Information Ltd*, Dec. 2003.

[20] . Website: http://www.nrl.navy.mil/vrs/factsheets/index.php, Oct 14

[21] W. Bennie and J. Cocke, "Wind tunnel investigation of the aerodynamic and structural deflection characteristics of the goodyear inflatoplane," naca-rm-l58e09p, nasa, Langley Aeronautical Laboratory, Langley Field, Va., Sept. 1958.

[22] W. http://www.myairship.com/database/prospect.html

[23] W. http://www.engr.uky.edu

[24] W. http://web.mit.edu/drela/Public/web/xfoil

[25] J. M. Rowe and S. Smith, "Challenges of modeling inflatable wings," AIAA Paper 2007–1848, 48th AIAA/ASME/ASCE/AHS/ASC Structurus, Structural Dynmaics, and Material Conference, Honolulu, HW, 2007.

[26] R. Comer and S. Levy, "Deflections of an inflated circular cylindrical cantilever beam," *AIAA Journal*, 1963.

[27] J. Main, A. Strauss, and S. Peterson, "Beam-type bending of space-based inflated membrane structures," *Journal of Aerospace Engineering*, 1995.

[28] J. Main, A. Strauss, and S. Peterson, "Load-deflection behavior of space-based inflatable fabric beams," *Journal of Aerospace Engineering*, 1994.

[29] D. Cadogan, T. S. T., F. Uhelsky, and M. MAcKuscik, "Morphing inflatable wing deployment for compact package unmanned aircarft vehicle," AIAA Paper 2004-1807, 45th AIAA/ASME/ASCE/AHS/ASC Structures, Structural Dynamics and Materials Conference, Palm Springs, CA, Apr. 2004.

[30] K. Munson, "Jane's unmanned aerial vehicles and targets," 2000.

[31] . Website: http://marsairplane.okstate.edu, Dec 14

[32] J. Jacob and S. Smith, "Design of hale aircraft using inflatable wings," AIAA Paper 2008–167, 46th AIAA Aerospace Sciences Meeting and Exhibit, Reno, NV, Jan. 2008.

[33] tech. rep., http://www.flightglobal.com/articles/2007/10/19/218799/nextgens-shape-changing-uav-morphs-in-flight.html, Oct. 2007.

[34] A. Simpson, J. Jacob, and S. Smith, "Inflatable and warpable wings for meso-scale uavs," AIAA Paper 2002-7161, AIAA Infotech@Aerospace, Arlington, Virginia, Sept. 2005.

[35] W. Loh and J. Jacob, "In flight aspect ratio morphing using inflatable wings," AIAA Paper 2008-xxxx, 46th AIAA Aerospace Sciences Meeting and Exhibit, Reno, NV, Jan. 2007.

VITA

Weng Kheong Loh

Candidate for the Degree of

Master of Science

Thesis: DEPLOYMENT DYNAMICS OF INFLATABLE WINGS

Major Field: Mechanical and Aerospace Engineering

Biographical:

Personal Data: Born in Ipoh, Perak, Malaysia on April 27, 1982.

Education:

Received the B.S. degree from OKlahoma State University, Stillwater, Oklahoma, United States, 2006, in Mechanical and Aerospace Engineering
Completed the requirements for the degree of Master of Science in Mechanical and Aerospace Engineering at Oklahoma State University,OKlahoma in December, December, 2008.

Name: Weng Kheong, Loh (Ben) Date of Degree: December, 2008

Institution: Oklahoma State University Location: Stillwater, Oklahoma

Title of Study: DEPLOYMENT DYNAMICS OF INFLATABLE WINGS

Pages in Study: 136 Candidate for the Degree of Master of Science

Major Field: Mechanical and Aerospace Engineering

Dynamic deployment of inflatable wings were investigated through laboratory, wind tunnel and flight testing. The goal of the research is to design an in-flight morphing wing aircraft using semi-span inflatable wings that morphs from low aspect ratio to high aspect ratio. Full scale pre-inflated flight tests were successfully conducted for an inflatable wing manufactured from polyurethane coated nylon that varies the aspect ratio of a small unmanned vehicle from approximately 3.4 to over 8.5, an 150% increase. A wing sleeve made of silicon tape was used to attached the semi-span inflatable wing section to the wing tip of the inboard rigid wing. Prior to in-flight deployment tests, wind tunnel tests were conducted to investigate the impact of dynamic pressure during deployment. Three wing designs were investigated: wing alone (WA), wing with stiffening elements (WSE), and wing with deployment control elements (DCE). Compressed air was used as the pressurized gas for inflation. Aerodynamic load and pressure measurements were made to determine the performances of deployment by varying angles of attack, free-stream velocities and inflation pressure while simultaneous recording deployment shape with high speed video. Regardless of the wing design and deployment behavior, in all deployments tests the wing was successfully deployed to its final shape at its design pressure. The WA contains no solid structure and solely relies on internal pressure to maintain shape. The WSE was reinforced with strips of flexible tape to increase structural stiffness over the WA design. However, both wing designs showed flapping and folding due to the aerodynamic loads during deployment. This unstable behavior was successfully mitigated by using hook and loop fasteners as DCE. The DCE test results showed a systematic and stable deployment even as the wing was deployed at stall conditions. Multiple arrangements with different lengths and surface areas were investigated to improve deployment performance. Full scale static and dynamic deployment tests using DCE have demonstrated that the deployment is symmetric and is able to maintain its structural integrity under dynamic pressure. However, both the wing internal pressure and surface roughness were found to impact the lift efficiency of the inflatable wing and lift could be maximized by using a pressure lower than the design pressure. Ground test under flight conditions demonstrated successful deployment. An onboard inflation system has been developed using a COTS solenoid valve and CO2 canister.

ADVISOR'S APPROVAL: Dr. Jamey Jacob